SYNTHESIS, STRUCTURAL AND BIOLOGICAL ANALYSIS OF ORGANIZED BIOMIMETIC SYSTEMS

Lubomir Vezenkov

Dottorato in Scienze Biotecnologiche – XXIII ciclo
Indirizzo Biotecnologie Industriali e Molecolari
Università di Napoli Federico II

Dottorato in Scienze Biotecnologiche – XXIII ciclo
Indirizzo Biotecnologie Industriali e Molecolari
Università di Napoli Federico II

SYNTHESIS, STRUCTURAL AND BIOLOGICAL ANALYSIS OF ORGANIZED BIOMIMETIC SYSTEMS

Lubomir Vezenkov

Dottorando:	Lubomir Vezenkov
Relatori:	Prof. Ettore Benedetti
	Prof. Jean Martinez
Correlatore:	D.ssa Muriel Amblard
Coordinatore:	Prof. Giovanni Sannia

Ai miei relatori,

a Muriel,

ai miei teammates,

alla mia famiglia…

…Grazie!!

INDEX

RIASSUNTO 1

SUMMARY 6

RESUME 8

I. INTRODUCTION 10

I.1. Foldamers 10

I.1.1. Foldamers structure 10

I.1.2. Foldamers function 12

I.2 CPP – Cell Penetratin Peptides and CPNP – Cell Penetrating Non Peptides 13

I.2.1 Cell Penetrating Peptides 13

I.2.2 Cell Penetrating Non-Peptides 15

I.2.3 Determination of the intracellular concentration of CPP and CPNP 16

I.2.4 CPP/CPNP-Drug bioconjugate intracellular localization 18

I.3 Cathepsin D 18

I.3.1 Cathepsin D and Cancer 19

I.3.2 Assay for CD enzyme activity 20

II. PROJECT AIMS 21

III. RESULTS AND DISCUSSIONS 23

III.1 Synthesis of Fmoc-DBT-OH and Fmoc-AMPA-OH 23

III.2 Structural studies of DBT and AMPA oligomers 24

III.2.1 Syntesis of DBT and AMPA oligomers for structural studies 24

III.2.2 Crystallization assays 25

III.2.3 NMR structural studies of linear DBT oligomers 26

III.2.3.1 Choice of deuterated solvent 26

III.2.3.2 'NOE walk' and assignment of the protons 27

III.2.3.3 Measurement of NOE and ROE volumes and determination of distance restrictions in the oligomers 29

III.2.3.4 Determination of the secondary structure of Ac-$(DBT)_6$-NH_2 by molecular modelization with distance restrictions 35

III.3 DBT and AMPA oligomers as cell penetrating non-peptides (CPNP) 36

III.3.1 Synthesis of oligomers tagged by fluorescein isothiocyanate 36

III.3.1.1 Synthesis of short DBT and AMPA oligomers tagged by fluorescein isothiocyanate 36

III.3.1.2 Synthesis of octa and nona-arginine and $(DBT)_{3-4}$-$(Arg)_9$ oligomers tagged by fluorescein isothiocyanate 37

III.3.2 Internalization of short DBT oligomers tagged by fluorescein 37

III.3.2.1 Cellular uptake of DBT Oligomers by MDA-MB-231 breast cancer cells 37

III.3.2.2 Intracellular Distribution of DBT Oligomers. 38

III.3.2.3 Toxicity of the DBT oligomers 40

III.3.2.4. Cellular uptake of DBT oligomer by different cell lines 41

III.3.2.5 Discussion 41

III.3.3 Internalization of chimeric OligoDBT-OligoArg oligomers tagged by fluorescein 42

III.3.4 Internalization of AMPA oligomers tagged by fluorescein 42

III.4. A Straightforward approach for cellular-uptake quantification of CPPs and CPNPs 43

III.4.1 Methodology 43

III.4.2 Discussion 51

III.5 Vectorization of pepstatine – *in vitro* inhibition of the Cathepsine D and anti-cancer activity 51

III.5.1 CD vectorized inhibitors design 52

III.5.2. Test for inhibition of the isolated CD enzyme 54

III.5.3. *In vitro* tests for cytotoxicity 56

III.5.4 Internalization assays of fluorescently labelled CD inhibitors 61

III.5.5 Discussion 61

IV. CONCLUSION AND PERSPECTIVES 64

IV.1 Structural studies of DBT and AMPA oligomers 64

IV.2 DBT and AMPA oligomers as cell penetrating non-peptides 64

IV.3 A straightforward approach for cellular-uptake quantification of CPPs and CPNPs 65

IV.4 Vectorization of pepstatine 65

V. MATERIALS AND METHODS 66

V.1 Materials 66

V.2 Characterization of the compounds 66

V.3 Liquid phase synthesis 67

V.4 SPPS 73

V.5 Biological experiments 78

V.6 MALDI TOF experiments 81

V.7 NMR exprerіments and structural studies 82

V.7.1 Proton chemical shifts of compounds Ac-$(DBT)_n$-NH_2 83

V.7.2 Distance restrictions measured for compound Ac-$(DBT)_6$-NH_2 from 2D NOESY experiment 84

ABBREVIATIONS 87

REFERENCES 89

SCIENTIFIC PRODUCTION LIST 94

EXPERIENCE ABROAD 96

APPENDIX

RIASSUNTO

I foldameri sono oligomeri di sequenza specifica simili a peptidi, proteine ed oligonucleotidi che si ripiegano in strutture tridimensionali ben definite.[1] Elementi strutturali per la costruzione dei foldameri sono composti come i β-peptidi, le oligouree ed i composti aromatici.[2] Anche se gli studi sui foldameri all'inizio erano maggiormente indirizzati verso la comprensione dei fattori che governano il loro ripiegamento, in seguito sono stati sviluppati alcuni foldameri con proprietà biologiche molto interessanti.[3] Ispirati dagli sviluppi di questo campo di ricerca, abbiamo progettato foldameri costruiti mediante l'uso di mimetici di ripiegamenti di tipo beta che sono stati selezionati mediante dinamica molecolare per la loro propensione ad adottare strutture organizzate quando oligomerizzati.[2] Fra i vari motivi strutturali selezionati dal programma di dinamica molecolare, due mimetici di *β-turns*, il (3S)[ammino]-5-(carbossimetil)-2,3-diidro-1,5-benzotiazepin-4(5H)-one o **DBT**[4] e l'acido 2-amminometil-fenil-acetico o **AMPA** (Figura **R.1**) sono stati scelti come elementi strutturali per la loro propensione ad adottare strutture elicoidali *in-silico* e per la loro facilità di sintesi.

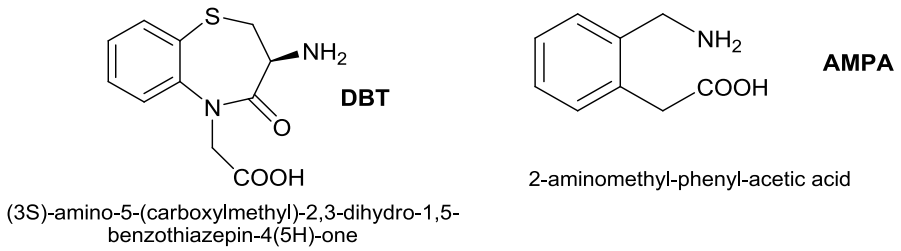

Figura R.1 *Mimetici di b-turns: le strutture di (3S)-amino-5-(carboxylmethyl)-2,3-dihydro-1,5-benzothiazepin-4(5H)-one o DBT ed il l'acido 2-amminometil-fenil-acetico o AMPA*

E' stata prima di tutto sviluppata una strategia di sintesi per l'ottenimento di grandi quantità di DBT N-protetto mediante il gruppo protettore 9-fluorenilmetossicarbonile (Fmoc). Questa sintesi ha permesso di ottenere dopo diversi stadi più di 25 grammi di Fmoc-DBT-OH con una resa globale di circa il 50%. L'AMPA é stato invece comprato e poi protetto con Fmoc. Gli ammino acidi non-naturali protetti mediante il gruppo Fmoc così ottenuti sono stati usati come monomeri di partenza per la costruzione di oligomeri mediante una sintesi peptidica di tipo standard in fase solida (*SPPS*). Il nostro primo obiettivo è stato quello di eseguire un'analisi strutturale degli oligomeri mediante NMR, dicroismo circolare e diffrattometria a raggi-X. Sono stati sintetizzati oligomeri di diversa lunghezza protetti all'N-terminale mediante acetilazione o mediante il gruppo 2-bromobenzilossicarbonil Z(Br) (Figura **R.2**) per gli studi di cristallizzazione al fine di ottenere cristalli singoli da usare in diffrattometria. Esempi degli oligomeri sintetizzati per gli studi strutturali sono riportati nella Tabella **R.1**.

Tabella R.1*. Esempi di oligomeri sintetizzati per studi strutturali*

Composti	Analisi strutturali
Ac-$(DBT)_n$-NH_2 ; n=[1-8]	NMR e cristallizzazione
Z(Br)-$(DBT)_n$-NH_2 n=[4-5]	Cristallizzazione
Ac-DBT-LBT-DBT-LBT-NH_2	NMR e cristallizzazione
Ac-$(AMPA)_n$-NH_2 n=[4-5]	NMR e cristallizzazione

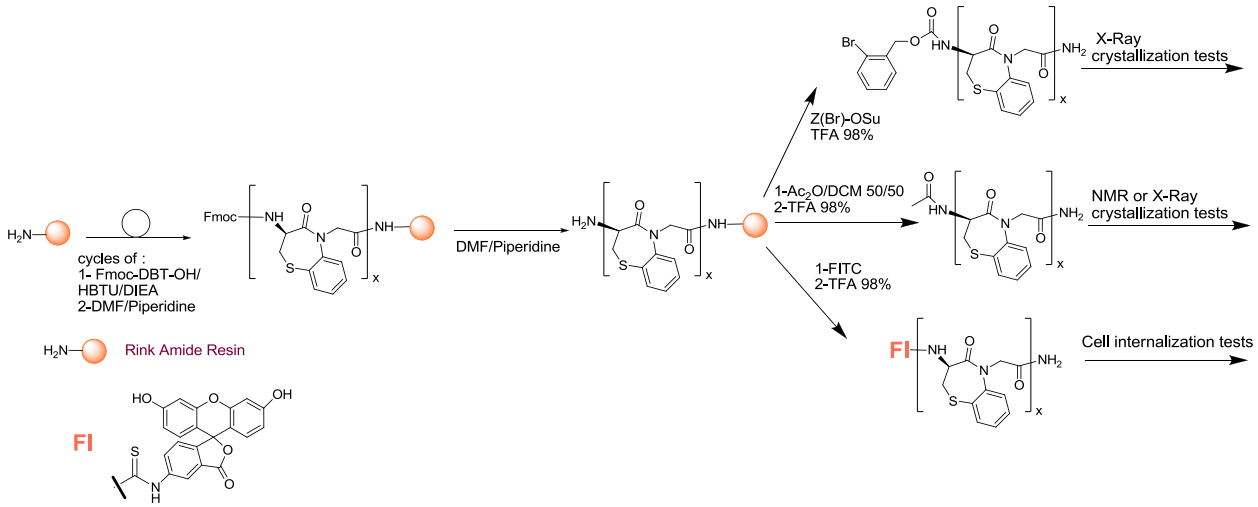

Figura R.2 *Sintesi generale in fase solida (SPPS) di oligomeri DBT protetti mediante il gruppo Z(Br) all'amino terminale per saggi di cristallizzazione, mediante il gruppo acetile per studi strutturali di NMR e mediante fluoresceina per i saggi di internalizzazione. Lo stesso approccio sintetico è stato usato per la sintesi degli oligomeri di AMPA*

Tutti i composti sono stati purificati mediante cromatografia preparativa HPLC e sono stati ottenuti con purezza molto elevata (>98%) ed infine caratterizzati mediante LC-MS. Sono state anche utilizzate tecniche NMR 1D e 2D per caratterizzare la struttura dei composti. Sono state evidenziate nelle varie molecole numerose interazioni a lunga distanza mediante esperimenti 2D ROESY e 2D NOESY. L'insieme di tutti questi dati suggerisce fortemente un'organizzazione strutturale ben definita degli oligomeri Ac-DBT_5-NH_2 ed Ac-DBT_6-NH_2. Piccoli cristalli delle stesse molecole sono stati ottenuti ma al momento la loro grandezza non risulta sufficiente per studi cristallografici mediante diffrazione dei raggi-X.

In uno studio parallelo è stato ipotizzato che piccoli oligomeri ottenuti dagli elementi strutturali di DBT o di AMPA potessero traslocare la membrana cellulare ed essere usati come nuova classe di non-peptidi che penetrano la cellula (cell penetrating non-peptides, CPNP).[5,1] Anche se questi peptidi non presentano carica come la maggior parte dei peptidi *cell-penetrating*, CPP[6] o i CPNP, si è considerato che in virtù della loro aromaticità, idrofobicità e struttura ben organizzata potessero avere interazioni non-specifiche con il doppio strato lipidico e perciò essere internalizzati nella cellula. Gli oligomeri corti sono stati sintetizzati su una resina Rink ammidica a cui è seguita la metodologia di sintesi in fase solida *SPPS* e successivamente fluorescinati all'N-terminale con fluoresceina isotiocianato (Figura **R.2**). Inizialmente l'*uptake* cellulare in cellule cancerose della mammella MDA-MB-231 di oligomeri tipo $(DBT)_{2\text{-}4}$ è stato analizzato mediante misure di emissione di fluorescenza (Figura **R.3**) e confrontate come controllo positivo al ben noto e potente CPP octarginina (Arg_8)[7] e come controllo negativo alla carbossifluoresceina (CF). La maggiore intensità di fluorescenza intracellulare è risultata essere quella di DBT_4 con un drastico decremento (>4 volte) per gli oligomeri DTB_3 e DTB_2 (Figura **R.3**).[8] Quindi l'*uptake* cellulare sembrava essere dipendente dalla lunghezza aumentando l'internalizzazione con la grandezza dell'oligomero. Inoltre la quantità di DBT_4 che era internalizzata era più significativa di quella di Arg_8 nonostante il fatto che DBT_4 non sia carico. Mediante microscopia confocale è stato stabilito che i nostri composti sono essenzialmente localizzati negli endosomi dopo 3 ore di incubazione e nei

liposomi dopo 16 ore di incubazione. In conclusione questi dati indicano l'abilità di questi oligomeri di essere internalizzati mediante un meccanismo endolisosomiale.

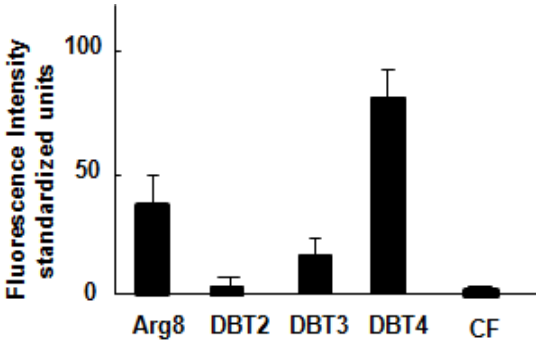

Figura R.3. *Determinazione dell'internalizzazione dei composti dopo 3 ore di incubazione a 37°C e a concentrazione di composto fluoresceinato 10^{-5} M.*

Anche se molti degli studi iniziali di *drug delivery* erano tesi ad evitare come obiettivo i lisosomi onde prevenire la successiva degradazione della molecola, studi più recenti hanno dimostrato la rilevante utilità clinica dell'uso di questo compartimento cellulare per la *drug delivery* nel trattamento di disturbi dell'accumulo nei lisosomi, nel morbo di Alzheimer e nel cancro.[9]

Nell'analizzare l'efficienza dell'internalizzazione dei nostri CPNP si è deciso di valutare direttamente la loro concentrazione all'interno della cellula. Anche se sono stati impiegati diversi metodi di individuazione dell'*uptake* cellulare di composti che penetrano in cellula come i coloranti fluorescenti o composti radioattivi, i risultati differiscono fortemente da uno studio all'altro a seconda del protocollo utilizzato ed in tutti i casi la quantificazione rimane difficile. Uno studio riportato da Burlina et al.[10] ha portato un grande miglioramento nel proporre un metodo quantitativo altamente riproducibile basato su MALDI-TOF MS per misurare la concentrazione del peptide internalizzato. Tuttavia, dopo la lisi cellulare, questo metodo richiede la cattura del CPP cui è legata la biotina da parte di granuli magnetici ricoperti di streptavidina. Questo stadio è particolarmente critico per l'accuratezza della quantificazione. Questo è il motivo per il quale si è deciso di sviluppare una nuova metodologia di carattere generale basata sulla spettrometria MALDI-TOF MS che non richieda alcuna purificazione o stadi di separazione. Si è studiata l'internalizzazione di composti CPP/CPNP marcati con l'acido α-ciano-4-idrossicinnamico (HCCA) seguendo i segnali in una matrice neutra dell'estere metilico dell'acido α-ciano-4-idrossicinnamico (HCCE) (Figura **R.4 B**). Questa matrice combinata (HCCA legato e HCCE) ha permesso di discriminare i segnali MS indotti dal peptide di interesse che erano presenti in bassa concentrazione da quelli dei peptidi non marcati molto abbondanti. Per aggiunta di precise quantitá di CPP/CPNP marcati con HCCA deuterato (Figura **R.4 A**) prima dell'esperimento MALDI-TOF MS, il CPP/CPNP internalizzato può essere quantificato sulla base del rapporto fra i picchi $[M+H]^+$ del CPP deuterato e quello non deuterato etichettato con HCCA (Figura **R.4 B**).[11]

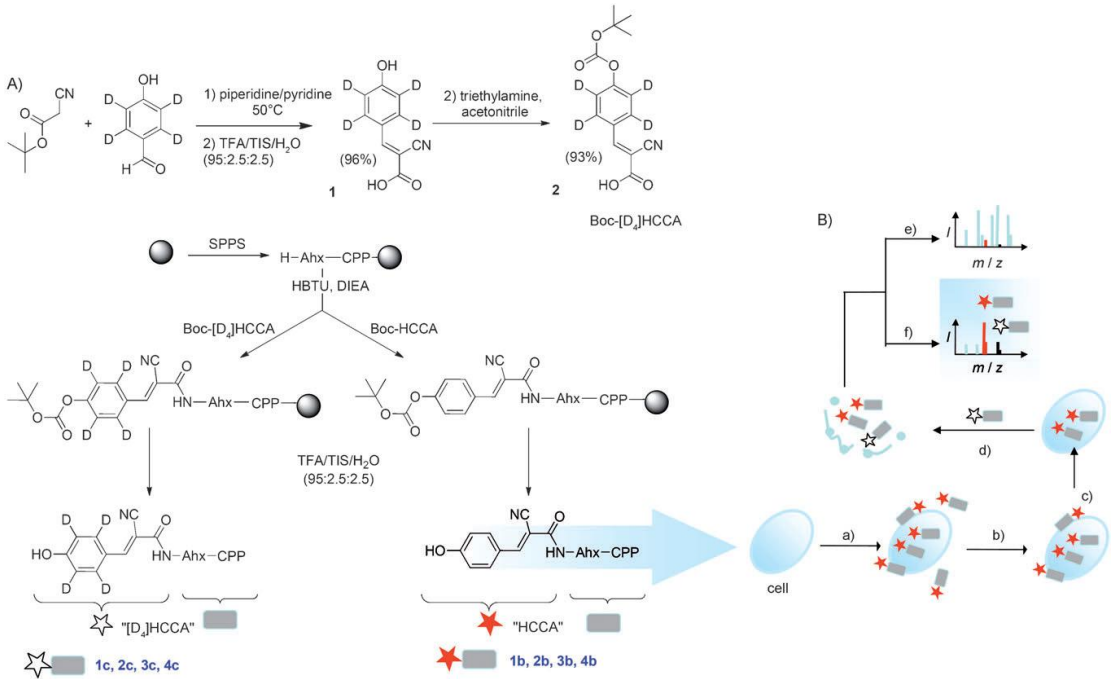

Figura R.4 A) *Sintesi dei CPP con HCCA non marcato (D_o) e marcato con deuterio (D_4).* ***B)*** *Strategia per la diretta quantificazione dell'uptake cellulare dei CPP (e un CPNP) mediante MALDI-TOF MS con l'uso dell'effetto di discriminazione HCCA/HCCE: a) incubazione delle cellule con CPP marcato con HCCA; b) stadio di lavaggio; c) stripping enzimatico della membrana cellulare; d) lisi cellulare, seguita dall'aggiunta di un ammontare preciso del CPP deuterato e marcato con HCCA come standard interno; e) analisi MALDI-TOF dell'intero lisato cellulare nella matrice HCCA; f) analisi MALDI-TOF dell'intero lisato cellulare nella matrice "neutra" HCCE. L'effetto di discriminazione dei segnali HCCA/HCCE produce un aumento del segnale del CPP nella miscela complessa. Il CPP internalizzato può essere quantificato sulla base del rapporto fra i picchi $[M+H]^+$ del CPP deuterato e di quello non deuterato marcato con HCCA. Boc = tert-butossicarbonilo, DIEA = N,N-diisopropiletilammina, HBTU = O-(benzotriazol-1-il)-N,N,N',N'-tetrametiliuronio esafluorofosfato, TFA = acido trifluoroacetico, TIS = triisopropilsilano*.

Un altro aspetto molto interessante della ricerca è stato quello riguardante la sintesi di bioconiugati fra i nuovi CPNP ed alcuni composti biologicamente attivi capaci di per se di attraversare la membrana cellulare. A tale scopo abbiamo scelto un potente inibitore dell'enzima catepsina D (CD), cioè la pepstatina. La catepsina D è una aspartico endopeptidasi lisosomiale solubile, sintetizzata nel reticolo endoplasmatico sotto forma di preprocatepsina D (pCD). pCD è una glicoproteina con due oligosaccaridi legati all'azoto bersaglio di strutture intracellulari vescicolari (lisosomi, endosomi, fagosomi).[12] Entrando nei compartimenti acidi endosomiali e lisosomiali si ottiene idrolisi proteolitica del pCD con formazione della forma enzimatica attiva della CD. In normali condizioni fisiologiche pCD è smistato ai lisosomi e si trova nella cellula, ma in alcune condizioni patologiche fisiologiche come il cancro pCD/CD sfugge al normale meccanismo e viene secreto dalla cellula. Una volta secreto all'esterno pCD può essere internalizzato per endocitosi via M6PR o da recettori ancora sconosciuti da entrambe le cellule cancerose e dai fibroplasti. Il pCD endocitosato va a maturazione dando luogo a CD attiva enzimaticamente. Un'attività extracellulare della CD o all'interno degli endosomi può essere responsabile dell'attivazione di diversi fattori di crescita e di recettori di fattori di crescita. Inoltre CD digerisce varie chemochine e può perciò attenuare la risposta immunitaria anti-

tumorale. Vari gruppi hanno dimostrato che la crescita tumorale non è inibita dal potente inibitore di CD pepstatina. La pepstatina anche se è un inibitore molto potente nello stato di transizione della CD è tuttavia incapace di attraversare la membrana cellulare. Inoltre l'attività della pepstatina *in vitro* ed *in vivo* è impedita dalla sua scarsa solubilità in acqua. Perciò se si può escludere l'importanza dell'attività enzimatica di CD al di fuori della cellula, rimane la possibilità di un'attivazione specifica dei fattori di crescita all'interno dei lisosomi o endosomi. Sono stati sintetizzati vari coniugati CPNP-pepstatina e saggiati *in vitro* per la loro capacità di inibizione della crescita di cellule MDA-MB-231 del tumore della mammella. Alcuni di questi coniugati mostrano un'alta tossicità, probabilmente susseguente l'inibizione della catepsina D negli endosomi. Uno dei più potenti composti investigati in tal senso è risultato essere JMV4463 (Figura **R.5**). Questo composto è stato ottenuto dalla coniugazione della pepstatina con $AMPA_4$ per la parte che localizza gli endosomi e per la parte responsabile della solubilità ad un derivato del glicol polietilenico e da un residuo di D-arginina. Si è così ottenuto una pepstatina vettorizzata che è allo stesso tempo solubile in acqua. I buoni risultati *in vitro* ottenuti per questo composto ci incoraggiano per i saggi *in vivo* da effettuare nel prossimo futuro. Abbiamo sintetizzato apprezzabili quantità di JMV4463 per poter ottenere sufficiente prodotto per effettuare questi saggi di attività anti-tumorale su ratti.

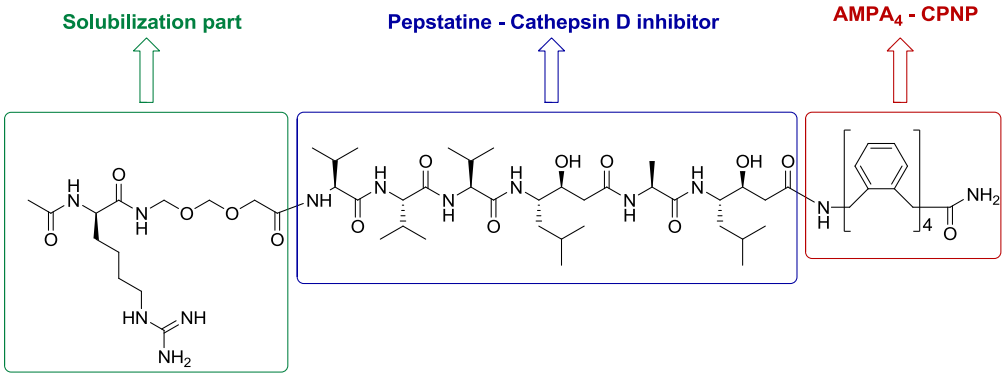

Figura R.5 *Il composto JMV4463 – un composto bioconiugato formato da tre parti. In rosso la parte di CPNP $(AMPA)_4$ sviluppata dal nostro gruppo, in blu il potente inibitore della catepsina D pepstatina ed in verde la parte responsabile della solubilizzazione.*

(1) *Goodman, C. M.; Choi, S.; Shandler, S.; DeGrado, W. F. Nat Chem Biol* ***2007****, 3, 252-62.*

(2) *Raynal, N.; Averlant-Petit, M.-C.; Bergé, G.; Didierjean, C.; Marraud, M.; Duru, C.; Martinez, J.; Amblard, M. Tetrahedron Letters* ***2007****, 48, 1787-1790.*

(3) *Bautista, A. D.; Craig, C. J.; Harker, E. A.; Schepartz, A. Curr Opin Chem Biol* ***2007****, 11, 685-92.*

(4) *Amblard, M., Raynal, N., Averlant-Petit, M. C., Didierjean, C., Calmes, M., Fabre, O., Aubry, A., Marraud, M., and Martinez, J. Tetrahedron Lett.* ***2005****, 46, 3733–3735.*

(5) *Trabulo, S.; Cardoso, A. L.; Mano, M.; de Lima, M. C. P. Pharmaceuticals* ***2010****, 3, 961-993.*

(6) *Sawant, R.; Torchilin, V. Mol Biosyst* ***2010****, 6, 628-40.*

(7) *Futaki, S.; Suzuki, T.; Ohashi, W.; Yagami, T.; Tanaka, S.; Ueda, K.; Sugiura, Y. J Biol Chem* ***2001****, 276, 5836-40.*

(8) ***Lubomir L. Vezenkov,*** *M. M., Jean-Francois Hernandez, Marie-Christine Averlant-Petit,; Olivier Fabre, E. B., Marcel Garcia, Jean Martinez and Muriel Amblard Bioconjugate Chem.* **2010,** *21* (10), 1850-1854.

(9) *Bareford, L. A., and Swaan P. W. Adv. Drug Delivery Rev* ***2007****, 59, 748–758.*

(10) *Burlina, F.; Sagan, S.; Bolbach, G.; Chassaing, G. Angew Chem Int Ed Engl* ***2005****, 44, 4244-7.*

(11) *David Paramelle, G. S.,* ***Lubomir L. Vezenkov****, Marie Maynadier, Christophe Andre,; Christine Enjalbal, M. C., Marcel Garcia, Jean Martinez, and Muriel Amblard. Angew. Chem. Int. Ed.* **2010,** *49* (44), 8240-8243

(12) *Petr Benes, V. V. a. M. F. Crit Rev Oncol Hematol.* ***2008****, 68, 12-28.*

SUMMARY

As a part of a program for foldamer design[1] two β-turn mimetics (3S)-amino-5-(carboxylmethyl)-2,3-dihydro-1,5-benzothiazepin-4(5H)-one or **DBT**[2] and 2-aminomethyl-phenyl-acetic acid or **AMPA** were selected as frameworks from a molecular modeling study for their suitability to adopt helical structure. At first we developed a highly efficient scale up synthesis of the DBT moiety protected by 9-fluorenylmetoxycarbonyl (Fmoc) group. By standard solid phase peptide synthesis (SPPS) we synthesized DBT oligomers of different lenghts and modifications were introduced at their N-terminus. Our first task was to perform structural analysis of the oligomers by NMR and X-Ray. Numerous NOE interactions in the DBT pentamer and hexamer molecules were detected by NMR 2D NOESY experiments. These data strongly suggest the organization of these DBT oligomers. Small crystals were obtained from the same molecules in DMSO but at the time being their size is not important enough for X-Ray crystallography studies. In a parallel study we hypothesized that short oligomers constructed by DBT or AMPA frameworks could translocate the cellular membrane and could be used as new cell penetrating non-peptides - CPNP (see section **I.2.2**).[3,4] Even though these compounds are not charged as most cell penetrating peptides (CPP)[5] or CPNP, we considered that by virtue of their aromaticity, hydrophobicity and their well-organized structure they could have a non-specific interaction with the lipid bilayer and thus be internalized into the cell. Short oligomers were synthesized on Rink amide (RA) resin following SPPS methodology and labelled at their N-terminus with fluorescein isothiocyanate (FITC). At first the cellular uptake of the $(DBT)_{2-4}$ oligomers in MDA-MB-231 breast cancer cells was analyzed by fluorescence emission measurement and compared to the potent and well-studied CPP octa-arginine $(Arg)_8$[6,7] as a positive control and carboxyfluorescein as a negative control. The highest intracellular fluorescence intensity was found for $(DBT)_4$ with a drastic decrease (>4-times) for $(DBT)_3$ and $(DBT)_2$ oligomers.[8] Thus, the cellular uptake appeared length-dependent with an increase of the internalization with the oligomer size. Moreover, the amount of $(DBT)_4$ that was internalized was more significant than that of $(Arg)_8$ despite the fact that it is uncharged. By confocal microscopy we determined that $(DBT)_4$ is mainly localized in the endosomes after 3 hours of incubation and in the lysosomes after 16 hours of incubation. Altogether, these data indicate the ability of these oligomers to target the endolysosomal pathway. Although most of the initial drug delivery studies aimed to avoid lysosomal addressing to prevent subsequent drug degradation, more recent studies demonstrated the relevant clinical utility to target this compartment for drug delivery in the treatment of lysosomal storage diseases, Alzheimer's disease, and cancer.[9]

While analyzing the internalization efficiency of our CPNP we decided to straightforward evaluate their concentration inside the cells. We studied our compounds internalization by total fluorescence emission measurement and by confocal microscopy (see sections **I.2.3**) but none of these techniques gave us the possibility to determine the exact amount of compound internalized per cell. A study reported by Burlina et al.[10] brought a great improvement in proposing a highly reproducible quantification method based on MALDI-TOF MS to measure the concentration of the internalized peptides. However, after cell lysis, this method

requires the capture of the biotin-labelled CPP by streptavidin coated magnetic beads. This step is particularly critical for the accuracy of the quantification. This is the reason why we decided to develop a new general methodology based on MALDI-TOF mass spectrometry (MS) which does not require any purification or separation steps. We studied the internalization of CPP/CPNP compounds by using an UV light-absorbing tag α-cyano-4-hydroxycinnamic acid (HCCA) and preparing the samples in a neutral matrix such as α-cyano-4-hydroxycinnamic methyl ester (HCCE). This combination (HCCA tag and HCCE matrix) enabled us to discriminate MS signals induced by peptides of interest that were present in low concentration from those of unlabelled more abundant peptides. By addition of a precise amount of deuterated-HCCA-tagged CPP/CPNP prior the MALDI TOF MS experiment, the internalized CPP/CPNP could be quantified on the basis of the ratio between the $[M+H]^+$ peaks of the deuterated and nondeuterated HCCA-tagged CPP.[11]

Another direction for research was to synthesize bioconjugates between our newly discovered CPNP and some biologically active compounds that are unable to cross the cell membrane. We selected pepstatine which is a powerful transition state inhibitor of the Cathepsin D (CD). Pepstatine while a very potent inhibitor of the CD is unable to cross the cellular membrane. Moreover pepstatine activity *in vitro* or *in vivo* is hampered by its poor solubility in water. CD is a soluble lysosomal aspartic endopeptidase synthesized in rough endoplasmic reticulum as preprocathepsin D (pCD).[12] Upon entering the acidic endosomal and lysosomal compartments proteolytic cleavages of the pCD result in the formation of the active enzymatic form of CD. Under normal physiological conditions pCD is sorted to the lysosomes and found intracellularly but in some pathological and physiological conditions like cancer pCD/CD escape the normal targeting mechanism and is secreted from the cell. Once secreted to the outside, pCD can be endocytosed via M6PR or yet unknown receptor by both cancer cells and fibroblasts. The endocytosed pCD undergoes maturation into the enzymatically active CD. An enzymatic activity of CD outside of the cell or inside the endosomes could be responsible for the activation of several growth factors and growth factor receptors. Several groups have proven that the tumour growth is not inhibited by the powerful CD inhibitor pepstatine. These results exclude the importance of the CD enzymatic activity outside of the cell but as already mentioned pepstatine is unable to penetrate into the cell thus CD activation of growth factors inside the endosomes or the lysosomes is still a possibility. Different CPNP-Pepstatine conjugates were synthesized and tested *in vitro* for their ability to inhibit MDA-MB-231 breast cancer cells growth. Some of these conjugates showed high cytotoxicity, probably via a Cathepsin D inhibition in the endosomes or the lysosomes. One of the most potent tested compounds was JMV4463. This compound was obtained by the conjugation of pepstatine with a CPNP as delivery system ($AMPA_4$) and with solubilizing moiety composed of polyethylene glycol and D-Arginine residue. The good *in vitro* results obtained with the vectorized pepstatine encouraged us to perform *in vivo* tests. We performed scale up synthesis of JMV4463 in order to obtain enough product for anti-cancer activity on mice in the near future.

RESUME

Le passage des médicaments à travers la membrane cellulaire représente souvent une limitation majeur dans un grand nombre de thérapies (anti-cancéreuse, anti-virale par exemple). Des peptides vecteurs connus comme les CPPs (cell penetrating peptides) ont été utilisés avec succès pour introduire à l'intérieur des cellules diverses molécules (protéines, peptides, siRNA, quantum dots) et présentent un fort potentiel dans l'adressage de médicaments. Parmi les différents CPPs décrits dans la littérature la plupart sont des peptides basiques ou amphiphiles.

Nous nous sommes intéressés à l'utilisation d'oligomères non chargés construits à partir de motifs contraints mimes de dipeptides comme vecteurs de pénétration cellulaire. L'internalisation cellulaire et leur localisation ont été établies à l'aide de dérivés fluorescents par microscopie confocale. L'étude de pénétration cellulaire par mesure de fluorescence a montré que des oligomères de (3*S*)-amino-5-carbonylméthyl-2,3-dihydro-1,5-benzothiazépine-4(5H)-one] (DBT) sont aussi puissants que les oligomères d'arginine (oligoArg), vecteurs de référence. Par microscopie confocale nous avons montré que ces composés sont internalisés dans les lysosomes. L'efficacité d'internalisation de nos composés a été confirmé par une méthode de quantification par spectrométrie de masse MALDI-TOF développée dans notre groupe. Cette méthode repose sur l'utilisation conjointe d'un marqueur UV-absorbant dérivé de l'acide α-cyano-4-hydoxycinnamique (HCCA) et d'une matrice MALDI adaptée. Un effet important de discrimination spectrale est obtenu, permettant une amplification du signal de la molécule d'intérêt dans un mélange complexe. Ainsi les faibles concentrations internalisées peuvent être détectées. Grace á cette technique et l'utilisation d'un étalon deutéré, nous avons caclulé la concentration intracellulaire de deux CPP de référence l'octa-arginine et la pénétratine. Nous avons aussi étudier l'internalization de petits oligomères construits à partir d'acide 2-aminométhyl-phényl-acétique (AMPA). Par microscopie confocal nous avons constaté que ces petits oligomers sont internalisés par voie endo-lysosomale.

L'efficacité de la pénétration cellulaire de ces petits oligomères aromatiques (oligoAMPA et oligoDBT) offre une nouvelle classe de vecteurs qui ont la particularité d'être non-cationiques et hydrophobes. De tels composés pourraient être utilisés pour la délivrance de médicaments dans le traitment des maladies comme le cancer, les maladies lysosomales ou la maladie d'Alzheimer.

Afin de montrer que cette nouvelle classe de vecteurs est capable d'internaliser des composés biologiquement actifs, nous les avons associé á un inhibiteur puissant de la Cathepsine D (CD) – la pepstatine. CD est une endopeptidase lysosomale qui dans des conditions normales est localisée dans les endosomes et les lysosomes. Pour cerains cancers, la CD est sur-exprimée et secrétée à l'exterieur de la cellule. La CD est problement impliquée dans la prolifération des cellules cancéreuses par l'activation de certains facteurs de croissances dans les endosomes. La pepstatine est une inhibiteur puissant de la CD. Cependant son efficacité thérapeutique potentielle est limitée par une faible capacité de pénétration des membranes cellulaires et une faible solubilité nécessitant de fortes doses pour l'inactivation de la CD *in vitro* et *in vivo*. Afin d'améliorer son

efficacité et sa biodisponibilité, des conjugués de la pepstatine avec nos vecteurs de pénétration cellulaire, oligo $(AMPA)_4$ et $(DBT)_4$, et une partie solubilisante ont été développés. Certains de ces bioconjugués ont montré une toxicité élevée (IC_{50} = 2.10^{-6}) *in vitro* sur différentes lignées cellulaires tumorales. Des tests *in vivo* sur des souris sont prévus pour le futur.

I. INTRODUCTION

My thesis work was performed in a close collaboration between the laboratories of 'Institut des Biomolécules Max Mousseron UMR 5247 Université Montpellier 1- France' and the 'Dipartimento delle Scienze Biologiche, C.I.R.Pe.B, Università Federico II di Napoli, Istituto di Biostrutture e Bioimmagini CNR' and the 'IRCM, Université Montpellier 1'. The main research topics of my project were the fields of the foldamers and cell penetrating compounds. These two fields emerged about the same time two decades ago and are becoming increasingly important and studied in the beginning of this decade.

I.1. Foldamers

I.1.1. Foldamers structure

In their attempt to mimic the natural folding of proteins, DNA and other natural molecules by smaller but yet stable non-natural oligomers, the researchers have developed the foldamers. Foldamers by definition are artificial oligomers with well-defined structure (for extensive reviews see [4],[13]). Pioneer work in this field was set by the groups of Gellman[14] and Seebach[15] who used β-amino acids as templates for well-structured oligomers in solution and in crystalline solid state. The development in the field was highlighted by the review 'Foldamers a Manifesto' by Gellman.[16] During the last 15 years a lot of different foldamers have been constructed and characterized based on different frameworks that were oligomerized.[4] The selection of the frameworks was often affected by the ease of the synthesis and the characterization of the oligomers. The interactions that define the secondary structure of the foldamers are similar to those of the proteins – H bonding, intrinsic conformational preference of the backbone, dispersion interactions, polar interactions and solvation. At the same time these unnatural oligomers are able to adopt organized structure for a lot shorter sequences than the natural proteins and peptides. Molecular modelling is often used to predict the possible conformations and most of the foldamers have been characterized by X-Ray crystallography, nuclear magnetic resonance (NMR) and circular dichroism investigations. Generally we can separate the foldamers in two categories depending on the presence or not of aromatic unit within the framework moiety:

-Aliphatic frameworks - examples of this group include the β-peptides[17], γ-peptides[18] and δ-peptides[19], mixed α/β peptides[20], oligoureas[21], azapeptides[22], pyrolinones[23], α-aminoxy-peptides[24] and peptoids[25] (Figure **I.1.1-1**). Between these foldamers the β-peptides are the most extensively studied. The different frameworks gave rise to different well defined secondary structures like helices and beta-sheets.[17b]

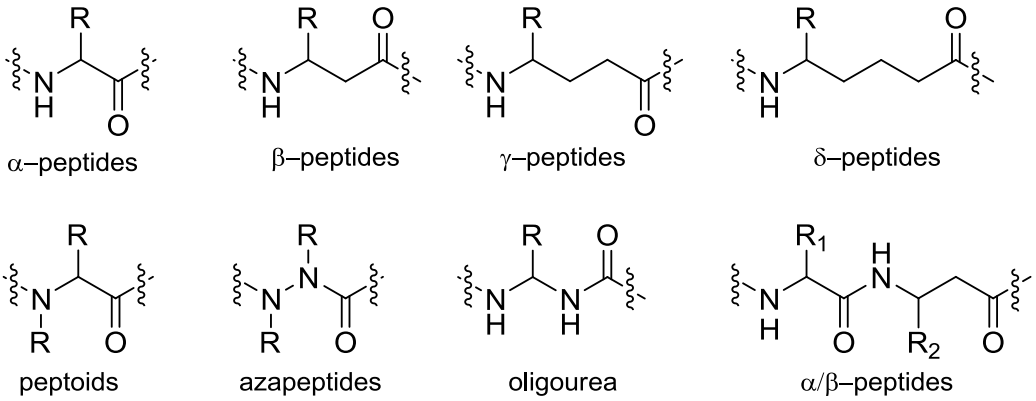

Figure I.1.1-1 *Examples for aliphatic foldamers*

-Aromatic frameworks - the same factors that govern the folding of the aliphatic oligomers are important for the aromatic foldamers but in this case the π-π stacking and the geometric constraints are also crucial.[4],[26] For this type of molecules the non-covalent interactions that define the secondary structures are often more local compared to those of the aliphatic foldamers. Usually the interactions are between consecutive units, fact that makes them easier to predict. Notable examples in the field are the works of Huc group on quinoline[27] and pyridin-derivated[28] oligoamides. Gong group have also designed and characterized oligoamide aromatic foldamers stabilized by a set of three-center intramolecular H-bonds.[29] Hamilton and coworkers constructed foldamers based on terphenyl.[30] Amblard and coworkers designed foldamers composed of 2-aminomethyl-phenyl-acetic acid (AMPA) (Figure **I.1.1-2**).[1]

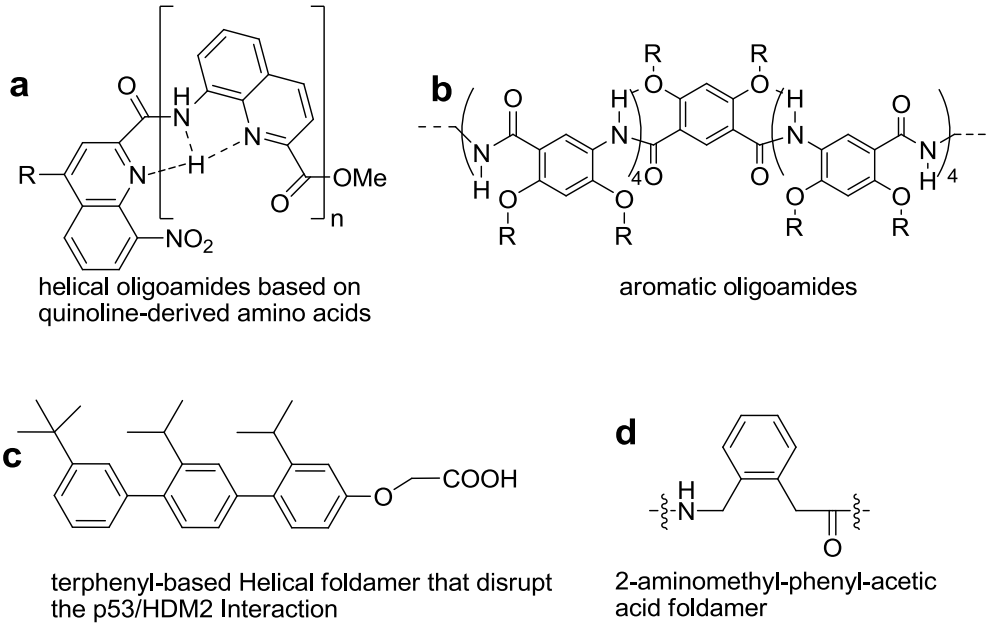

Figure I.1.1-2 *Examples for aromatic foldamers* ***a)*** *quinoline based foldamer[27],* ***b)*** *oligoamide foldamer stabilized by three-center intramolecular H-bonds[29],* ***c)*** *terphneyl foldamer[30],* ***d)*** *foldamer constructed from 2-aminomethyl-phenyl-acetic acid[1] (AMPA)*

I.1.2. Foldamers function

While the studies on foldamers were, at the beginning, more often driven by the understanding of the factors that govern their folding later, some foldamers were also developed with very interesting biological properties.[4],[13] The foldamers have many advantages over the natural peptides and the proteins. They are generally more stable to enzymatic degradation and they require fewer monomeric units to adopt an organized secondary structure, so they could be used as smaller more stable mimetics of the natural oligomers. This was very well illustrated by downsizing the natural host defense antimicrobial peptide Magainin[31] from 2000-3000 Da to 1000-2000 Da for the β-peptide analogues, 1000 Da for the arylamide antimicrobial foldamers[32] and to around 500 Da for the phenylalkylnyl-based antimicrobial compound[33] (Figure **I.1.2**).

By virtue of their well-defined structure, the relationships between sequence and structure in the foldamers scaffolds are predictable. Therefore, they constitute privileged structures to distribute functional groups according to a specific three-dimensional arrangement. Consequently they provide especially relevant tools for the design of miniature α-helical mimetics able to block specific protein-protein interactions by mimeting protein-binding domains. In this field, Hamilton and coworkers constructed terphenyl backbone foldamer that mimics the distribution of side chains at positions i,i+4 and i+7 on one face of an α-helix.[30] They used this template to successfully mimic the BH3 pro-apoptotic helix from Bak and to disrupt the Bak-Bcl-x_L interaction.[34] In more recent studies the same group developed terphenyl-based helical mimetics that disrupt the p53/HDM2 interaction.[30] In a similar study Gellman et al. designed a chimeric α/β-peptide that binds to the Bcl-x_L with an affinity of around 1nM that competes the tightest-binding BH3-derived α-peptides.[35] Later the same group reported a new more resistant to proteases α/β-peptide with similar activity obtained by sequence based design.[36] In a recent work, they reported the co-crystallization of mixed α/β-peptide with the anti-apoptotic Bcl-x_L.[37] These peptides could be used eventually as anti-cancer drugs because they could induce apoptosis in the cancer cells via their binding with the anti-apoptotic Bcl-x_L.

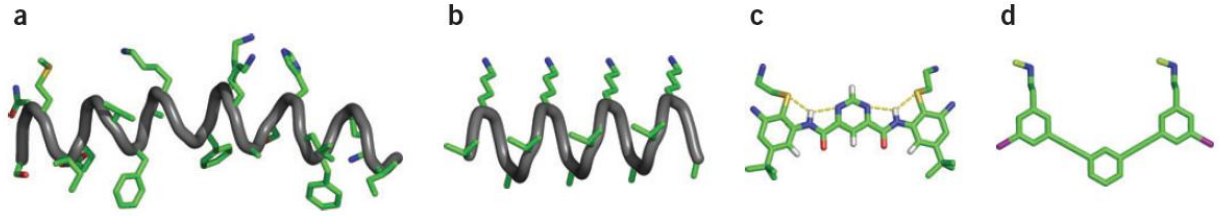

Figure I.1.2 a) *Natural antimicrobial peptide magainin,* ***b)*** *β-peptide analogue of the magainin,* ***c)*** *arylamide analogue of the magainin,* ***d)*** *phenylalkylnyl-based analogue of the magainin.*

One of the very interesting applications of the foldamers is to use them as scaffolds for the synthesis of cell penetrating non-peptides or CPNP. As this point is of particular interest for our work, it will be discussed separately in the next chapter.

I.2 CPP – Cell Penetratin Peptides and CPNP – Cell Penetrating Non Peptides

I.2.1 Cell Penetrating Peptides

One of the major biological barriers for the drug delivery is the hydrophobic cell membrane. Only a few molecules that fit within a certain size range, polarity and charge are able to cross the cell membrane. At the same time a lot of potentially very powerful drugs like peptides, proteins and recently short interfering RNA (SiRNA) are unable to translocate the lipid bi-layer because of their size and charge. One of the possible ways to overcome this problem is to use the so called cell penetrating peptides or CPP. Since two decades ago, these 'Trojan horse' molecules have emerged as promising tools for delivery of large set of cargos of different types and sizes (for recent reviews see[5],[3],[38],[39]). One of the first examples for CPPs is the polycationic, arginine rich TAT peptide (TATp), derived from the 86-mer trans-activating transcriptional activator (TAT) protein encoded by human immunodeficiency virus type 1 (HIV-1).[40] TATp sequence is **YGRKKRRQRRR**. In another pioneer work, Prochiantz and coworkers have discovered the amphipathic penetratin derived from the homeodomain of Drosophila Antennapedia.[41] Penetratin sequence is **RQIKIWFQNRRMKWKK**. The oligoarginines **Arg_8** or **Arg_9** derived from the polycationic TAT peptide were discovered by the groups of Wender and Futaki.[7],[6] These synthetic peptides exhibited often a better uptake than TATp and penetratine. All these CPP were cationic and/or amphipathic peptides. The internalization pathway or combination of pathways for the CPP is very controversial and results vary from one study to another. The interaction with the charged anionic molecules of the cellular membrane seems to be very important.[42] Divalent hydrogen binding between the guanidino moiety of the arginine and the phosphates, sulphates and carboxylates (Figure **I.2.1-1**) is reported as one of the driving forces of the internalization. Indeed, binding of these permeating peptides to cell surface proteoglycans could promote the interaction of the CPPs with the cellular membranes, facilitating the subsequent interactions necessary for the translocation process; in an alternative scenario, this same binding step could induce by itself certain endocytotic mechanisms, leading to CPP internalization.

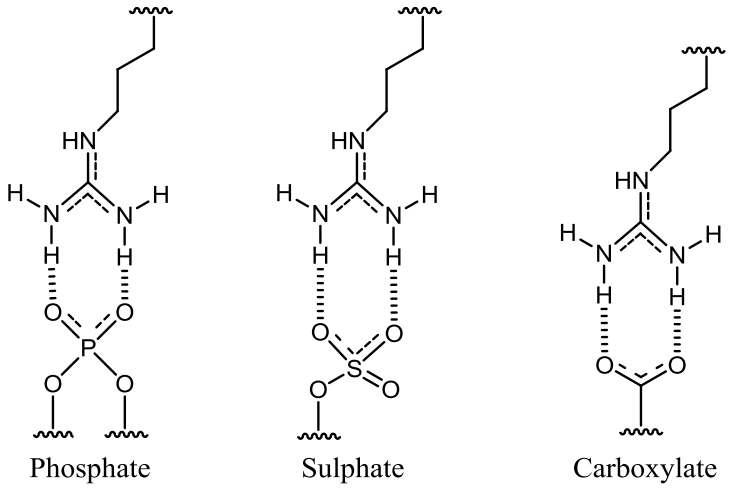

Figure I.2.1-1 *Strong divalent hydrogen bonds could be formed by side-chain guanidino moiety of arginine with phosphates, sulfates, and carboxylates of the cell membrane*

Different paths of internalization have been observed depending on the type of CPP, their concentration, the type of the cell line, the cargo attached to the CPP, and even the counter ion of the cationic residues.[38] The major pathways seem to be either energy dependent endocytosis or energy independent direct internalization. The possible endocytotic pathways reported in the literature are the caveola mediated endocytosis, macropinocytosis and clathrin-mediated endocytosis.[3] The proposed mechanisms for direct translocation are the torodial pore, barrel stave pore, inverted micelle and carpet model.[3] The internalization pathway for most of the CPP seems to be a combination of two or more of these mechanisms. For example the oligoarginine is reported to penetrate cells at 4°C and at 37°C which suggests a mixture between energy dependent and energy independent internalizations.[43] CPPs conjugated to small cargos seem more able to penetrate via the direct internalization mechanisms while big cargos are internalized mainly via endocytosis. Generally there are two approaches for the internalization of drugs by CPP/CPNP (Figure **I.2.1-2**):

- The covalent strategy in which the drug is covalently linked to the CPP. Following this strategy have been internalized small molecules[44], peptides and proteins[45], PNA and PMO[39], imaging agents[46] and so on.

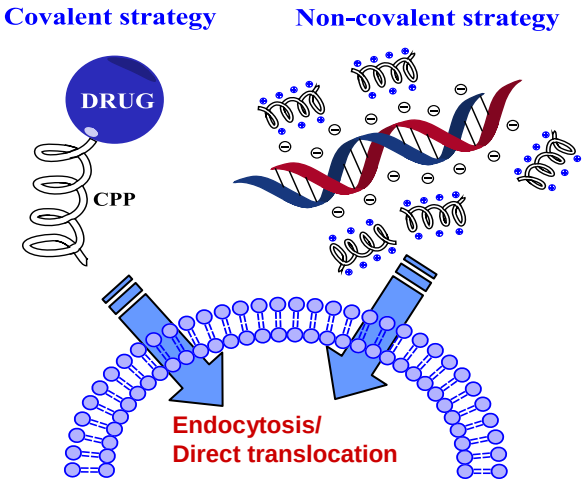

Figure I.2.1-2 *Strategies for internalization of drugs by CPP/CPNP*

- The non-covalent strategy in which the usually anionic drug (SiRNA or DNA) is complexed by the cationic CPP.[5] Cholesterol coupled to polyarginine[47], the chimeric peptide MPG[48] and many others have been successfully used for the internalization of SiRNA or DNA. This strategy is also applied for the internalization of nanoparticles.[5] A small dogma in the field is that all CPPs are charged cationic compounds. In fact hydrophobic segments from protein signal sequences or membrane translocating sequences (MTS)[49], as well as non-charged polyproline[50] peptides were described as effective cell membrane transporters. Recently Futaki et al.[51] reported a small hydrophobic sequence **PFVYLI** that successfully translocated cargos across the cell membrane. While most of the work in the field is directed to charged poly-cationic peptides we should note that for the internalization of CPP or CPNP an interaction with the cell membrane is crucial. While this interaction is often electrostatic at first, we should not exclude the possibility of hydrophobic interactions with the lipid rafts or other parts of the membrane to induce internalization. Some toxicity effects are linked to the administration of high doses of poly-cationic

compounds[52] thus the development of non-charged vectors is of considerable interest.

I.2.2 Cell Penetrating Non-Peptides

As we previously described, foldamers are very interesting framework for CPNP because of their small size, resistance to protease degradation and well defined structure. Seebach and coworkers performed experiment with polycationic β-peptides[53] and obtained similar results to those of polycationic α-peptides but with compounds that were resistant to enzyme degradation. Wender and coworkers reported a polycationic peptoid[54] and recently an oligocarbonate molecular transporter[55] obtained by ring opening oligomerization. Chmielewski and coworkers[56] described hydroxyproline oligomers bearing precisely arrayed hydrophobic and cationic appendages that were internalized in some cases 35 times better than the TATp. The principal drawback of these molecules is their difficult synthesis. Gellman and coworkers designed amphipathic β-peptides that internalized into cells at concentration of 8 μM.[57] Further studies revealed an endocytotic pathway of internalization.

Recently some CPNPs that differ significantly from peptides were developed. Huc group designed aromatic amide foldamers functionalized with peripheral cationic side chains that delivered FITC to HeLa cells[58] with an efficiency similar to TATp. In one of the most interesting studies to date, Selwood and coworkers[59] reported the so called SMoC (small molecule carrier) (Figure **I.2.2-1**). This compound is comprised of a biphenyl core functionalized with 4 guanidinium groups in an arrangement that mimics the display of side chains of an α-helix. SMoC was able to mediate dyes and recombinant proteins into a variety of cell lines with efficiency similar to that of TATp. By using 4G-SMoC the 23.5 kDa DNA replication suppressor gaminin was successfully delivered to human fibroblast. 4G-SMoC-gaminin effectively suppressed DNA synthesis in NIH-3T3, WI-38 HDF, HeLa S3 adenocarcinoma cells, and MOLT-4 leukemic lymphoblasts *in vitro*. One should note that this powerful CPNP is only about 600 Da making it one of the smallest known cell penetrating compounds. The high density of the guanidinium charges and the hydrophobicity of the two phenyl rings seem very important for its internalization.

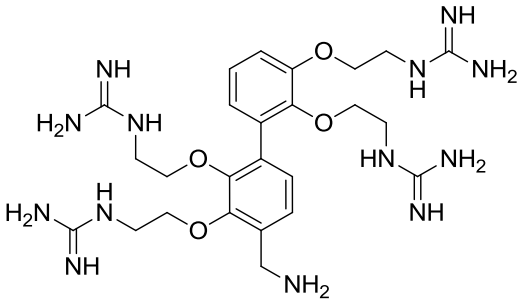

Figure I.2.2-1 *SMoC vector*

As in the case of the CPP, not all CPNP are charged compounds. While studding the enzymology and biochemistry of the protein palmitoylation Stefan et al. discovered a small cell penetrating non-charged lypo-peptide[60] (Figure **I.2.2-2**) that was internalized by Jurkat lymphocytes. In a very elegant study Simons and coworkers have vectorized a potent transition state inhibitor of the β-secretase cleavage of β-amyloid precursor protein and thus stopped the β-amyloid peptide

production.[61] The inhibitor was inactive *in vitro* because of its inability to reach the endosomes where the β-secretase enzyme is the most effective. To confront this problem the authors have linked the inhibitor to a sterol moiety (Figure **I.2.2-2**) via a polyethylene glycol linker. This bioconjugate was internalized and localized in the endosomes supposedly via an interaction with the lipid rafts and subsequent endocytosis. The sterol linked inhibitor was able to inhibit the β-secretase enzyme activity at very low concentration of 200 nM *in vitro* and also increased the survival rate of triple transgenic Drosophila expressing human wild type β-amyloid peptide.

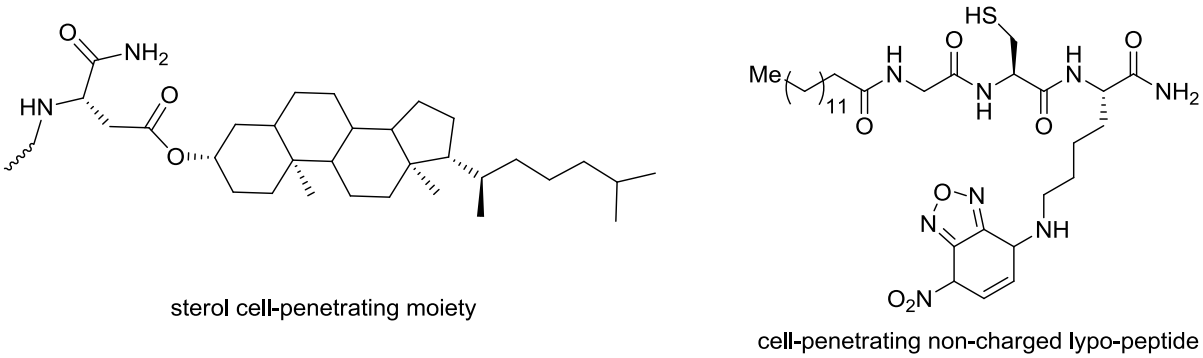

Figure I.2.2-2 *Different non-charged CPNP*

I.2.3 Determination of the intracellular concentration of CPP/CPNP

Different methods for detection of CPP and CPNP inside the cell have been developed each of them with its distinctive advantages and drawbacks. As none of these methods is perfect the development of new ones is of considerable scientific interest.

Total fluorescence emission measurement (TFEM)

In this experiment cells are first incubated with fluorescently labelled compound for a certain time (Figure **I.2.3-1**). A first washing is performed to take away the residual non-internalized compound.

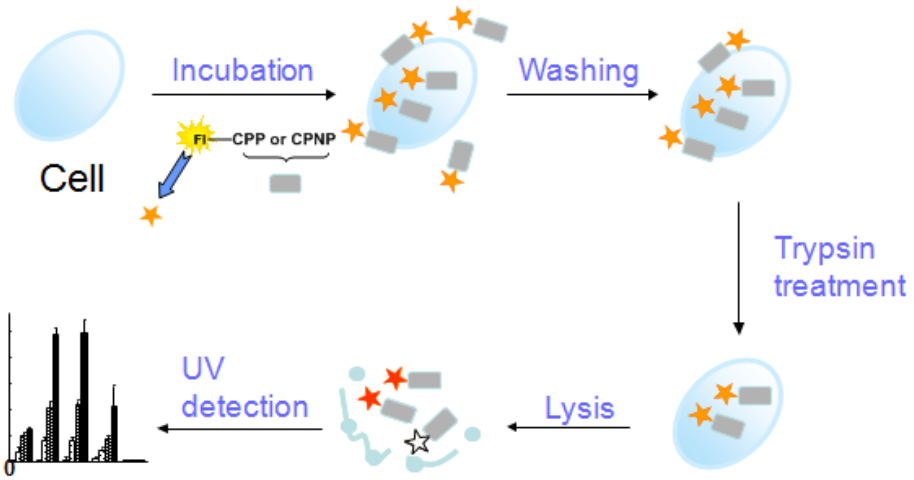

Figure I.2.3-1 *Basics of total fluorescence emission measurement*

After that, a trypsin treatment is performed in order to digest the cell membrane-adsorbed cell-penetrating compounds.[62] After this treatment, cell lysis is performed.

The obtained media is irradiated with UV light. Then estimation of the internalized compound could be made by detection of the UV emission of the fluorescent tag. The drawback of this technique is that it is relevant only when CPPs are compared to another one in the same experimental conditions because no accurate estimation of the intracellular concentration could be made. Another problem is the fact that some times CPPs or CPNPs are not effectively removed by the washing steps thus some residual fluorescence from non-internalized compounds is detected.

Fluorescence-activated cell sorting

One of the standard procedures for detection of a fluorescently labelled CPP and CPNP inside the cells is the fluorescence-activated cell sorting or FACS. FACS is a specialized type of flow cytometry that provides a method for sorting a heterogeneous mixture of biological cells into two or more containers, one cell at a time, based upon the specific light scattering and fluorescent characteristics of each cell.[63] It is a useful scientific instrument, as it provides fast, objective and quantitative recording of fluorescent signals from individual cells as well as physical separation of cells of particular interest. The advantage of FACS is that it allows separating different population of cells depending on the quantity of internalized fluorescently labelled compound. This methodology has the same disadvantages as the total fluorescence measurement.

Confocal microscopy

Confocal microscopy is an optical imaging technique used to increase optical resolution and contrast of a micrograph by using point illumination and a spatial pinhole to eliminate out-of-focus light in specimens that are thicker than the focal plane.[64] Plane images of cells incubated with fluorescently labelled compounds could be obtained by this technique. Prior to internalization experiment, cells could be incubated with markers for different organelles so that the exact localization of CPP/CPNP inside the cell could later be determined (Figure **I.2.3-2**).

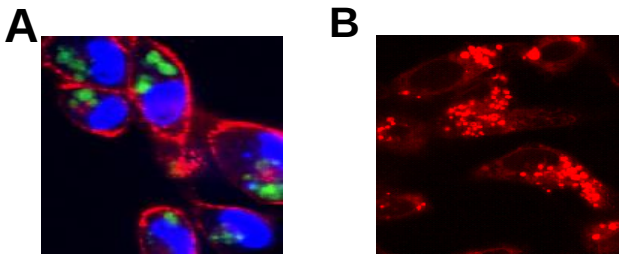

Figure I.2.3-2 *Examples of confocal images of cells incubated with markers for:* ***A)*** *the cell membrane (red) and nucleus (blue)* ***B)*** *the lysosomes (red).*

This technique is very useful in a combination with the previous two mentioned (FACS and TFEM) because it could answer the question if the compound is really internalized inside the cell or just attached to the membrane. However, as the previously described techniques, it cannot give an accurate quantification of the internalized compound.

MALDI TOF MS techniques for the accurate calculation of the intracellular concentration of CPP or CPNP

All the previously mentioned methods for detection are unable to give an accurate calculation of the intracellular concentration of CPP/CPNP. To resolve this problem Burlina and al. have developed a highly reproducible quantification method based on MALDI-TOF mass spectrometry.[10] In this method cells are incubated with biotin-labelled CPP in a similar way as in the case of the TFEM. After washing steps a cell lysis is performed and the biotin-labelled CPPs are captured by streptavidin coated beads. The beads are washed and a known amount of deuterated biotin labelled CPP (D-CPP) is added. After that the beads are analyzed by MALDI-TOF MS. The peaks of the $[M+H]^+$ deuterated and non-deuterated CPP are integrated and by their ratio the intracellular concentration could be determined with very good precision.

The step of biotin-labelled CPP capture from streptavidin is critical for the accuracy of the quantification. Indeed the lysate could contain molecules that may hamper the CPP capture by the streptavidin coated beads. The development of a similar method but devoid of any separation procedure is of considerable practical interest.

I.2.4 CPP/CPNP-Drug bioconjugate intracellular localization

As we have already discussed a lot of effort has been put in the design of potent CPP or CPNP vectors. Even more important than the intracellular concentration of the vector is its compartmentalization inside the cell. Anti-cancer drugs should often be delivered to the cytosol or the nucleus.[44] SiRNA should be delivered to the RISC apparatus in the cytosol[65], DNA strands to the nucleus. For a lot of these drugs, once internalized endosomal escape is very important thus different techniques have been developed to avoid the endosomal entrapment. Nuclear and cytosol localization sequences have been designed to help the drug reach its specific destination.[48]

At the same time very interesting targets are located in the endosomes as the already mentioned β-secretase enzyme responsible for the Alzheimer's disease.[61] Another target inside the endosomes of the cancer cells is the Cathepsin D enzyme. As this enzyme was a prime target for our group we will discuss its implication in cancer development in more detail in the next chapter.

I.3 Cathepsin D

Cathepsin D (CD) is a soluble lysosomal aspartic endopeptidase synthesized in rough endoplasmic reticulum as preprocathepsin D (pCD).[12] pCD is a glycoprotein with two N-linked oligosaccharides (mannose-6-phosphate lysosomal localization signals) that is targeted to the intracellular vesicular structures (lysosomes, endosomes, phagosomes)

Upon entering the acidic endosomal and lysosomal compartments proteolytic cleavages of the pCD result in the formation of the active enzymatic form CD. Under normal physiological conditions pCD is sorted to the lysosomes and found intracellularly but in some pathological and physiological conditions like cancer pCD/CD escape the normal targeting mechanism and is secreted from the cell. Once

secreted to the outside pCD can be endocytosed via M6PR or yet unknown receptor by both cancer cells and fibroblasts. Once endocytosed, pCD undergoes maturation into the enzymatically active CD. CD has been studied mainly for its implication in cancer development and is subjected as an independent tumor marker.

I.3.1 Cathepsin D and Cancer

Numerous studies clearly demonstrate that pCD secreted from cancer cells serve as an autocrine factor for cell growth of breast cancer and other types of cancer such as lung cancer.[12] Breast cancer cells with down-regulated expression of pCD by antisense gene transfer displayed reduced growth *in vivo* and *in vitro.*[66] Similar results were obtained after incubation with pCD anti-bodies.[67] The exact implication of CD on the cancer growth is much debated and is still an object of study. There are two predominant theories for the CD action on cancer proliferation. One is that the effect is dependent on the enzymatic activity of the CD and the other one is that the mitogenic activity is independent of the enzymatic activity. The exact mechanism of action of the over-expressed CD in cancer cells is probably a combination of both.

Cathepsin D enzymatic related effect on mitogenic activity

An enzymatic activity of CD could be responsible for the activation of several growth factors and growth factor receptors.[68] Moreover it is possible that CD is responsible for the degradation of the extracellular matrix. CD digests various chemokines and may thus attenuate anti-tumor immune response. Several groups have proven that the tumor growth is not inhibited by the powerful CD inhibitor pepstatine A (Figure **I.3.1**).[69]

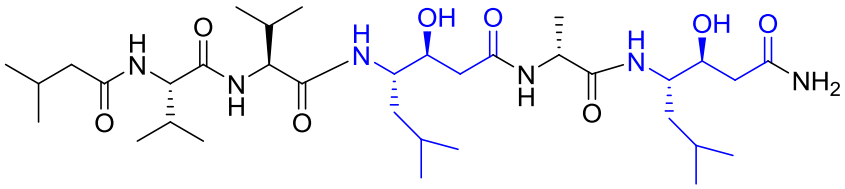

Figure I.3.1.*Pepstatine A – an 7 nM inhibitor of the Cathepsin D.*[70] *Pepstatine is unable to cross the cell membrane and is ineffective in vitro or in vivo. Statine crucial residues for inhibitory activity are shown in blue.*

Pepstatine while a very potent transition state inhibitor of the CD (IC_{50} = 7nM) has a low ability to cross the cellular membrane.[70] Moreover pepstatine activity *in vitro* or *in vivo* is hampered by its poor solubility in water. So if we could exclude the importance of the CD enzymatic activity outside of the cell a specific activation of growth factors inside the endosomes is still a possibility. Synthesis of pepstatine conjugated to CPP or CPNP for better internalization is of considerable interest because it allows us to study the importance of CD inhibition inside the cell and its implication on cancer growth. The CPP or CPNP used for this experiment should deliver the cargo preferably to the endosomes and lysosomes where the CD enzymatic activity is the most important. A pepstatine-CPP or pepstatine-CPNP conjugate could be an interesting anti-breast cancer drug candidate.

Pro Cathepsin D non-enzymatic related mitogenic activity

Some studies have shown that the treatment of cancer cell with enzymatically inactive pCD mutant has the same effect as the treatment with the wild type CD. This research suggests that a non-enzymatic effect of the pCD might also be important for the cell proliferation.[71] The exact mechanism of the pCD mitogenic effect remains unclear. Some scientific groups have shown that pCD binds to the surface of breast cancer cells.[71] Thus an interaction with an unknown cell receptor with signalling properties could be responsible for the increased cells proliferation.

I.3.2 Assay for CD enzyme activity

To measure CD enzymatic activity we used protocol reported by Erikson and coworkers.[72] They used fluorogenic peptide substrate of CD which contains fluorophore and quencher groups in the same molecule. The fluorescent signal in the uncleaved substrate is quenched due to resonance energy transfer between the fluorophore and the quencher groups. In this case EDANS (5-[(2-aminoethyl)amino]naphthalene-1-sulfonic acid) and DABCYL (4-(4-dimethylaminophenylazo) benzoic acid) were respectively the fluorophore and the quencher (Figure **I.3.2**).

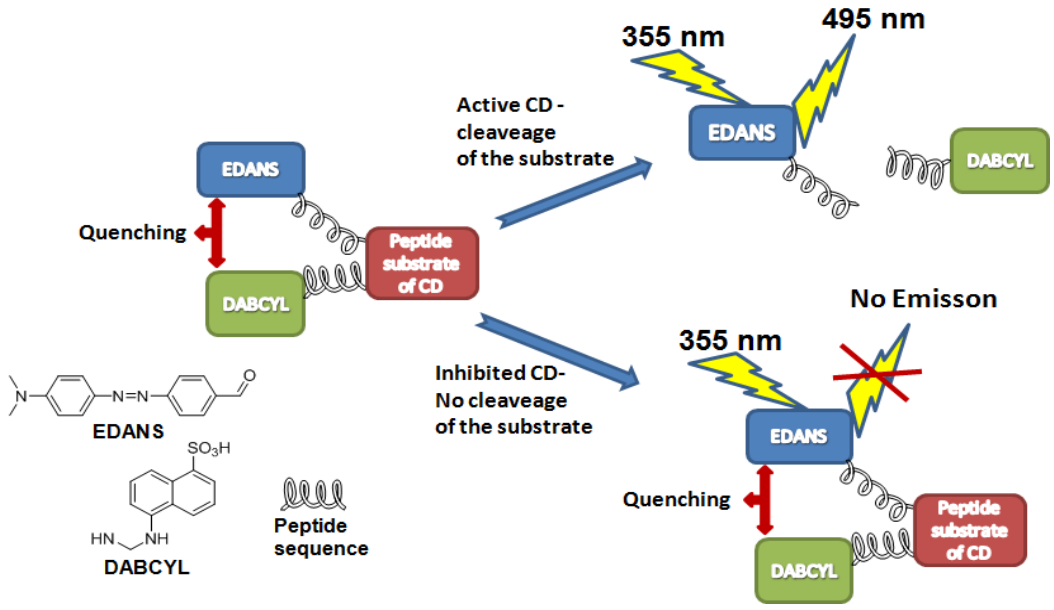

Figure I.3.2 *Test for enzymatic activity of the CD based on fluorogenic peptide substrate*

This donor-acceptor pair is characterized by a number of advantages such as the extremely good spectral overlap of EDANS emission with the strong absorption band of DABCYL, good quantum yield, stability against photobleaching and Stokes shift of over 100 nm for EDANS. Here we used the quenched fluorescent synthetic peptide substrate EDANS–CO–CH_2–CH_2–CO–Arg-pro-Ile-Phe-Phe-Arg-leu-Gln–DABCYL–OH with a cleavage site of Phe-Phe, previously described by Baechle and collaborators to be specific of CD.[73] When CD is activated the cleavage site of Phe-Phe is degraded, the fluorescent probe is free from the quencher and thus fluorescence is emitted. On the opposite when CD is inhibited there is no cleavage of the fluorogenic peptide substrate and thus no fluorescence emission. By this method the residual activity of the CD after incubation with an inhibitor at certain concentration could be measured.

II. PROJECT AIMS

As a part of a program for foldamer design, oligomers composed from different β-turn mimetics were constructed in-silico and tested by molecular dynamics for their ability to adopt organized structure.[1] Among the different motifs selected by this program, two dipeptide mimetics, (3*S*)-amino-5-(carbonylmethyl)-2,3-dihydro-1,5-benzothiazepin-4(5H)-one or **DBT**[2] and 2-aminomethyl-phenyl-acetic acid or **AMPA**[1] (Figure **II.1**), were selected as frameworks for their suitability to adopt helical structure. Our first task was to develop a highly efficient scale up synthesis of these two moieties protected by Fmoc group onto their amino function. Next these Fmoc protected unnatural aminoacids were used to construct, via standard solid phase peptide synthesis (SPPS), oligomers of different lengths and modifications introduced at their N-terminus. We planned to study the structure of these oligomers by NMR, circular dichroism and X-Ray crystallography. Such organized oligomers could be used for inhibition of protein-protein interactions or as frameworks for antibiotics and CPNP.

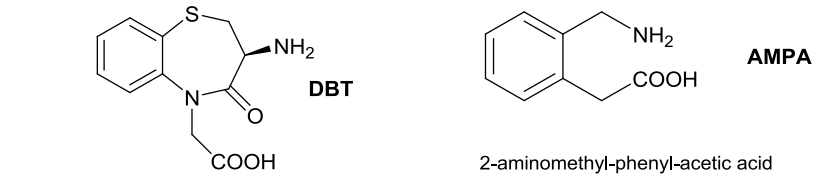

Figure II.1. *(3S)-amino-5-(carboxylmethyl)-2,3-dihydro-1,5-benzothiazepin-4(5H)-one or* ***DBT*** *and 2-aminomethyl-phenyl-acetic acid or* ***AMPA*** *structures*

In a parallel study we hypothesized that short oligomers constructed by DBT or AMPA moieties could translocate the cellular membrane and be used as a new class of CPNP (see section **I.2.2**). Oligomers from different size were synthesized and marked by a fluorescent dye. Our discovery that AMPA tetramers and especially DBT tetramers are potent CPNP that are able to transport fluorescent dyes with high efficiency encouraged us to further investigate their biological activities and set new aims to my thesis. First we planned to straightforward evaluate the concentration of the CPNP internalized inside the cells by developing a new general methodology based on MALDI-TOF mass spectrometry (MS) which does not require any purification or separation steps.

In order to study an eventual interaction of the benzothiazepine oligomers with a specific receptor and then better understand the internalization mechanism of our CPNP, compounds like the fluorescein labelled LBT tetramer with inversed chiral configuration were synthesized.

Another direction for research was to synthesize bioconjugates between our newly discovered CPNP and some biologically active compounds that are unable to cross the cell membrane on their own. We planned to vectorize pepstatine - a powerful inhibitor of the Cathepsin D (see section **I.3.1**). Pepstatine while a potent transition state inhibitor of the CD is hindered *in vitro* or *in vivo by* its poor solubility in water and its inability to cross the cell membrane. Our aim was to improve pepstatine bioavailability by connecting it to a CPNP and solubilizing moieties. These

bioconjugates were tested for their ability to inhibit CD and cancer cells growth. By doing this we should be able to:

-prove that our set of CPNP is able to traffic biologically relevant cargos

-evaluate the effect of CD inhibition inside the endosomes and the lysosomes on the cancer cell proliferation

-discover a new target for breast anticancer therapy

Different CPNP-Pepstatine conjugates were synthesized and tested for cell toxicity on MDA-MB-231 breast cancer cells *in vitro*. Some of the AMPA oligomers conjugated to pepstatine showed high toxicity which encouraged us to perform tests *in vivo* on mice with one of our best compound (JMV4463). For that purpose, important quantities (about 100 mg) of compound JMV4463 were synthesized.

III. RESULTS AND DISCUSSION

III.1 Synthesis of Fmoc-DBT-OH and Fmoc-AMPA-OH

As mentioned in the project aims we needed the (3*S*)-amino-5-(carboxylmethyl)-2,3-dihydro-1,5-benzothiazepin-4(5H)-one **(DBT)** and 2-aminomethyl-phenyl-acetic acid (**AMPA**) moieties protected by the Fmoc group in order to use them later for standard SPPS. We synthesized the Fmoc-DBT-OH via 7 steps liquid phase synthesis (Figure **III.1** and Materials and Methods) starting from 125 mM of H-D-Cys-OH.HCl (Materials and methods). We obtained about 62.5 mM (29 gr) of Fmoc-DBT-OH corresponding to a global yield of around 50%. More than 100 grams of Fmoc-DBT-OH were synthesized during the course of my PhD thesis fallowing this efficient strategy. With the obtained quantity we were able to synthesize an important number of DBT oligomers for structural and biological studies.

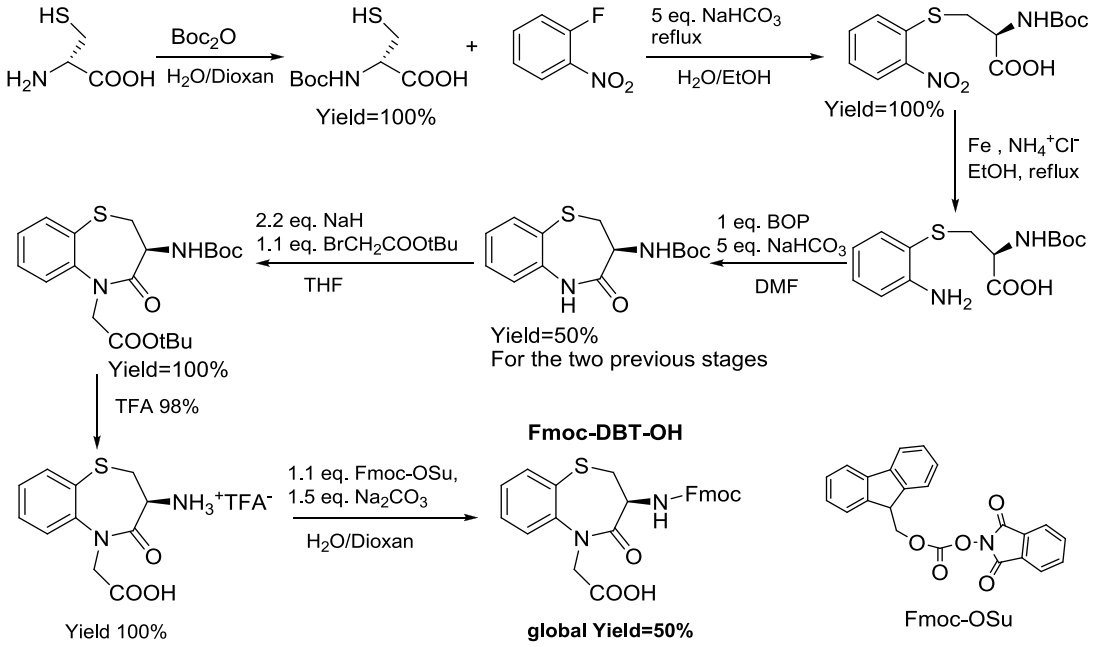

Figure III.1 *Synthesis of Fmoc protected (3S)-amino-5-(carboxylmethyl)-2,3-dihydro-1,5-benzothiazepin-4(5H)-one or* ***Fmoc-DBT-OH***

The Fmoc-LBT-OH monomer with inversed chiral configuration of the amino-group was synthesized following the same methodology but starting from H-L-Cys-OH. AMPA was purchased by commercial supplier and protected with Fmoc group by Fmoc-OSu in the same reaction conditions as for the DBT (see Materials and Methods)

III.2 Structural studies of DBT and AMPA oligomers

III.2.1 Syntesis of DBT and AMPA oligomers for structural studies

Synthesis of linear oligomers

The secondary structure determination of the DBT and AMPA oligomers was one of the principal aims of my thesis. This important task should help the construction of biomimetics with correctly positioned crucial functions on a target-by-target basis. In order to do this we synthesized via standard SPPS on Ring amide (RA) polystyrene (PS) resin using HBTU/DIEA as a coupling reagent, AMPA and DBT oligomers of different lengths and we capped them at the N-terminus with acetyl group or Z(Br) (2-bromobenzyl oxycarbonyl). The heavy Br atom is supposed to give a better resolution of the X-Ray structure if a compound is crystallized. At the end the compounds were cleaved from the resin by TFA and purified by preparative HPLC chromatography (see Materials and Methods). The synthesis of the oligomers is summarized on Figure **III.2.1-1**

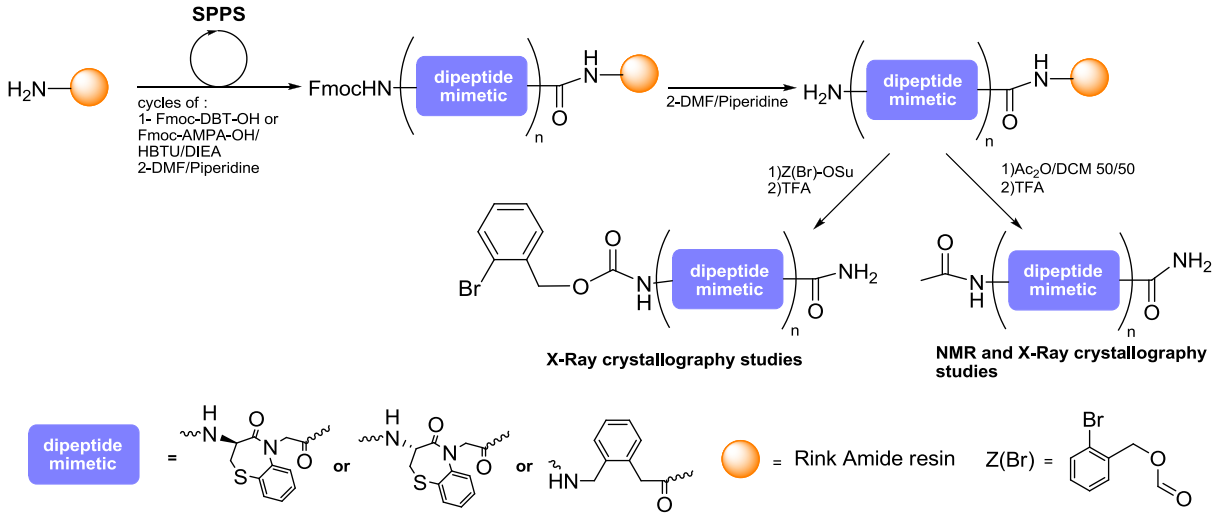

III.2.1-1 *General SPPS synthesis of DBT, LBT and AMPA oligomers capped by Z(Br) or acetyl group at the N-terminus for crystallization and NMR structural studies respectively.*

The AMPA and DBT oligomers synthesized by this method are summarized in Table **III.2.1-1**

Table III.2.1-1 *Linear oligomers synthesized for structural studies*

Compounds	Type of structural tests
Ac-$(DBT)_n$-NH_2 n=[1-8]	NMR studies and Crystallization essays
Z(Br)-$(DBT)_n$-NH_2 n=[4-5]	Crystallization essays
Ac-DBT-LBT-DBT-LBT-NH_2	NMR studies and Crystallization essays
Ac-$(AMPA)_n$-NH_2 n=[4-5]	NMR studies and Crystallization essays

Synthesis of cyclic oligomers

Cyclic foldamers are interesting scaffolds for CPNPs, antibiotics and nanostructures. Linear DBT hetero and homo-oligomers were synthesized by SPPS and subsequently cyclized in solution. The first DBT moiety was anchored to the 2-

chlorotrityl PS resin in the presence of DIEA. After that DBT homo-oligomers and $[Lys(Boc)–DBT]_n$ hetero-oligomers were synthesized via standard SPPS by HBTU/DIEA activation (Figure **III.2.1-2**). The hetero-oligomers were cleaved from the resin by a solution of TFE/DCM 3/7 v/v in order to keep the Boc protection of the lysine residue side chain. The cyclization steps were performed by BOP/$NaHCO_3$ activation in DMF at low concentration of the oligomers (200 µM) in order to avoid dimerization. After cyclization, a treatment with a solution of 99% TFA was performed and the cyclic compounds were purified by HPLC preparative chromatography. In the case of DBT homo-oligomers the compounds were cleaved directly by TFA 99% and cyclized via BOP activation in the presence of $NaHCO_3$ as base in DMF at concentration of 200µM. After cyclization the compounds were purified by HPLC preparative chromatography.

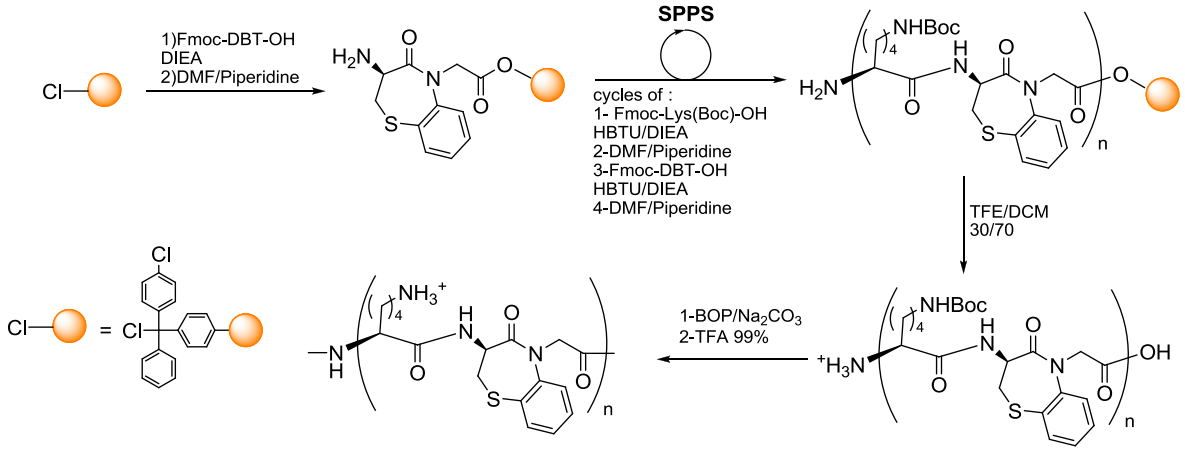

Figure III.2.1-2 *General synthesis of -(Lys-DBT)$_n$- cyclic hetero-oligomers. The same strategy was applied for the synthesis of the -(DBT)$_n$- cyclic homo-oligomers but they were directly cleaved from the resin by TFA 99% and then cyclized by BOP activation in DMF.*

The cyclic hetero and homo-oligomers obtained following this strategy are summarized in Table **III.2.1-2**. We were unable to obtain the cyclic compound -$(DBT)_2$-. During the attempt for cyclization of H-$(DBT)_2$-OH only dimerization of this compound was obtained even at 200 µM concentration. This dimer is probably too constrained to cyclize.

*Table **III.2.1-2** Cyclic oligomers synthesized for structural studies*

Compounds	Type of structural tests
-$(DBT)_3$-	NMR studies and Crystallization essays
-$(DBT)_4$-	NMR studies and Crystallization essays
-$(Lys\text{-}DBT)_3$-	NMR studies and Crystallization essays
-$(Lys\text{-}DBT)_4$-	NMR studies and Crystallization essays

III.2.2 Crystallization assays

Crystallization essays were performed with the compounds reported in section **III.2.1** in order to obtain crystals suitable for X-Ray structural studies. The choice of the solvent for these experiments was motivated by the compounds solubility. For example the longer DBT linear and cyclic oligomers were soluble only in DMSO. The compounds and the solvents used for crystallization essays are reported in Table

III.2.2. Small crystals were obtained from Ac-$(DBT)_6$-NH_2 in DMSO but their size was not important enough for X-Ray crystallography studies. Powder diffraction experiments are currently performed with compounds: -$(Lys\text{-}DBT)_3$-, -$(DBT)_3$- and Ac-$(DBT)_6$-NH_2.

*Table **III.2.2** Compounds and solvents used for the crystallization assays*

Compound	Crystallization essay solvent
Ac-$(DBT)_n$-NH_2 n=[1-4]	DCM, DMSO, TFE, CH_3CN
Ac-$(DBT)_n$-NH_2 n=[5-8]	DMSO, DCM
Ac-$(AMPA)_n$-NH_2 n=[4-5]	DMSO, DCM
Z(Br)-$(DBT)_n$-NH_2; n=[4-5]	DMSO
-$(DBT)_n$-; n=[3,4]	DMSO
-$(Lys\text{-}DBT)_n$-; n=[3,4]	EtOH

III.2.3 NMR structural studies of linear DBT oligomers

Our main effort for structural characterization by NMR was concentrated on the series of compounds Ac-$(DBT)_n$-NH_2 with n=[1-8] as we had no data about their secondary structures. Cyclic homo and hetero-oligomers were also studied but their symmetrical structures gave rise to too much signals overlays.

III.2.3.1 Choice of deuterated solvent

Our first task was to choose deuterated solvent for the NMR structural studies of the DBT oligmers. Most of these compounds were insoluble in pure water, TFE, MeOH or EtOH, thus we excluded these solvents. This narrowed our choice to $CDCl_3$ and DMSO. Figure **III.2.3.1** shows the ^1H NMR spectra of Ac-$(DBT)_4$-NH_2 obtained in d_6-DMSO or in $CDCl_3$. The peaks of the protons in the spectrum obtained in DMSO are a lot better defined and resolved than the broad peaks obtained in $CDCl_3$. These results could be explained by the existence of several conformers in intermediate chemical exchange in $CDCl_3$. The sharp resonances in d_6-DMSO suggested a single well defined conformation or fast exchange between two or more conformers. 2D [^1H, ^1H] NOESY experiments were performed with compound JMV4169 in d_6-DMSO and in $CDCl_3$ at 0.5 mM concentration. Practically no NOE signals were observed in the $CDCl_3$ solvent, whereas the spectrum obtained in d_6-DMSO showed several proton-proton interactions that could suggest more defined organization of the oligomer in this solvent (Figure **III.2.3.3-4 A**). Possible explanation is that the structure of JMV4169 in DMSO is promoted by solvophobic interactions that are more pronounced in the case of a polar solvent. Moreover, DMSO was a better choice for the structural studies also because it is more similar to water due to its polarity and ability to form hydrogen bonds.

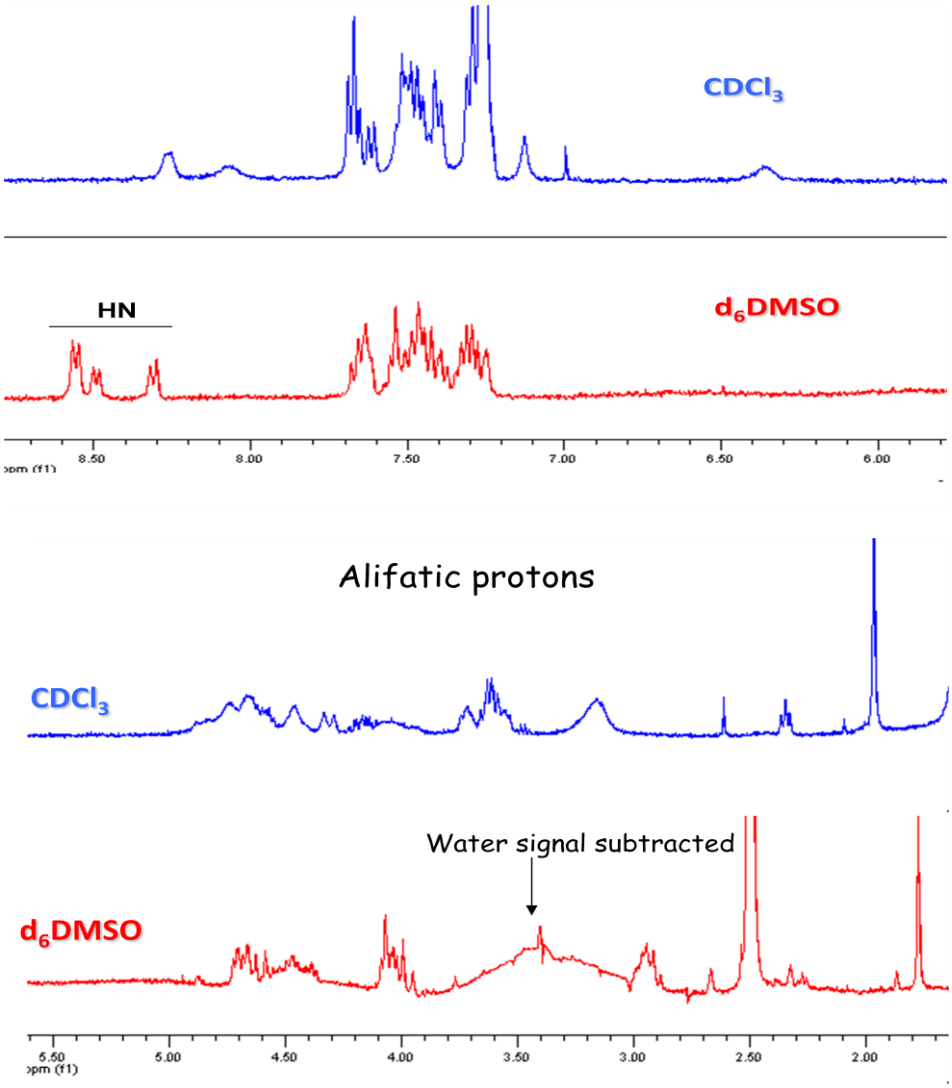

Figure III.2.3.1 *^{1}H NMR of Ac-$(DBT)_4$-NH_2 obtained in d_6-DMSO or $CDCl_3$ at 25℃.*

III.2.3.2 'NOE walk' and assignment of the protons

Compounds Ac-$(DBT)_n$-NH_2 with n=[1-8] were extensively studied in d_6-DMSO by 1D ^{1}H, 2D [^{1}H, ^{1}H] NOESY, 2D [^{1}H, ^{1}H] ROESY, 2D [^{1}H, ^{1}H] TOCSY and 2D [^{1}H, ^{1}H] COSY NMR experiments. The spectra were analysed by the CARA 1.5.5 software. The atom nomenclature we chose for the DBT moiety follow that commonly used for amino acids and is summarized on Figure **III.2.3.2-1**

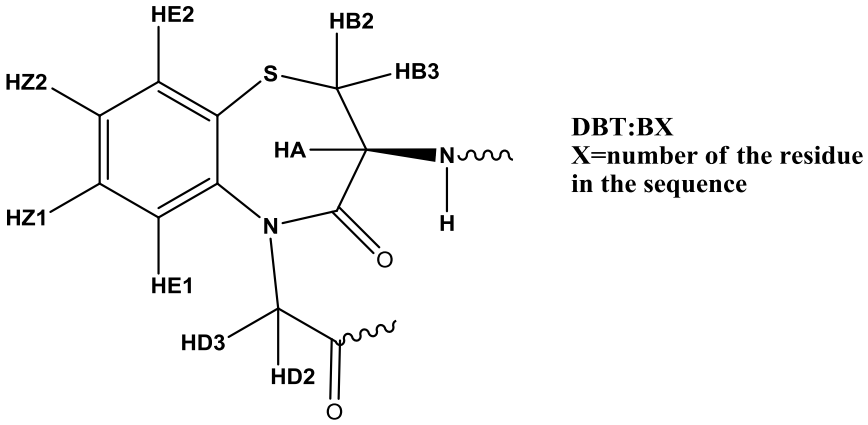

Figure III.2.3.2-1 *Nomenclature used for the DBT moiety. Atom names are followed by DBT:BX where X corresponds to the number of the residue in the sequence (N-terminal residue being the first one and the C-terminal being the last one). For example the HA atom of the C terminal residue in the case of Ac-(DBT)$_4$-NH$_2$ is noted HA DBT:B4 and HA of the N terminal residue is assigned HA DBT:B1*

Figure **III.2.3.2-2** shows the so called 'NOE walk' we performed to assign the chemical shifts of the protons of the Ac-(DBT)$_3$-NH$_2$ oligomer starting from the C- and N-terminus of the molecule. Starting from the N-terminus we determined H DBT:B1 by its interaction with the acetyl group protons. Then we identified HA DBT:B1 by its cross peak with H DBT:B1. HB2 and HB3 DBT:B1 were determined by their interaction with HA DBT:B1. HE2 DBT:B1 was assigned by its intense interaction with HB2,3 DBT1. We were then able to assign the aromatic protons of the first residue using interactions detected by 2D COSY and 2D TOCSY NMR experiments. Through the aromatic HE1 DBT:B1 we were able to indentify HD2,3 DBT:B1. Then through interactions with HE1 DBT:B1 and HD2,3 DBT:B1 we were able to determine H DBT:B2. Once H DBT:B2 assigned the same algorithm was used to determine the protons of the second and third residue.

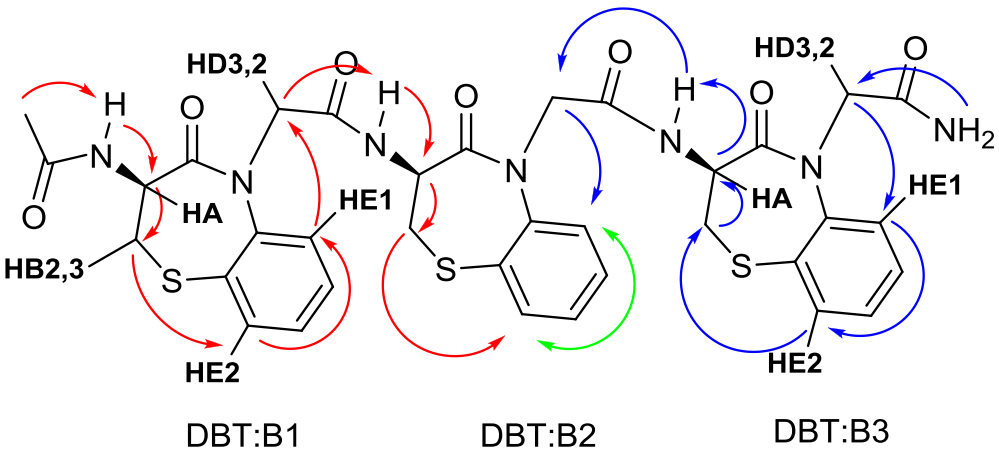

Figure III.2.3.2-2 ***'****NOE walk' for the assignment of the atoms of the Ac-(DBT)$_3$-NH$_2$ oligomer starting from the C- and N- terminal residues (Blue and red arrows). The same strategy was used for the assignment of the protons of the oligmers Ac-(DBT)$_n$-NH$_2$ n=[1-6]. In the case of the Ac-(DBT)$_n$-NH$_2$ n=7,8 was observed too much overlay of the proton signals for the accurate assignment.*

Alternatively the NOE walk could start from the C-terminus where HD2,3 DBT:B3 could be determined by their cross peak with the amide protons. HE1 DBT:B3 was identified by its interaction with HD2,3 DBT:B3. Then by TOCSY and COSY spectra we assigned the aromatic protons of the 3th DBT residue and most importantly HE2 DBT:B3. We determined HB2,3 DBT:B3 by its cross peak with HE2 DBT:B3. HA DBT:B3 and H DBT:B3 could then easily be assigned. Next step was to determine HD2,3 of the second residue by their interactions with H DBT:B3. The same algorithm was then used to assign the protons of the second and first residues. Using similar 'NOE walks' we were able to assign all the protons of the oligomers Ac-$(DBT)_n$-NH_2 n=[1-6] (Materials and Methods Section **V.7.1**) . In the case of the Ac-$(DBT)_n$-NH_2 n=7,8 was observed too much overlay of the proton signals for accurate assignment.

III.2.3.3 Measurement of NOE and ROE volumes and determination of distance restrictions in the oligomers

Study of Ac-$(DBT)_n$-NH_2 with n=[1-4] by 2D ROESY experiment

First we concentrated our effort on the series of compounds Ac-$(DBT)_n$-NH_2 with n=[1-4] because in their spectra was observed a lot less overlay compared to the longer oligomers. The comparison between the ROESY and NOESY experiments showed more cross-peaks in the ROESY spectrum, especially between the aliphatic HD2,3 protons and the aromatic protons (see Figure **III.2.3.3-1** for the ROESY spectrum of Ac-$(DBT)_4$-NH_2 and Figure **III.2.3.3-4 A** for the NOESY spectrum). These findings could be explained by the fact that ROESY spectra are more adapted for the analysis of small or medium sized molecules. Indeed this kind of molecules has correlation times which lead to very small or zero NOEs on high-field spectrometer, where the correlation time is a function of the molecular shape and size. Thus we decided to examine first the ROESY spectra.

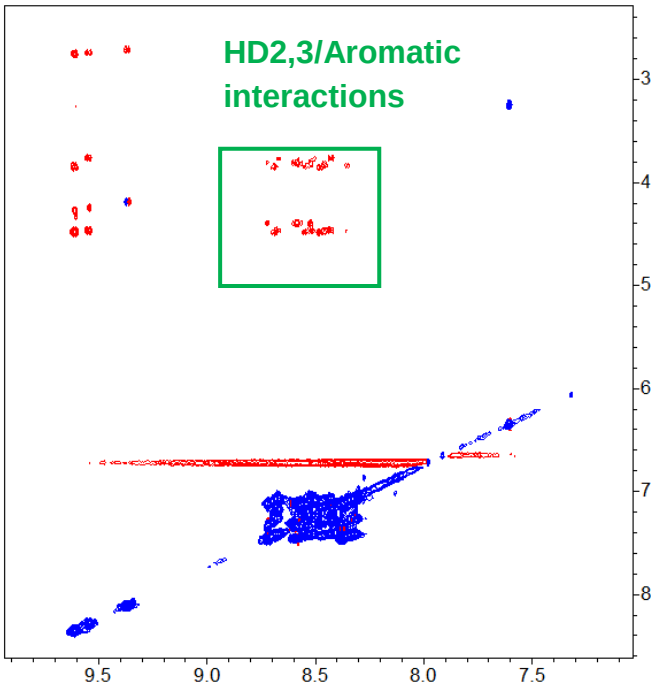

Figure III.2.3.3-1 *ROESY spectrum (MT=250ms) of Ac-$(DBT)_4$-NH_2.*

Figure **III.2.3.3-2** sums up some of the characteristic ROEs we observed in Ac-$(DBT)_4$-NH_2. In order to obtain distance restrictions, we carried out manual integration of the volumes of the ROEs by means of NEASY, a tool of CARA software**.** We used the volume of the interaction between the vicinal HD2 and HD3 atoms in the DBT:B1 residue as reference to transform these volumes into distances.

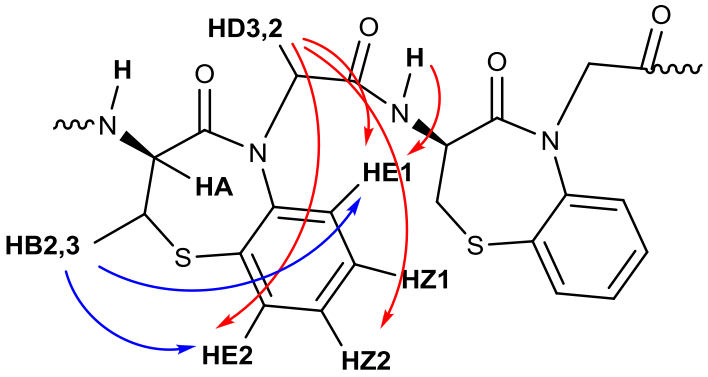

Figure III.2.3.3-2 *ROEs observed in the ROESY (MT=250ms) spectrum of Ac-$(DBT)_4$-NH_2. The distance between HD2,3 and HE1 was estimated around 4 Å equal to the distance between HD2,3 and HE2. These interactions were ruled by us as artefacts.*

During the preliminary analysis of these data we observed that the distances between HD2,3-HE1 and HD2,3-HE2 in the same residue were very similar (in the range of 4 Å). Unfortunately there is no possible conformation of the DBT moiety that respect these distance restrictions. In fact there is no possible structure in which HE2 is closer than 5 Å to HD2,3. Thus we had to judge these ROE interactions as artefacts. In fact ROESY is probably the most artefact-ridden one of all 2D methods. TOCSY-ROE combinations are particularly tricky, because they have the same phase as true ROEs. A TOCSY transfer between strongly coupled protons like HE1 and HE2, in combination with a ROE between HD2,3 and HE1 could give a false ROESY peak between HD2,3 and HE2 (Figure **III.2.3.3-3**). Such artefacts could seriously hamper the calculation of the exact distances inside the molecule or even give interactions that do not exist at all. Thus we could not use the distance constraints obtained from ROESY spectra for the structure determination of compounds Ac-$(DBT)_n$-NH_2 with n=[1-4]. Such artefacts are less common for the NOESY sequence. This fact pushed us to look deeper into the NOESY spectra.

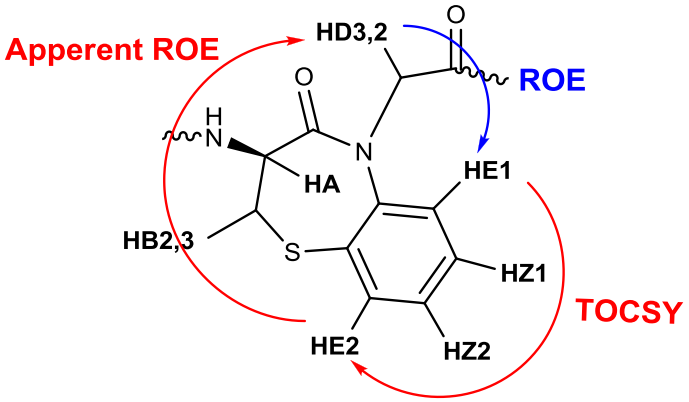

Figure III.2.3.3-3 *Mechanism for the detection of false ROEs in case of protons with very strong TOCSY coupling.*

Structural studies of Ac-$(DBT)_6$-NH_2 by the 2D NOESY experiment

As we already mentioned, NOESY spectra of compounds Ac-$(DBT)_n$-NH_2 n=[1-4] showed few NOE interactions, as expected for such small molecules (Figure **III.2.3.3-4 A**). We examined higher DBT oligomers – Ac-$(DBT)_n$-NH_2 n=[5-8] by 2D NOESY experiments. Spectrum of compound Ac-$(DBT)_5$-NH_2 and especially spectrum of compound Ac-$(DBT)_6$-NH_2 showed numerous NOEs that strongly suggested a well defined secondary structures of these compounds. Spectra of compounds Ac-$(DBT)_n$-NH_2 n=7,8 exhibited similar patterns but also a lot of overlay so correct assignment of the protons was difficult. Figure **III.2.3.3-4** is a comparison between the NOESY spectra of the Ac-$(DBT)_4$-NH_2 and Ac-$(DBT)_5$-NH_2. On the tetramer spectrum were observed few intra-residual NOEs between the aliphatic protons with the aromatic protons and the aromatic with the amide protons (Figure **III.2.3.3-4 A**). For the pentamer we identified numerous inter and intra-residue interactions between the amide protons and the aromatic protons, aliphatic-aliphatic protons interactions and a lot more aliphatic-aromatic protons interactions (Figure **III.2.3.3-4 B**). This could be explained by the fact that the pentamer has a better defined structure compared to the tetramer or that the tetramer has a correlation time such that the NOE are less intense. Moreover, we examined the chemical shifts of the amide protons of the first and second DBT residues (Figure **III.2.3.3-5**). The chemical shift of the amide proton of the first residue is constantly shifted up-field when we elongate the oligomer until we reach the pentamer and is slightly down-fielded from the pentamer to the octamer. The amide proton signal of the second residue is at first shifted down-field between the monomer and the trimer, then it is shifted up-field until the pentamer but its chemical shift is constant from the pentamer to the octamer. These data suggest the progressive organization of the DBT oligomers in DMSO with the elongation of their sequences and the formation of well defined secondary structure starting from the DBT pentamer. These observations were supported by the different NOE patterns observed for the tetramer and the pentamer (Figure **III.2.3.3-4**).

We decided to examine more closely the Ac-$(DBT)_6$-NH_2 NOESY spectrum (MT 250ms) obtained in d_6-DMSO. In fact this spectrum showed even more NOE interactions than the spectrum obtained for the pentamer (Figure **III.2.3.3-6**). At the same time there was not as much overlay as in the case of the heptamer and the octamer.

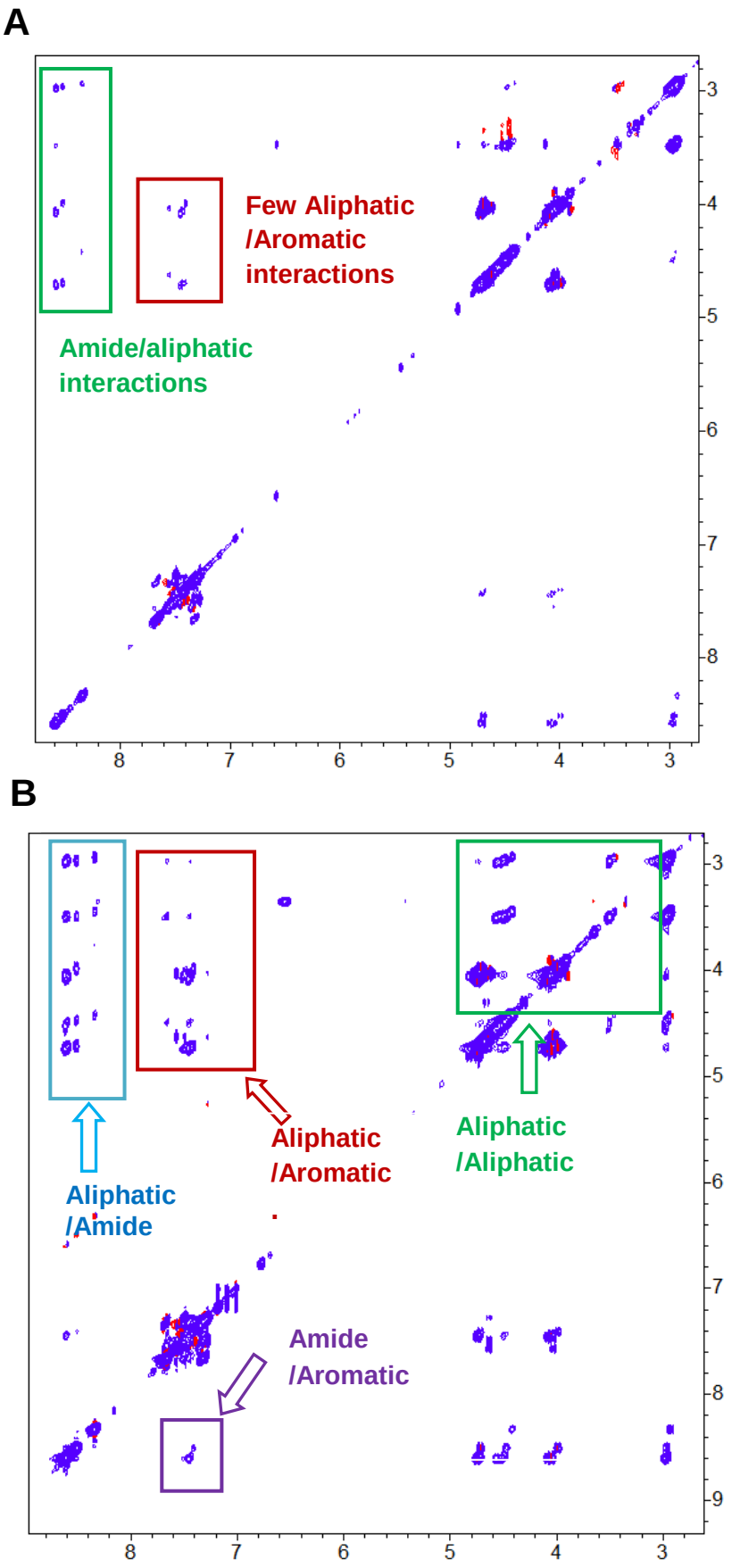

Figure III.2.3.3-4 A) *NOESY spectrum (MT=250ms) of compound Ac-(DBT)$_4$-NH$_2$.* ***B)*** *NOESY spectrum (MT=250ms) of compound Ac-(DBT)$_5$-NH$_2$.*

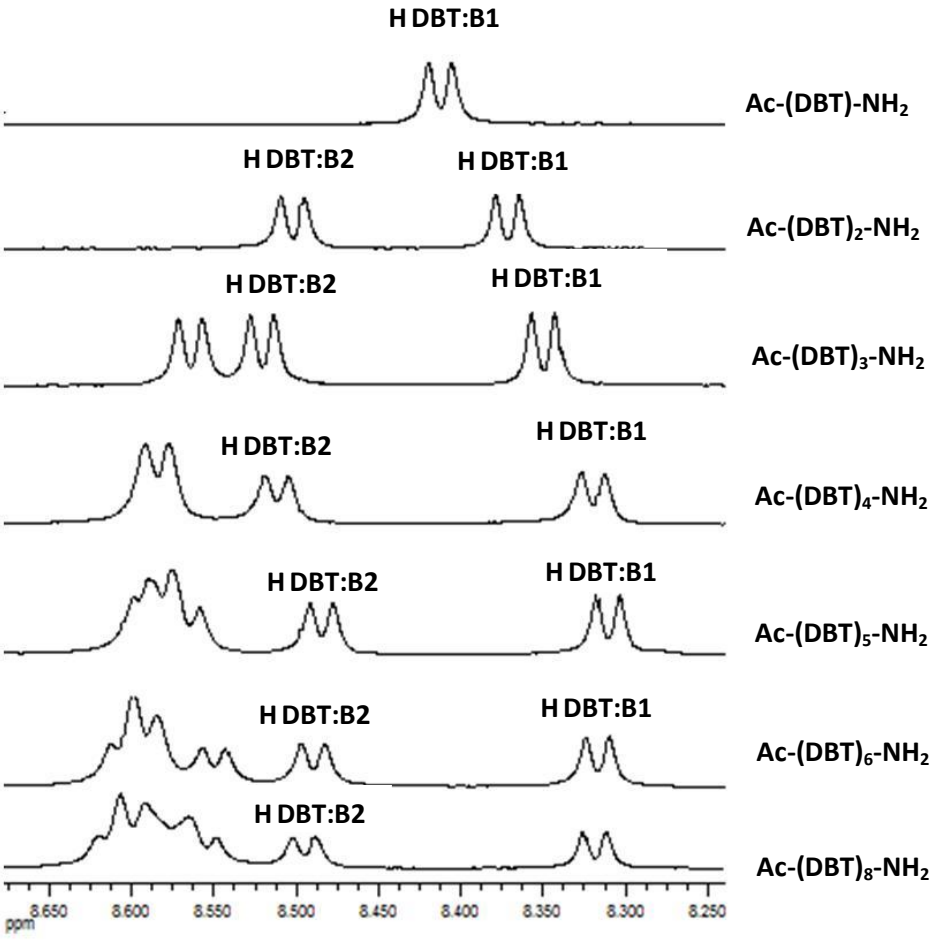

Figure III.2.3.3-5 *Chemical shifts of the amide protons for DBT oligomers of different length*

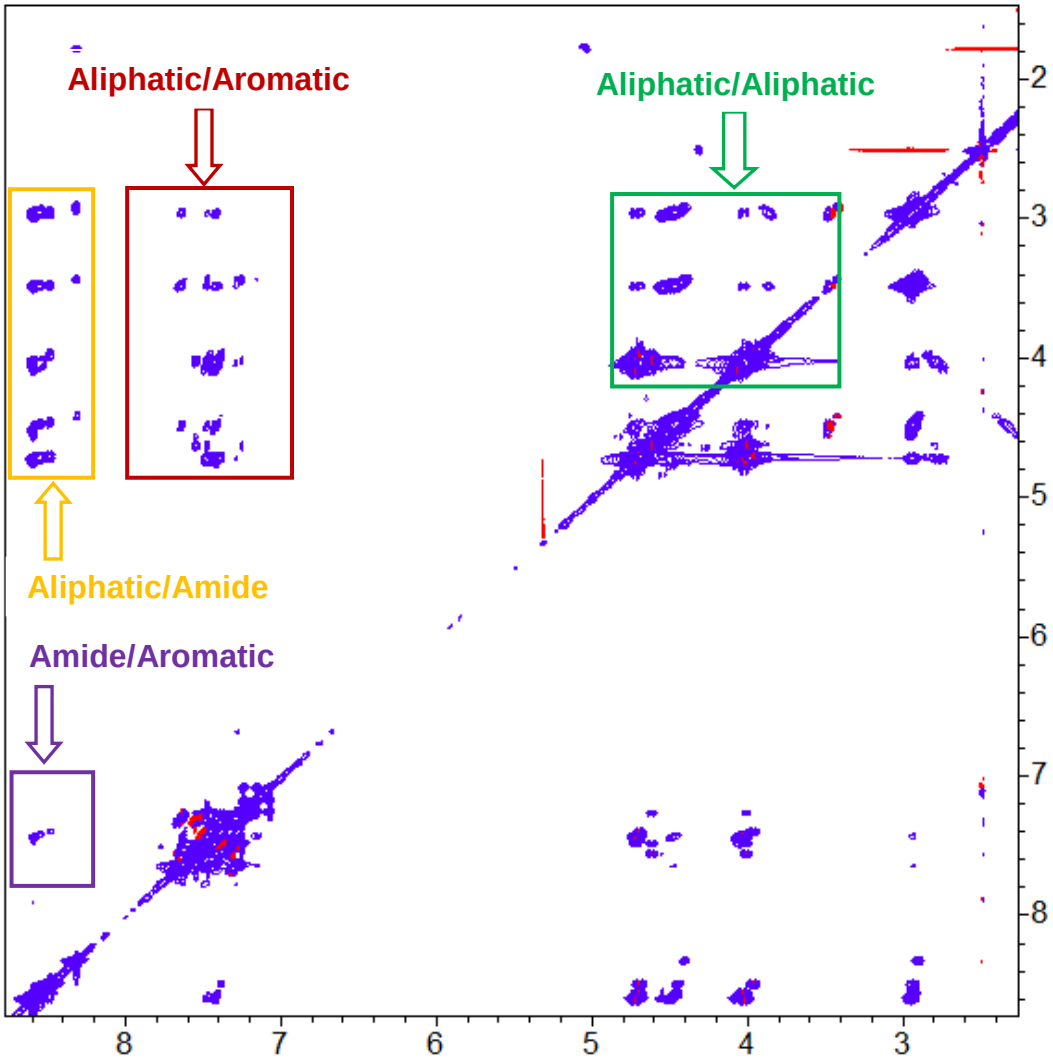

*Figure **III.2.3.3-6** NOESY spectrum (MT=250ms) of compound Ac-(DBT)$_6$-NH$_2$.*

The Ac-(DBT)$_6$-NH$_2$ spectrum could be separated in four parts:

<u>-aliphatic-aromatic NOE interactions (red colour on Figure **III.2.3.3-6**)</u>

First very important observation was that we did not observe the same artefacts as in the case of the ROESY spectra (Figure **III.2.3.3-1**). Important for the determination of the structure are the intense interaction between the HA proton and the aromatic protons in the same residue. These interactions suggest a constraint and well defined conformation of the DBT residues inside the oligomer. We assigned intra-residue interactions between:

- HD2,3-HE1 and HD2,3-HZ1 in the same residue (valid for all the residues).
- HB2,3-HE2 and HB2,3-HZ2 in the same residue (valid for all the residues).

We assigned also some very important inter-residue interactions like:

- HE1 DBT:B2 with HB2 DBT:B3;
- HE1 DBT:B1 with HA DBT:B2;
- HE1 DBT:B1 with HB3 DBT:B2;
- HD3 DBT:B2 with HB2 DBT:B3;

- HD3 DBT:B4 with HB2 DBT:B5;
- HD3 DBT:B3 with HB2 DBT:B4;
- HZ2 DBT:B2 with HA DBT:B3

-Aliphatic-aliphatic proton interactions (orange colour on Figure **III.2.3.3-6**)

In the ROESY and NOESY spectra of compounds Ac-$(DBT)_n$-NH_2 n=[1-4] we observed very few aliphatic-aliphatic interactions (Figure **III.2.3.3-4 A**). In the case of Ac-$(DBT)_6$-NH_2 2D NOESY spectrum we observed intense aliphatic-aliphatic proton interactions but unfortunately due to the overlay it was hard to assign and quantify them. Nevertheless these data show the better structural organization of Ac-$(DBT)_6$-NH_2 compared to the shorter oligomers. One of the interactions that we were able to quantify was HA DBT:B1 with HB2 DBT:B1. We used the volume of this interaction as reference to convert the NOE volumes into distance restriction.

-Aliphatic-amide proton interactions (purple colour on Figure **III.2.3.3-6**)

These interactions are not so important for the determination of the secondary structure but were crucial for the assignment of the protons. Some examples for the NOEs detected:

- H DBT:B6 - HD2 DBT:B5;
- H DBT:B5 - HD2 DBT:B4;
- H DBT:B4 - HD2 DBT:B3;
- H DBT:B2 - HD2 DBT:B1;
- H DBT:B3 - HD3 DBT:B2;
- H DBT:B6 - HD3 DBT:B5;
- H DBT:B5 - HD3 DBT:B4;
- H DBT:B4 - HD3 DBT:B3

-Aromatic-amide proton (violet colour on Figure **III.2.3.3-6**)

These interactions could be very important for the determination of the secondary structure. The interactions we detected were of type H DBT:Bi with HE1 DBT:Bi-1.

A table with all the measured volumes and distances (with upper and lower limits) could be found in the Materials and Methods section (Section **V.7.2)**. While measuring the volumes and distances we encountered certain problems. First one was the overlay. In case of important overlay between NOEs we considered the maximum distance between the protons to be 5.5 Å. Another problem was that HD2 and HD3 had similar NOE values with all the other atoms. The same problem was observed for protons HB2 and HB3. This problem is often observed for geminal protons and usually is solved during the structure calculations by means of the introduction of pseudo atoms.

III.2.3.4 Determination of the secondary structure of Ac-$(DBT)_6$-NH_2 by molecular modelization with distance restrictions

The calculated distance restrictions in Ac-$(DBT)_6$-NH_2 (reported in section **III.2.3.3** and Materials and Methods) are currently being used for the determination of the oligomer structure by a molecular modelization study.

III.3 DBT and AMPA oligomers as cell penetrating non-peptides (CPNP)

As mentioned in the introduction (section **I.1.2.**) foldamers are attractive platform for the design of cell penetrating non-peptide compounds (CPNP).[3,4] We hypothesized that short oligomers constructed by DBT or AMPA frameworks could translocate the cellular membrane and thus be used as a new class of CPNP (see section **I.2.2**). Even though these compounds are not charged as most CPP[5] or CPNP we considered that by virtue of their aromaticity, hydrophobicity and their well-organized structure they could have a non-specific interaction with the lipid bilayer and thus be internalized into the cell. This chapter of the manuscript will mainly focus on the ability of these short hydrophobic oligomers to transport fluorescent dyes and short linkers inside the cell while in the '**V**' chapter we will concentrate on their ability to transport biologically relevant cargos like the powerful inhibitor of the Cathepsin D - pepstatine.

III.3.1 Synthesis of oligomers tagged by fluorescein isothiocyanate

III.3.1.1 Synthesis of short DBT and AMPA oligomers tagged by fluorescein isothiocyanate

Oligomers of different lengths were synthesized (see Materials and Methods) on a solid support using RA PS resin, by successive addition of N-Fmoc protected DBT/AMPA (Fmoc-DBT-OH/Fmoc-AMPA-OH) in the presence of HBTU as coupling reagent and DIEA as a base. In order to track their cellular internalization by fluorescence microscopy, fluorescein isothiocyanate was used to label the oligomers (Figure **III.3.1.1**).

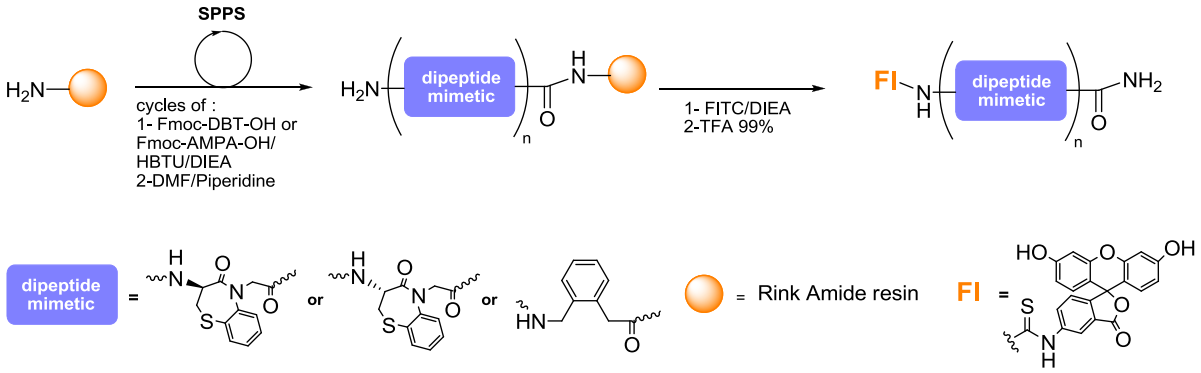

Figure III.3.1.1 *Synthesis of fluoresceine labelled oligo-(D- and L-BT) and oligo-AMPA*

The fluorescent tag was either directly attached to the N-terminus of the poly(DBT)/poly(AMPA) anchored to the resin or attached to the N-terminus via a short linker. The importance of the configuration and the structure of the oligomers were assessed by the preparation of the LBT derivative (JMV4228) and the D/LBT alternated oligomer (JMV4287), respectively. The compounds synthesized following this strategy are summarized in Table **III.3.1.1** In the case of compound JMV4497, a short solubilizing moiety between the CPNP oligomer and the fluorescein was introduced. The solubilizing moiety is composed of a short polyethylene glycol linker and D-Arg residue. The introduction of such moiety was motivated by the poor solubility of the longer AMPA oligomers in aqueous media.

Table III.3.1.1 *Fluorescein labelled DBT and AMPA oligomers synthesized for internalization studies.*

Compounds	JMV number
Fl-$(DBT)_2$-NH_2	**JMV2949**
Fl-$(DBT)_3$-NH_2	**JMV2968**
Fl-$(DBT)_4$-NH_2	**JMV3229**
Fl-$(LBT)_4$-NH_2	**JMV4228**
Fl-DBT-LBT-DBT-LBT-NH2	**JMV4287**
Fl-$(AMPA)_3$-NH_2	**JMV4236**
Fl-$(AMPA)_4$-NH_2	**JMV4237**
Fl-O_2Oc-r-$(AMPA)_4$-NH_2	**JMV4497**

III.3.1.2 Synthesis of octa and nona-arginine and $(DBT)_{3-4}$-$(Arg)_9$ oligomers tagged by fluorescein isothiocyanate

In order to study the internalization of our set of compounds we needed a positive control. As such, we chose the well-studied and potent CPPs octa and nona-arginine (Section **I.2.1**). The octa and nona-arginine were synthesized following the standard SPPS methodology on RA PS resin with HBTU/DIEA activation. They were tagged on the amino-end by fluorescein isothiocyanate via an aminohexanoic acid linker in order to avoid secondary reactions reported by Subra et al.[74]

Some publications in the literature point that an association of oligo-arginine with a hydrophobic moiety could result in a very powerful cell penetrating compound. Such compounds could also be used to internalize DNA or SiRNA via the non-covalent strategy.[47] Inspired by these data, we synthesized via SPPS on RA PS resin chimeric oligoDBT-oligoArginine bioconjugates. We linked the DBT trimer and tetramer to the nona-Arginine via an Ahx linker and then we tagged the compounds by fluorescein. The synthesized arginine oligomers and mixed DBT-Arginine oligomers are summarized on Table **III.3.1.2.**

*Table **III.3.1.2.** PolyArginine containing compounds synthesized as positive tests and chimerical CPNP*

Compounds	JMV number
Fl-Ahx-$(Arg)_8$-NH_2	-
Fl-Ahx-$(Arg)_9$-NH_2	**JMV3888**
Fl-Ahx-$(DBT)_3$-Ahx-$(Arg)_9$-NH_2	**JMV4568**
Fl-Ahx-$(DBT)_4$-Ahx-$(Arg)_9$-NH_2	**JMV4569**

III.3.2 Internalization of short DBT oligomers tagged by fluorescein

III.3.2.1 Cellular Uptake of DBT Oligomers by MDA-MB-231 breast cancer cells.

At first, the cellular uptake in MDA-MB-231 breast cancer cells of the oligomers (JMV2949, JMV2968, JMV3229, JMV4228, JMV4287) was analysed by fluorescence emission measurement (Figure **III.3.2.1-1 A**, see section **I.2.3.**) and compared to fluorescein labelled octa-arginine (Arg_8) as a positive control and

carboxyfluorescein (CF) as a negative control. In order to determine the internalized fraction of the compounds, a 5-min trypsin treatment was realized to remove membrane-bound transduction compounds. It is worth noting that the percentage of membrane-bound DBT oligomers was not as important as in the case of the Arg_8. Probably this polycationic compound has a higher affinity for the lipid membrane via its association to the anionic phospholipids and proteoglycans. The highest intracellular fluorescence intensity was found for DBT_4 (JMV3229) with a drastic decrease (>4-times) for DBT_3 (JMV2968) and DBT_2 (JMV2949) oligomers. Thus, the cellular uptake appeared length-dependent with an increase of internalization with the oligomer size. Moreover, the amount of DBT_4 that was internalized was more significant than that of Arg_8 despite the fact that it is uncharged. Even though the increase in efficiency from DBT_2 to DBT_4 could be associated with an increase of the hydrophobicity, the high difference between DBT_3 and DBT_4 might be also attributed to a progressive organization of the oligomer structure. Compound LBT_4 (JMV4228) constructed by the oligomerization of an L-benzothiazepinone moiety was as potent as its D-counterpart suggesting that the configuration of the BT moiety was not important and that the CPNPs do not interact with a specific receptor but rather with hydrophobic plasma membrane components. Compounds constructed from the alternation of D and LBT exhibited a 2-times decreased uptake. This result could be explained by a change in the oligomer structure.

A dose-response analysis was performed to compare the uptake of the BT-oligomers with octa-arginine (Figure **III.3.2.1-1 B**). The penetration of all compounds appeared to be dose-dependent. However in contrast to Arg_8, uptake of JMV compounds still increased at high doses (5.10^{-5} M). The kinetics study performed with 10^{-5} M JMV3229 (**III.3.2.1-2 A**) showed that its cellular entry was at least as efficient at 1 h as that of Arg_8. Then, JMV3229 uptake increased up to 16 h to reach a 6-time higher intracellular concentration than Arg_8, for which maximal concentration is reached at 1 h. A temperature-dependent analysis performed at 4°C and 37°C (**III.3.2.1-2 B**) showed that the cellular uptake exhibited a 3-times decrease at low temperature, hence suggesting the involvement of an energy-dependent endocytotic pathway. The remaining fluorescence was most probably due to cell membrane-bound oligomers as shown in Figure **III.3.2.2 D**.

III.3.2.2 Intracellular Distribution of DBT Oligomers.

Confocal laser scanning microscopy (CLSM) (see section **I.2.3**) analyses were also performed on living MDA-MB-231 cells to assess internalization and intracellular distribution. These experiments were associated with a kinetic study of $Fl\text{-}(DBT)_4\text{-}NH_2$ oligomer internalization. Figure **III.3.2.2 A** shows the internalization of JMV3229 in cellular organelles after 3 h of incubation with the highest accumulation at 16 h and an apparent decrease at 24 h in accordance with the kinetic study reported in Figure ***II.3.2.1-2 A***. Co-staining with a membrane marker (lipid-raft labelling) indicated that this hydrophobic compound was not held in the lipid membrane at 37°C. However, at 4°C, the majority of the compound was co-localized with the membrane marker (Figure **III.3.2.2 D**) rather than internalized, confirming the temperature effect on the intracellular uptake described in Figure **III.3.2.1-2 B** and supporting an energy-dependent internalization mechanism.

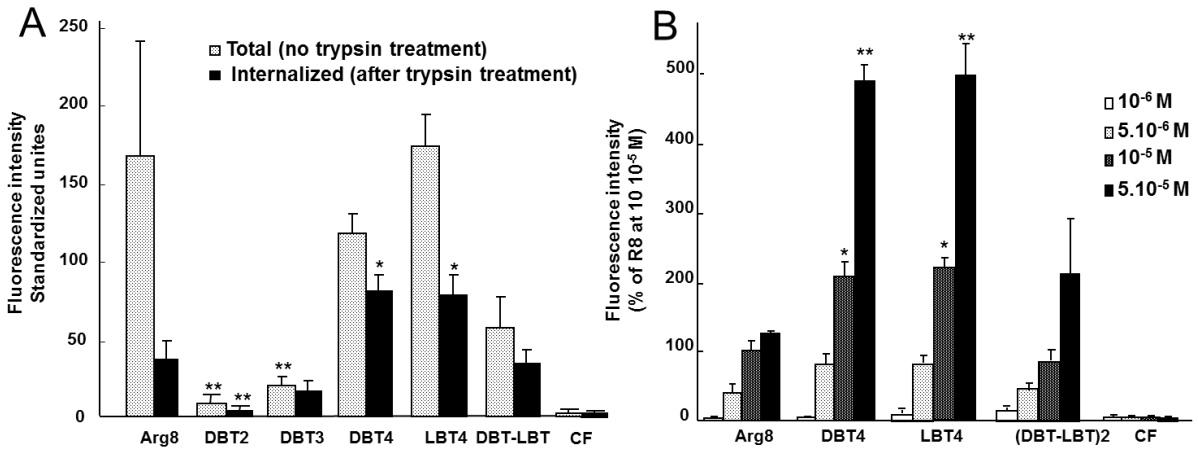

Figure III.3.2.1-1 *Uptake of Arg_8 and DBT oligomers in MDA-MB-231 cells. Data are the means ±SD from three independent experiments. In B) cells were treated by trypsin before fluorescence measurements.* ***A)*** *Determination of total and internalized compounds after incubating cells for 3 h at 37 °C with 10^{-5} M of fluorescently labelled compounds. *p < 0.05, **p < 0.01 relative to Arg_8 values with or without trypsin treatment, respectively (Student's t test).* ***(B)*** *Comparison of fluorescence emission after incubation for 3 h with several concentrations ranging from 10^{-6} to 5.10^{-5} M. *p < 0.05, **p <0.01 relative to Arg_8 values at the same concentration (Student's t test).*

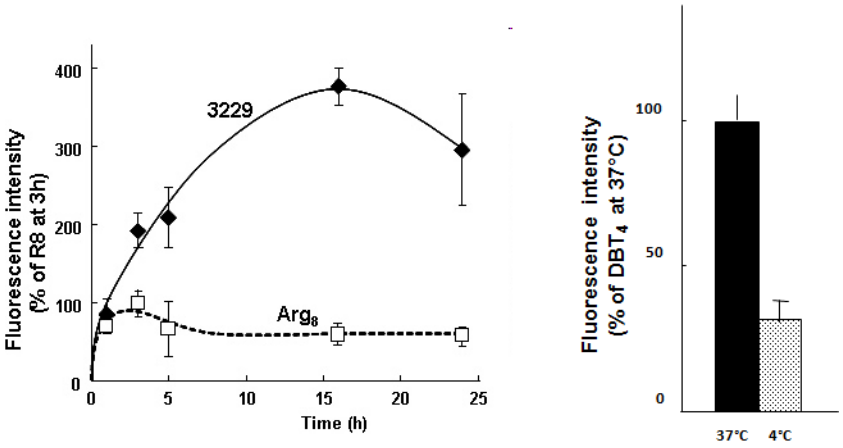

Figure III.3.2.1-2 A) *Kinetics of internalization of JMV3229 and Arg_8 at 10^{-5} M.*
B) *Effect of temperature on the cellular uptake of JMV3229 at 3 h.*

To gain more insight into JMV3229 internalization, co-stainings were performed with other fluorescent markers for subcellular components such as the nucleus, endosomes, and lysosomes. The results showed that JMV3229 was mostly co-localized with an endosomal marker at 3 h (Figure **III.3.2.2 B**) and with a lysosomal marker at 16 h (Figure **III.3.2.2 *C***). Similar data were obtained for the L-counterpart JMV4228. This indicated an endosomal uptake of these oligomers followed by a lysosomal accumulation.

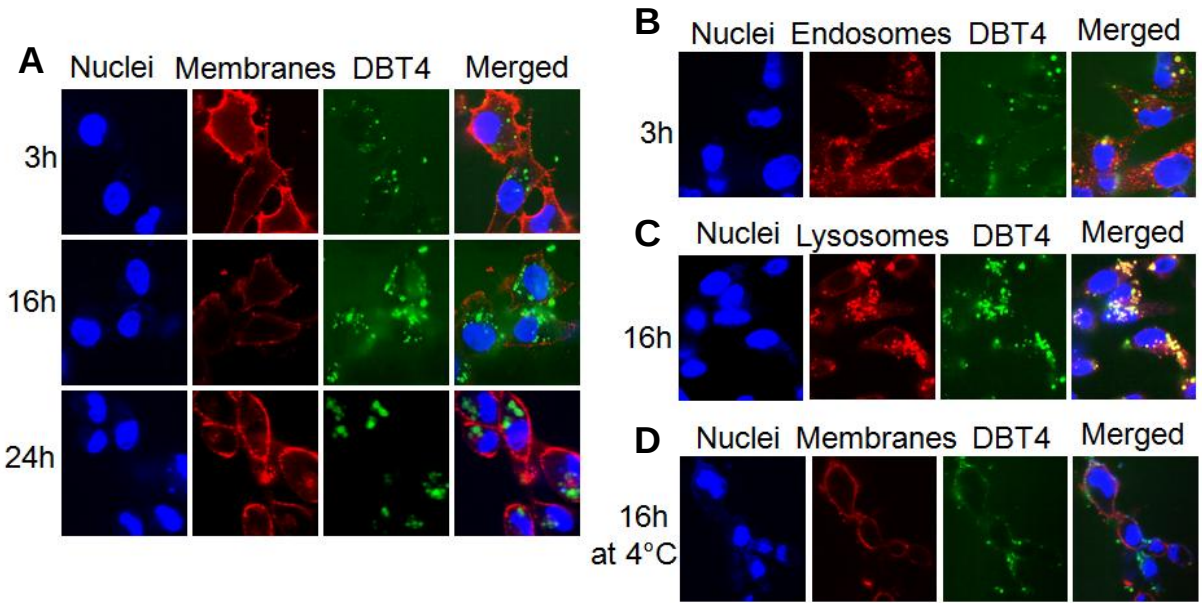

Figure III.3.2.2 *Confocal microscopy images of living MDA-MB-231 breast cancer cells incubated with JMV3229 compound at 10^{-5} M concentration. Images are representative of at least 3 independent experiments.* ***A)*** *Distribution of JMV3229 after 3, 16, and 24 h of incubation at 37°C.* ***B)*** *Co-localization of JMV3229 with the endosomal marker at 3 h at 37°C.* ***C)*** *Co-localization of JMV3229 with the lysosomal marker at 16 h at 37°C* ***D)****. Distribution of JMV3229 at 4°C and co-localization of the oligomers with the membrane marker.*

III.3.2.3 Toxicity of the DBT oligomers

The cytotoxicity of this new class of molecules was also determined in MDA-MB-231 cells by using MTT viability assay (Figure **III.3.2.3** and Materials and Methods). After a 5 day-incubation, these compounds exhibited no significant effect on the cell viability at 10^{-5} M concentration. These results indicated that oligoDBTs could be safely used as vectors for cell drug delivery.

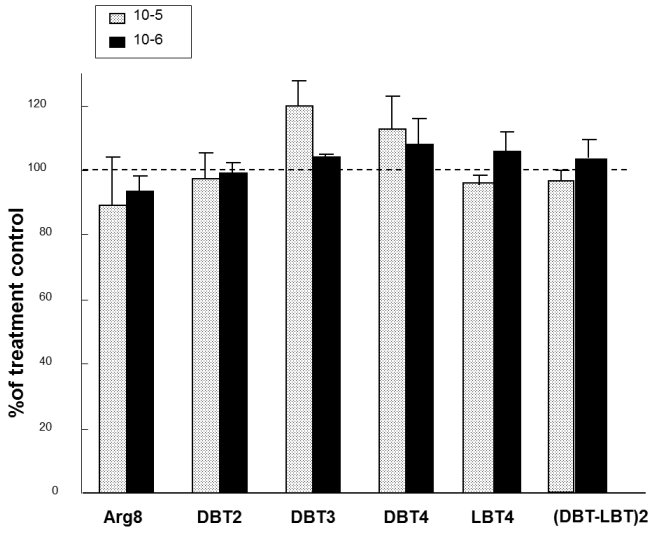

Figure III.3.2.3 *MTT cell viability assay. Cytotoxicity of compounds after a 5-day incubation at a concentration of 10^{-5} or 10^{-6} M. Values are mean ± SD of three independent experiments performed in triplicates. Values are expressed as a percentage of control cells incubated with vehicle alone (1% DMSO).*

III.3.2.4. Cellular uptake of DBT oligomer by different cell lines

To assess the capacity of DBT oligomers to be internalized by different cell lines we performed internalization tests with prostate, colon, osteosarcome and breast (2 types) cancer cell lines (Figure **III.3.2.4**). The internalization was studied by total fluorescence emission measurement. The same pattern of internalization as that of MDA-MB-231 was observed for the other tested cell lines. DBT and LBT tetramers were internalized in the same manner by all cell lines and they were both better internalized than the potent polycationic CPP Arg_8.

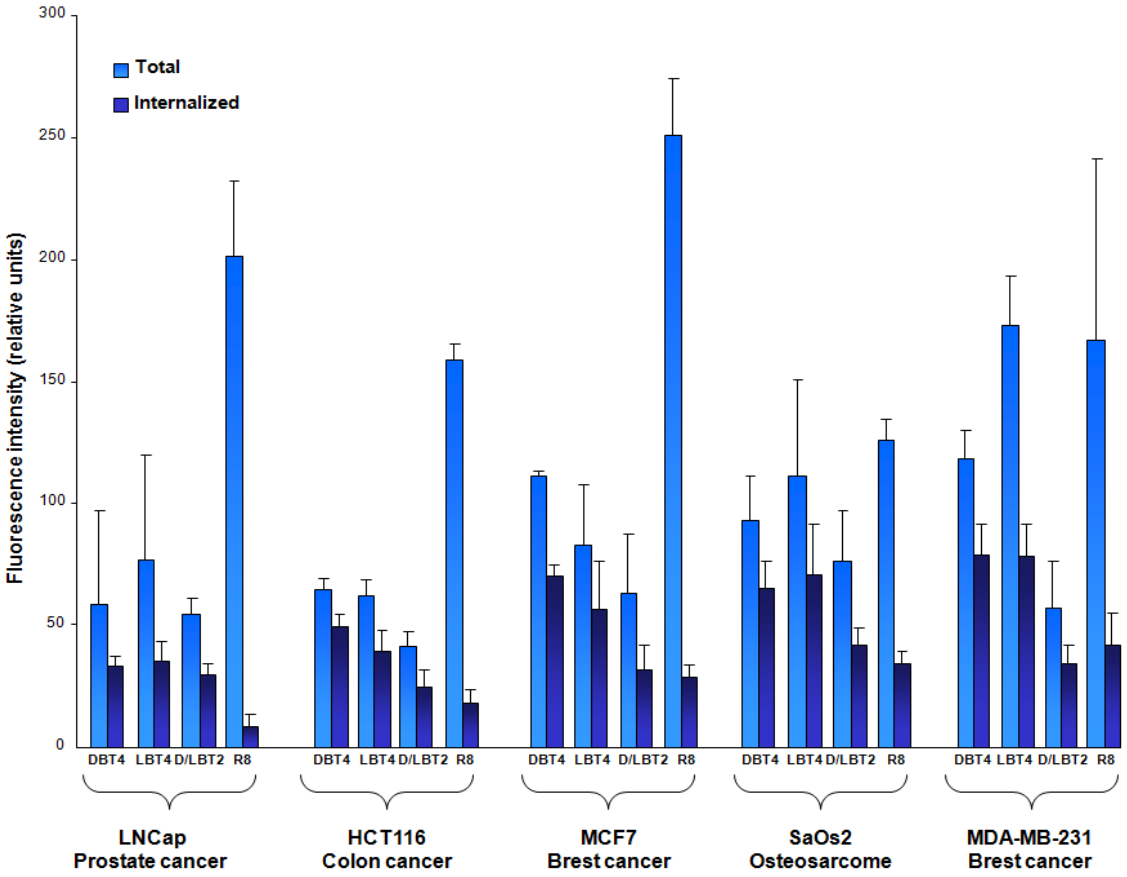

Figure III.3.2.4. *Uptake of Arg_8 and DBT oligomers in different cell lines. Total - cells were not treated by trypsin before fluorescence measurements. Internalized - cells were treated by trypsin before fluorescence measurements.*

III.3.2.5 Discussion

Altogether, these data indicate the ability of our new class of CPNPs to target the endolysosomal pathway. Although most of the initial drug delivery studies aimed to avoid lysosomal addressing to prevent subsequent drug degradation, more recent studies demonstrated the relevant clinical utility to target this compartment for drug delivery in the treatment of lysosomal storage diseases, Alzheimer's disease, and cancer.[9] The described by us CPNPs are characterized by their lack of charge, small size, well defined secondary structure, high intracellular uptake and resistance to proteases. Their mechanism of internalization is non-specific receptor dependent and probably implicates an interaction with the hydrophobic regions of the cell membrane like the lipid rafts. While a promising candidate for vectorization of biologically

relevant cargos, the DBT oligomers probably share similar drawbacks with the CPPs like the lack of cell specificity.

III.3.3 Internalization of chimeric OligoDBT-OligoArg oligomers tagged by fluorescein

Confocal laser scanning microscopy (CLSM) (see section **I.2.3**) analyses were performed in living MCF7 cells to assess internalization and intracellular distribution of compound Fl-Ahx-$(DBT)_4$-Ahx-$(Arg)_9$-NH_2 (JMV4569). These experiments were associated with a kinetic study of the oligomer internalization (Figure **III.3.3 A**). The experiments were performed at a very low concentration of 10^{-7} M at 37°C. At the 3th hour we observed internalization of the compound with more important accumulation at the 16th hour. Co-staining with a membrane (lipid-raft labelling) and nucleus markers indicated that the compound was not held in the lipid membrane at 37°C. At the same concentration (10^{-7} M) no internalization of the potent CPP $(Arg)_9$ was observed after 16 hours (Figure **III.3.3 B)**

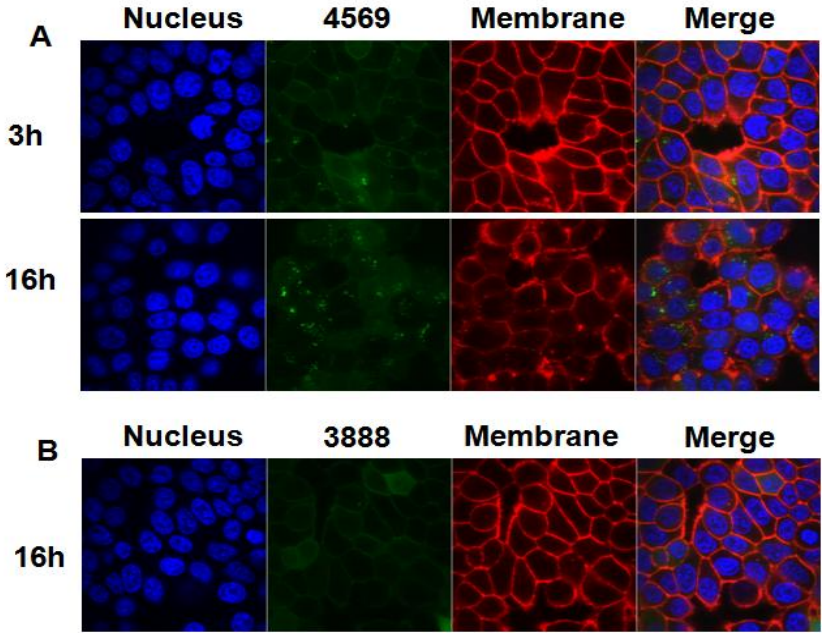

Figure III.3.3 *Confocal microscopy images of living MCF7 breast cancer cells incubated with JMV4569 or JMV3888 at 10^{-7} M. Images are representative of at least 3 independent experiments.* ***A)*** *Distribution of JMV4569 after 3 and 16 hours of incubation at 37°C and co-localization with membrane marker.* ***B)*** *Distribution of JMV3888 after 16 hours of incubation at 37°C and co-localization with membrane marker.*

These data shows the high potential of these chimerical compounds as CPNP. These oligomers will be tested for their ability to deliver SiRNA via a non-covalent strategy. Even though these results are encouraging much work remains to be done as total fluorescence emission measurements of the internalization efficiency and *in vitro* tests for SiRNA internalization.

III.3.4 Internalization of AMPA oligomers tagged by fluorescein

CLSM analyses (see section **I.2.3**) were performed in living MDA-MB-231 cells to assess internalization and intracellular distribution of compound Fl-O_2Oc-r-$(AMPA)_4$-NH_2 (JMV4497). These experiments were associated with a kinetic study of

the oligomer internalization (Figure **III.3.4 A**). The experiments were performed at a concentration of 10^{-5} M at 37°C. At 3 hours we observed internalization of the compound with more important accumulation at 16 hours. Co-staining with a membrane marker (lipid-raft labelling) indicated that the compound was not held in the lipid membrane. At 16 hours a big part of the internalized compound was co-localized with the lysosome marker (Figure **III.3.4 B**).

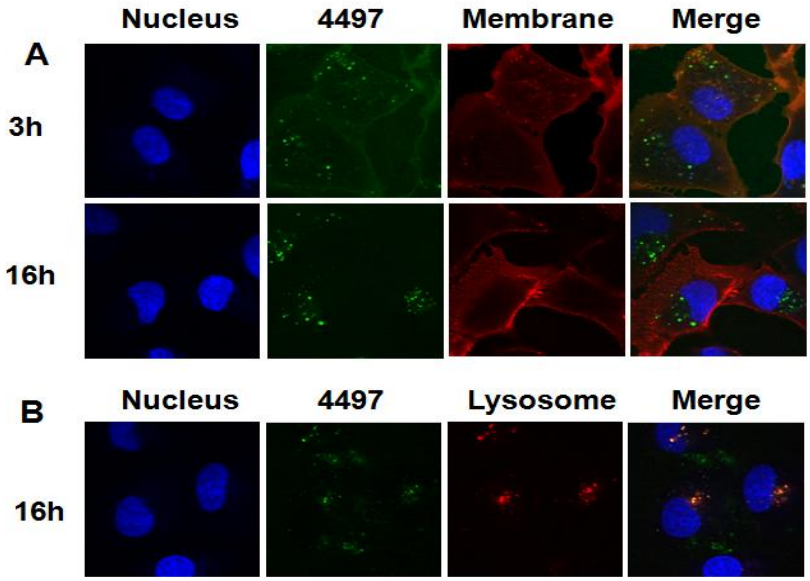

Figure III.3.4 *Confocal microscopy images of living MDA-MB-231 breast cancer cells incubated with compound JMV4497. Images are representative of at least 3 independent experiments.* ***A)*** *Distribution of JMV4497 after 3 and 16 hours of incubation at 37°C and co-localization with membrane and nucleus marker.* ***B)*** *Distribution of JMV4497 after 16 hours of incubation at 37°C and co-localization with lysosome marker.*

These data suggest that $(AMPA)_4$ like the $(DBT)_4$ could be used as a CPNP. This compound shares the same non-cationic hydrophobic nature and well organized structure as $(DBT)_4$. Both compounds $(DBT)_4$ and $(AMPA)_4$ possess four aromatic unites that are probably an important feature for their internalization. Similarly to the $(DBT)_4$, $(AMPA)_4$ is delivered to the lysosomes and thus could be used to deliver drugs for the treatment of cancer (see section **III.5**), lysosomal storage disease and Alzheimer's disease. Moreover, $(AMPA)_4$ is characterized by its even smaller size than that of $(DBT)_4$.

III.4. A Straightforward approach for cellular-uptake quantification of CPPs and CPNPs

III.4.1 Methodology

Most studies of CPPs or CPNPs internalization efficiency are performed by fluorescence emission measurement, FACS display or confocal microscopy (see section **I.2.3**). All these techniques share the same disadvantage – they cannot quantify the exact amount of compound internalized per cell or the intracellular concentration. Most of the studies are made in comparative manner. New CPP or CPNP fluorescence emission is compared to a well-known CPP like TATp or oligoArg. To confront this problem Burlina et al. developed a highly reproducible quantification method based on MALDI-TOF MS to straightforward measure the

concentration of the internalized peptides (see section. **I.2.3**).[10] Taking advantage from our group experience with proteomics studies we designed an improved method that does not require any separation or chromatographic steps. Our group has previously reported an original approach in which peptides derivatized by α-cyano-4-hydroxycinnamic acid (HCCA) were readily identified by selective enhancement and discrimination of their MALDI TOF MS signals in a neutral matrix, such as α-cyano-4-hydroxycinnamic methyl ester (HCCE).[75] The HCCA moiety is an UV absorbing tag that has the property to dramatically enhance the relative MALDI TOF MS signal strength of the compounds it is attached to. The HCCE matrix has the property to reduce the MS signal strength of all the compounds except the ones that are tagged by the HCCA moiety. This combination (HCCA tag and HCCE matrix) enabled us to discriminate signals induced by peptides of interest that were present in low concentrations from those of unlabelled more abundant peptides. To quantify the compounds after their internalization we synthesized deuterated 'heavy' HCCA(D_4) (Figure **III.4.1-1)**.

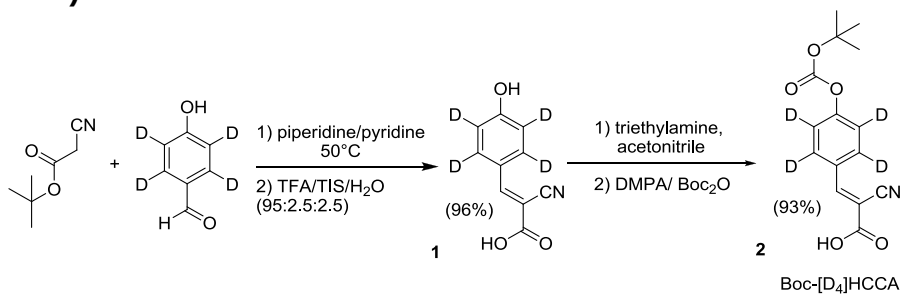

Figure III.4.1-1 *Synthesis of deuterated HCCA(D_4) protected by Boc group on the hydroxyl function*

CPPs/CPNPs were prepared by microwave assisted solid-phase synthesis on RA PS resin coupled with light (D_0) or heavy (D_4) HCCA on their N-terminus through an aminohexanoic acid (Ahx) spacer (Figure **III.4.1-2 A**). The ability of these compounds to penetrate cells was readily determined by comparison of the MS signals induced by tagged compounds with those of the over-represented untagged materials. Thus, no separation procedure was required. The material that penetrated cells was quantified by comparison of the signals due to the light tag with the corresponding signals of the deuterated heavy HCCA. The methodology (described in Figure **III.4.1-2 B**) was validated by using four different compounds: the two widely used CPPs penetratin and nona-arginine $(Arg)_9$ (see section **I.2.1**), our potent CPNP $(DBT)_4$ (described in section **III.3.2)** and a tripeptide (FAK) as a negative control (Table **III.4.1**).

Initially to prove our concept we checked that HCCA-tagged peptides could be detected in a crude cell lysate by MALDI-TOF MS up to a 10^{-10} M, which corresponds to the possible concentration of internalized compound in the sample after cell lysis.[10] To highlight the HCCE/HCCA matrix-discrimination effect, N-terminal acetylated peptides were prepared and mixed at different concentrations along with HCCA-tagged peptides in a crude cell lysate. Equimolar mixtures of HCCA-CPPs and Ac-CCPs diluted in water/acetonitrile were mixed in a cell lysate to afford a 5.10^{-6} M to 5.10^{-11} M concentration of each peptide species.
The samples were prepared either in an HCCA matrix or in a neutral HCCE matrix to assess the discrimination effect (see Figure **III.4.1-3**). The MALDI-TOF spectra were quite clean, and very few signals were observed from the cell lysate or the buffer. HCCA tagged peptides were still readily detected at 5.10^{-9} M in the HCCA matrix and

5.10^{-10} M in the HCCE matrix. Ac-CPPs with the exception of Ac-$(DBT)_4$-NH_2 were not detected at a concentration of 5.10^{-8} M in HCCE matrix (Figure **III.4.1-3**)

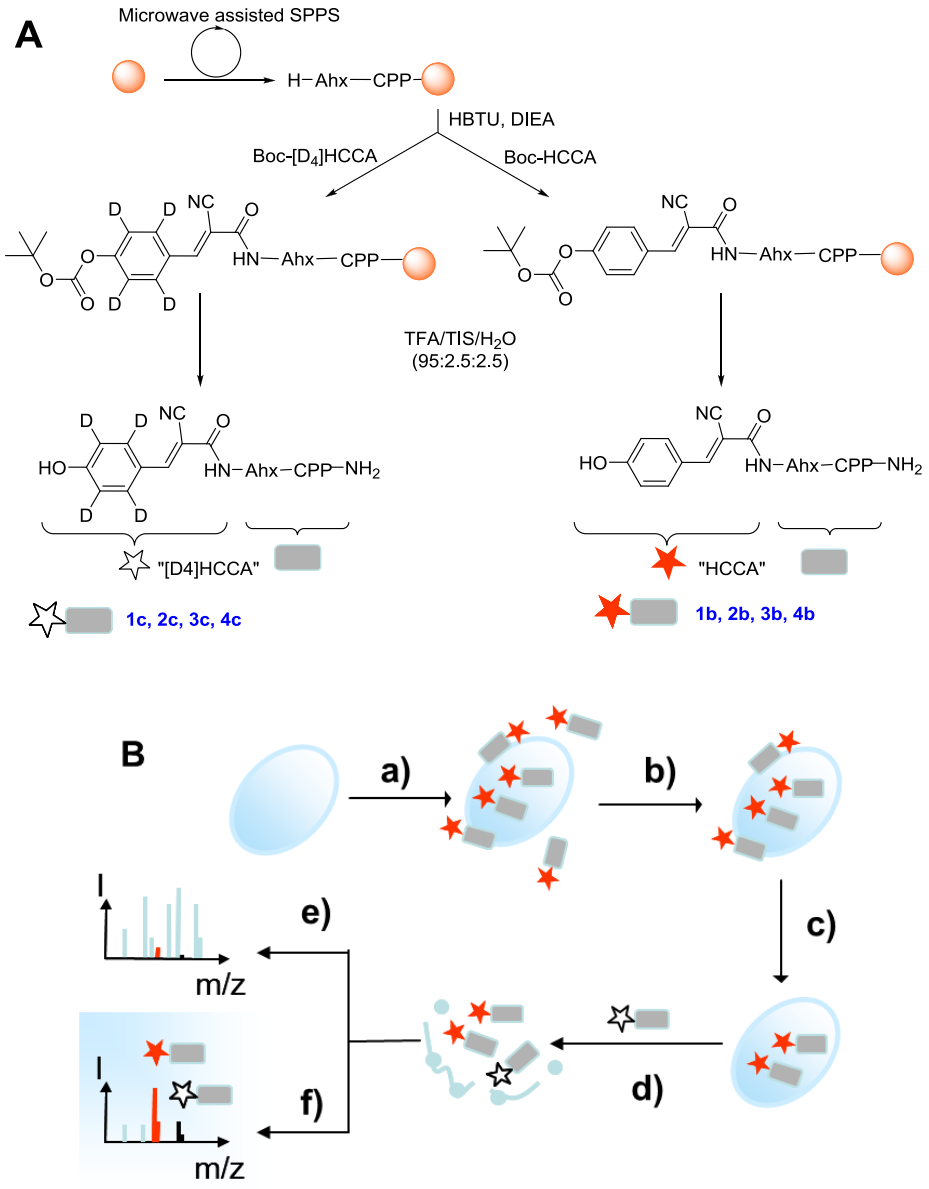

Figure III.4.1-2 A) *Synthesis of light (D_0) and heavy (D_4) HCCA-tagged CPPs.* ***B)*** *Strategy for the direct quantification of the cellular uptake of CPPs (and a CPNP) by MALDI-TOF MS by using the HCCA/HCCE discrimination effect: a) incubation of cells with the HCCA-tagged CPP; b) washing step; c) enzymatic stripping of the cell membrane; d) lysis of cells, followed by the addition of a precise amount of the deuterated-HCCA-tagged CPP as an internal standard; e) MALDI-TOF analysis of the whole cell lysate in the HCCA matrix; f) MALDI-TOF analysis of the whole cell lysate in the "neutral" HCCE matrix. The HCCA/HCCE signal-discrimination effect enables the enhancement of the CPP/CPNP signal in a complex mixture. The internalized CPP can be quantified on the basis of the ratio between the $[M+H]^+$ peaks of the deuterated and nondeuterated HCCA-tagged CPP.*

Table III.4.1 *Compounds tested for cellular uptake. Mass spectrometry intracellular uptake concentration results.*

Compounds	Id	N-term	Sequence	m/z $[M+H]^+$	m/z $[M+Na]^+$	Intracellular uptake	Intracellular Uptake*
Penetratin	**1a** **1b** **1c**	**Ac-** **HCCA-** **HCCA(D_4)-**	-Ahx-RQIKIWFQNRRMKWKK-NH_2	2400.4 2529.4 2533.4	2422.4 2551.4 2555.4	**11.21 µM**	**3 3.5 µM**
$(Arg)_9$	**2a** **2b** **2c**	**Ac-** **HCCA-** **HCCA(D_4)**	-Ahx-RRRRRRRRR-NH_2	1578.0 1707.0 1711.0	1600.0 1729.0 1733.0	**11.08 µM**	**4 4.5 µM**
$(DBT)_4$	**3a** **3b** **3c**	**Ac-** **HCCA-** **HCCA(D_4)**	-Ahx-$(DBT)_4$-NH_2	1109.3 1238.3 1242.3	1131.3 1260.3 1264.3	**8.7 µM**	-
FAK, Negative control	**4a** **4b** **4c**	**Ac-** **HCCA-** **HCCA(D_4)**	-Ahx-FAK-OH	520.3 649.3 653.3	542.3 671.3 675.3	**none**	-

**Intracellular uptake concentration reported in the publication of Burlina et al.[10] using biotin labelled analogues*

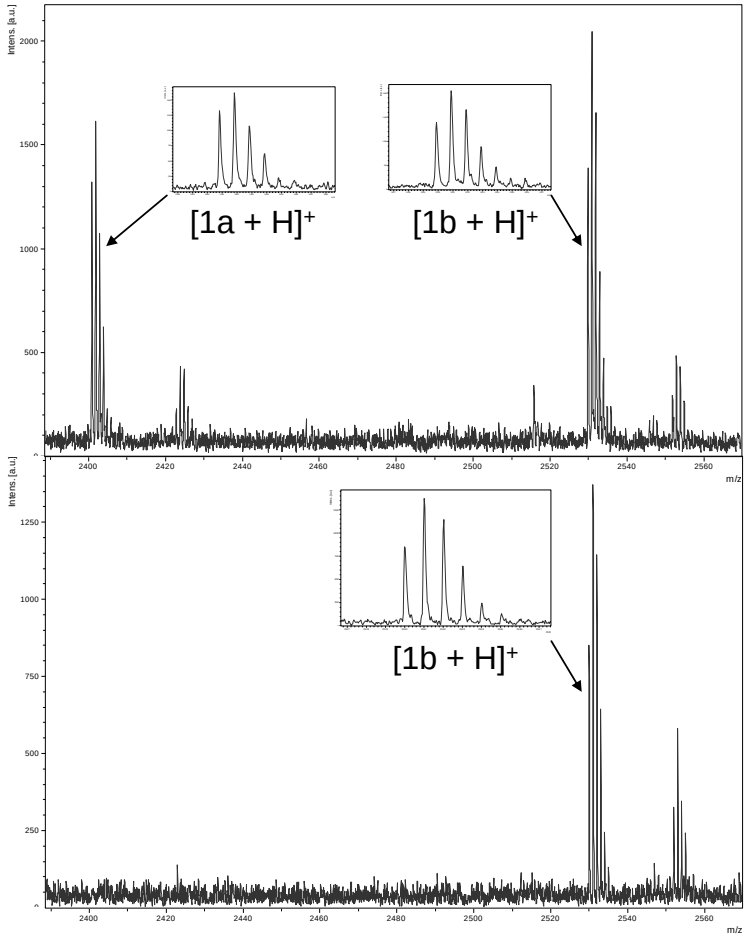

Figure III.4.1-3 *MALDI-TOF MS spectra of equimolar mixtures of Ac- and HCCA-penetratin (5.10^{-8} M each) in cell lysate. Above spectrum was obtained in HCCA matrix and the down spectrum in HCCE matrix.*

Generally, the HCCA-discriminating effect increased when the concentration of the analyte (HCCA-CPP or Ac-CPP) decreased. This phenomenon makes HCCA tagging a method of choice for the detection and quantification of low abundance compounds in a complex mixture. Furthermore, the baseline of spectra obtained in the HCCE matrix was flatter than that of spectra obtained in the HCCA matrix. This

flat baseline is particularly favourable for the purpose of peak integration and quantification. The expected discrimination effect was less significant with the $(DBT)_4$ sequence: the intensity of the Ac-Ahx-$(DBT)_4$-NH_2 $[M+Na]^+$ peak at m/z 1131.3 was only two times lower than that of the HCCA-Ahx-$(DBT)_4$-NH_2 $[M+Na]^+$ peak at m/z 1260.4 in the HCCE matrix (see Figure **III.4.1-4**) The DBT moiety is probably able to absorb UV light in a similar manner as that of the HCCA moiety.

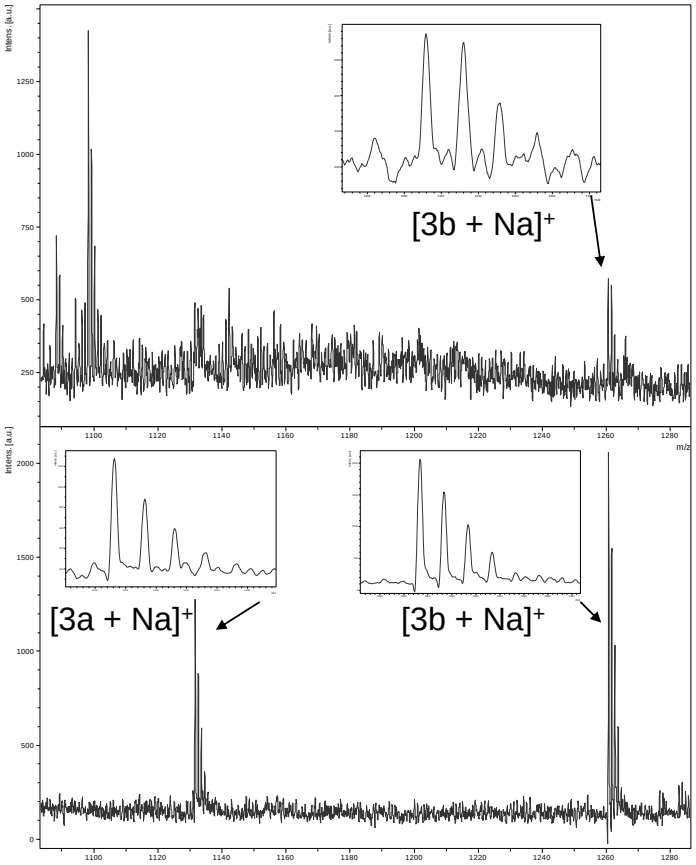

Figure III.4.1-4 *MALDI-TOF Mass spectra of equimolar mixtures of Ac- and HCCA-$(DBT)_4$ (5.10^{-8} M each) in cell lysate. The above spectrum was obtained in HCCA matrix and the down spectrum in HCCE matrix.*

Once that we confirmed that HCCA tagged CPP and CPNP could be detected in very low concentration in complex mixtures we moved to *in vitro* tests. Internalization experiments were performed on the MDA-MB-231 cell line according to the modified protocol described by Burlina et al.[10] (Figure **III.4.1-2 B**). The HCCA-tagged compounds 1b, 2b, 3b, and 4b were incubated at a concentration of 10 µM with 2.10^5 MDA-MB-231 breast cancer cells for 3 hours at 37℃. The biological samples were then split into two pools to be submitted or not to trypsin stripping of cell-membrane-bound CPPs (see section **I.2.3**). The cells were lysed for 20 minutes with lysis buffer containing 2-amino-2-hydroxymethylpropane- 1,3-diol (Tris) and ethylenediaminetetraacetic acid (EDTA), and the membrane fragments were removed by centrifugation. The supernatant was collected and added to known amounts of the corresponding deuterated CPP. In this way, both internalized CPPs and internal standards ($[D_4]$HCCA-labelled CPPs) were exposed to degradation by proteases remaining in the medium.

The samples were deposited directly on the MALDI probe, mixed with a HCCA or neutral HCCE matrix, and analysed. Spectra were averaged for statistical sampling from a hundred laser shots recorded on different spots of the deposit. Figure **III.4.1-5** gives a good idea of the HCCA/HCCE discrimination effect on HCCA tagged CPPs. Acetylated and HCCA-tagged Penetratin (1a and 1b respectively) were submitted to internalization tests. They were both analysed in HCCA or HCCE matrix. Compound 1a was only hardly detectable in the cell lysate in HCCA matrix, while 1b was detectable in HCCA matrix and represented the major MS peak in HCCE matrix.

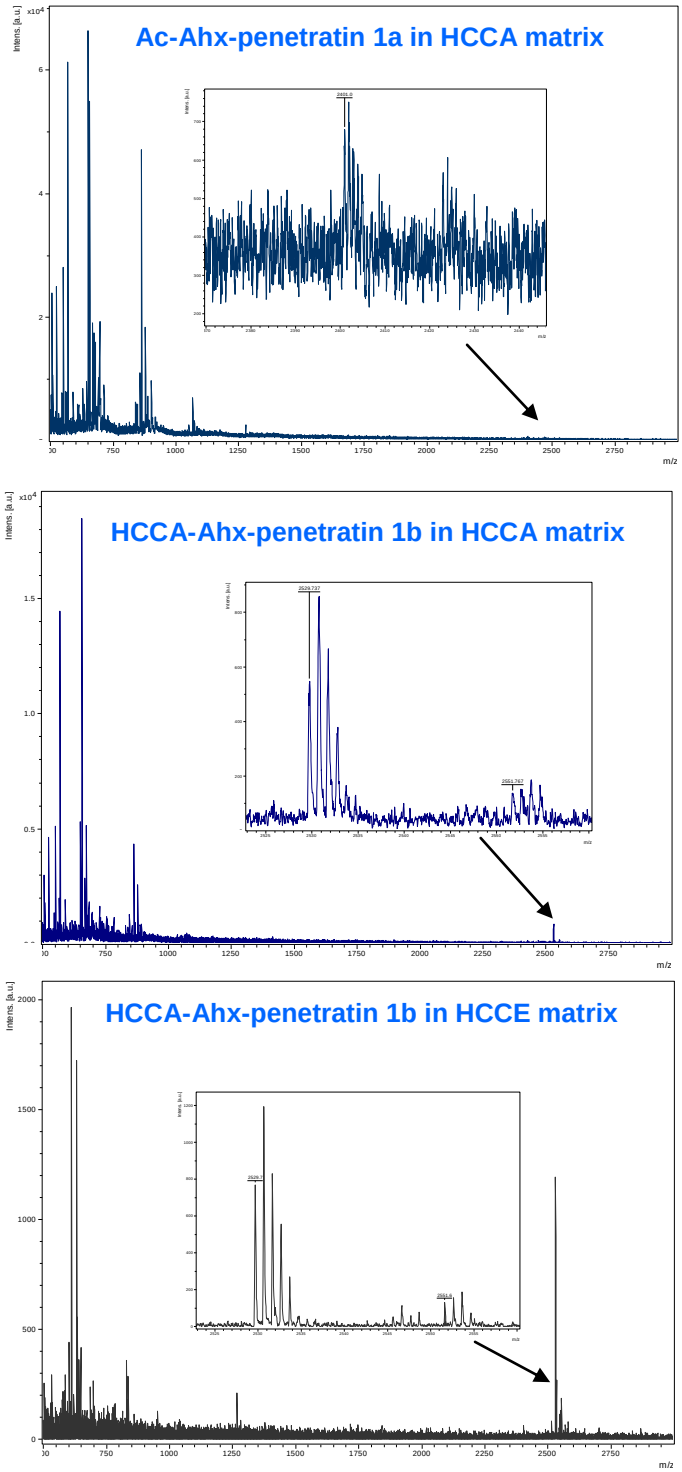

Figure III.4.1-5 *MALDI TOF MS spectra of internalized Ac-Ahx-penetratine and HCCA-Ahx-penetratine. Samples were obtained in HCCA or HCCE matrix.*

The spectra obtained in HCCE matrix were used for the peak integration and quantification as they gave better signal to noise ratio. The areas of all isotope peaks of the light and heavy compounds corresponding to mono-protonated compounds $[M+H]^+$ were used for quantification. In the case of DBT derivatives (Table **III.4.1**, 3b and 3c), the isotope peaks of the sodiated ions $[M+Na]^+$ were chosen for quantification, as they are more intense than those of the mono-protonated ions. The mass increment of 4 Da between the compounds tagged with light HCCA and heavy, isotopically labelled $[D_4]$ HCCA gave two isotopic distributions that partially overlapped at the edges. For example, the ion at m/z 2533.6 in Figure **III.4.1-6** was produced by the cumulated contributions of the light-HCCA tagged molecule containing four naturally occurring ^{13}C atoms (very tiny abundance) and of the heavy-$[D_4]$ HCCA tagged counterpart (major intensity). The ratio of these two isotopic contributions was estimated and taken into account in all results after calculation and integration of the isotopic patterns by using the algorithm SNAP (Sophisticated Numerical Annotation Procedure) from the software FlexAnalysis. This algorithm helped us to determine and separate the exact isotopic pattern of molecules tagged with light and heavy HCCA, even when overlapping occurred.

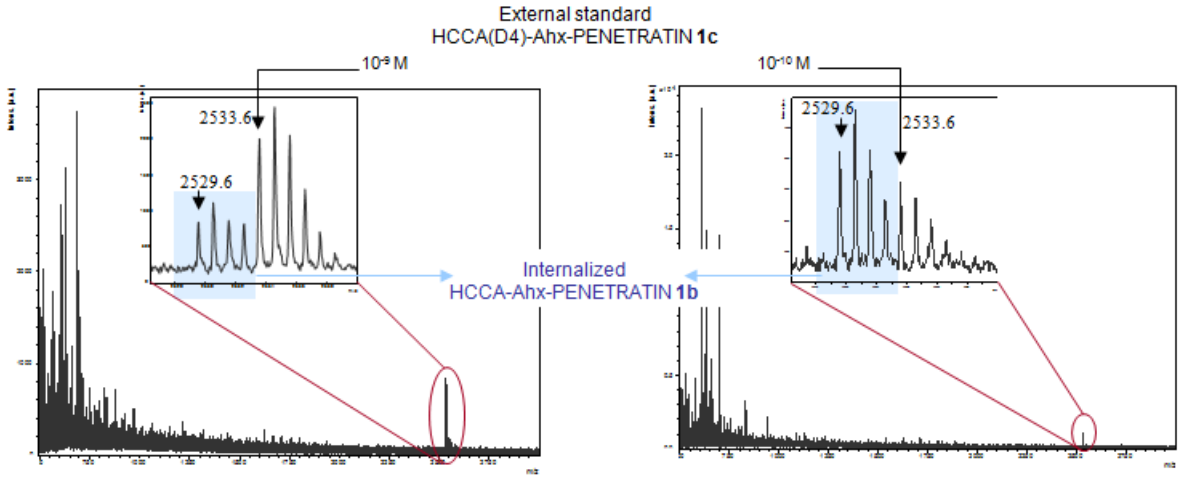

Figure III.4.1-6 *Quantification of HCCA-Ahx-penetratin (1b) through the addition of its deuterated counterpart at a concentration of 10^{-9} or 10^{-10} M (samples were prepared in an HCCE matrix).*

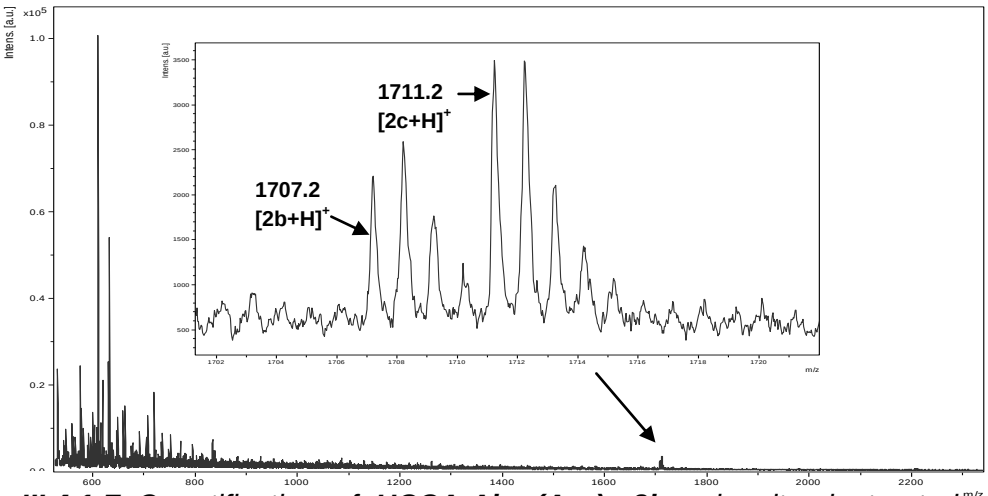

Figure III.4.1-7 *Quantification of* ***HCCA-Ahx-(Arg)$_9$ 2b*** *using its deuterated counterpart introduced at 10^{-9} M concentration in the sample (samples were prepared in HCCE matrix)*

The absolute quantification was more precise when light and heavy compounds displayed similar intensities and thus similar concentrations in the sample.

A logarithmic range of concentrations of the deuterated standards was used to determine accurate concentration values. Each CPP concentration was calculated by using the more accurately known concentration values of the [D_4]HCCA-tagged compound.

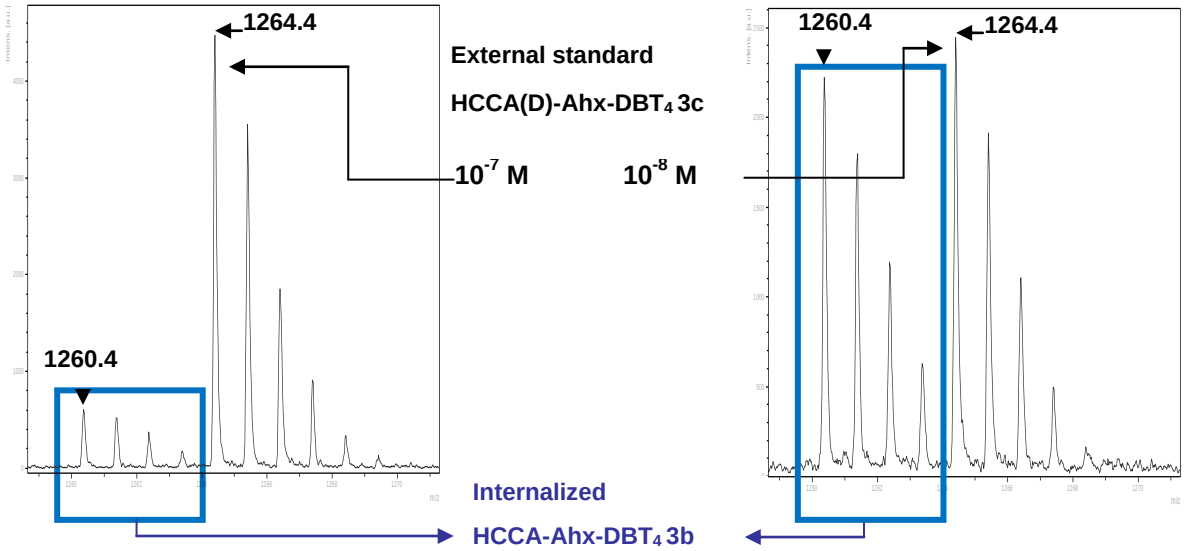

Figure III.4.1-8 *Quantification of HCCA-Ahx-$(DBT)_4$ (3b) through the addition of its deuterated counterpart at a concentration of 10^{-7} or 10^{-8} M (samples were prepared in an HCCE matrix).*

Quantification was performed with ratios varying from 0.1:1 to 4:1. The analysis of several deposits of the same cell lysate yielded highly reproducible results (a maximum of 10% variation between samples). The analysis of different deposits of various biological samples (cell lysates with a variable number of MDA-MB-231 cells) also showed good reproducibility. By using this protocol, we calculated the intracellular concentration of the four compounds (Table **III.4.1**). A concentration of 1.21 µM for the penetratin derivative 1b was found (see the spectrum used for quantification on Figure **III 4.1-6**) and 1.08 µM for the $(Arg)_9$ derivative 2b (see the spectrum used for quantification on Figure **III 4.1-7**). These two values are in full accordance with the previously reported MS quantification of N-terminally biotinylated CPPs. As expected, the negative-control peptide 4b was not detected in the cell lysate; the internal standard 4c was detected at a concentration of 10^{-8} M. The highest intracellular concentration (8.70 µm) was found for the labelled $(DBT)_4$ CPNP 3b (see the spectrum used for quantification on Figure **III 4.1-8**). This value corresponds to an absolute amount of 13.10^{-18} Mol in a single cell.

The experiments were repeated with the pool of trypsin untreated cells. A comparison of the two series reflected the proportion of the CPP (or CPNP) that remained bound to the membrane. Depending on the CPP (or CPNP), the amount of internalized compounds was 10–100 times lower after trypsin treatment (Figure **III.4.1-9**). We should note that in the case of the CPNP $(DBT)_4$ this difference was less important probably due to its non-cationic character.

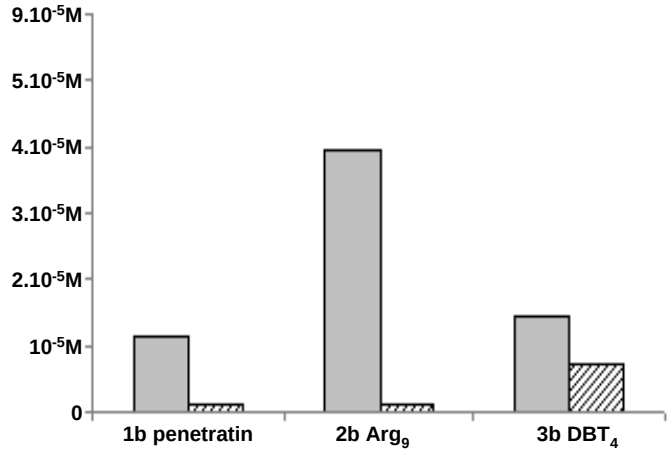

Figure III.4.1-9 *Amount of compounds detected after incubation of compounds* ***1b, 2b, 3b*** *with MDA-MB-231 cells and lysis of the cells. Stripped bars and gray bars correspond to cells submitted or not to five minutes trypsin treatment, respectively. Negative control* ***4b*** *is not presented in the figure as no peptide was detected.*

III.4.2 Discussion

We have described a straightforward and efficient method for the quantification of cell-penetrating compounds internalization. The originality of the methodology relies first on the use of the combination of HCCA as a UV-light-absorbing tag and the neutral HCCE matrix, which enabled the very sensitive detection of the compounds of interest by mass spectrometry even in complex biological samples, and second on the stable isotope labelling of such compounds for their reliable quantification. The procedure does not require any purification step, including biotin-based capture. The later is extremely important and makes this method one of the most simple and precise reported in the literature. Like some of the fluorescence emission measurement techniques, this method should be used in combination with confocal microscopy. This combination gives the possibility to determine the localization and the exact intracellular concentration of the CPP/CPNP. The results obtained with $(DBT)_4$ and $(Arg)_9$ are in complete agreement with the fluorescence-based assays reported in section **III.3** and further affirmed the importance of the DBT tetramer as a powerful CPNP.

III.5 Vectorization of pepstatine – *in vitro* inhibition of the Cathepsine D and anti-cancer activity

As mentioned in section **I.3,** Cathepsin D (CD) has complex role in the cancer development probably via its enzymatic activity inside the endosomes or the lysosomes but also as a ligand to a yet unknown extracellular receptor. Some groups have studied the inhibition of Cathepsin D *in vitro* by incubation of cancer cells with pepstatine. Even though pepstatine is a powerful transition state inhibitor of the CD, it had no effect on the cell growth. The lack of inhibitory activity should be attributed to the fact that pepstatine has very poor solubility in water and is unable to penetrate into the cells.[69] Thus, it appeared crucial to study the CD inhibition *in vitro* and *in vivo*

by vectorized pepstatine. Such study was of a considerable interest because it should allowed us to:

- Study the importance of CD enzymatic activity for the cancer development
- Prove that our set of CPNP is able to traffic biologically relevant cargos
- Find potent anti-breast cancer compounds

A perfect vector for the pepstatine is one that directs the compound to the endosomes and the lysosomes – the cell compartments where CD enzymatic activity is the most important. Thus oligo-AMPA and oligo-DBT have seemed particularly attractive candidates for the vectorization of the pepstatine because of their ability to deliver fluorescent dyes to the endosomes and the lysosomes (See sections **III.3.2 and III.3.4**).

III.5.1 CD vectorized inhibitors design

The first set of vectorized pepstatine inhibitors that we synthesized were the compounds Pepstatine-$(Arg)_9$-NH_2, Pepstatine-$(AMPA)_4$-NH_2 and Pepstatine-$(DBT)_4$-NH_2 (table **III.5.1 A**). As vectors, we used our CPNP $(AMPA)_4$ and $(DBT)_4$ (see sections **III.3.2** and **III.3.4**) and the well studied CPP nona-arginine. These compounds and all following CD inhibitors were synthesized by standard SPPS on RA PS resin by HBTU/DIEA activation (see Materials and Methods). From this first generation of vectorized CD inhibitors only Pepstatine-$(AMPA)_4$-NH_2 showed any toxicity *in vitro* while all compounds were active on the secreted CD enzyme. One of the possible explanations for the poor activity of Pepstatine-$(Arg)_9$-NH_2 could be the fact that this small peptide is internalized to the cytosol instead of the endosomes or the lysosomes. While promising, the Pepstatine-$(AMPA)_4$-NH_2 bioconjugate has a poor solubility which hampered the reproducibility of the biological results. Effectively, it is stated that one of the reasons for the low anti-tumoral activity of the potent pepstatine CD inhibitor *in vitro* or *in vivo* is its low solubility in water.[69] To overcome this problem we synthesized a new set of vectorized pepstatine analogues connected to a solubilizing moiety on their N-terminus. As a solubilizing moiety we used short polyethylene glycol linker 8-amino-3,6-dioxaoctanoic acid (O_2Oc) and polar D-amino acids residues like D-Asp, D-Lys and D-Arg. We used D-amino acids because of their resistance to protease degradation. These compounds are summarized on table **III.5.1 B**. All of these oligomers showed medium to high cytotoxicity with the exception of compound Ac-D-Asp-O_2Oc-pepstatine-$(AMPA)_4$-NH_2 which showed no toxicity at all. The most toxic compounds were JMV4463 (Figure **III.5.1**) and JMV4622. Encouraged by this result we synthesized a similar compound to JMV4463 but vectorized by $(DBT)_4$ instead of $(AMPA)_4$. To our surprise this bioconjugate was not toxic (table **III.5.1 C**). We also synthesized bioconjugates as negative controls that includes:

-Compounds JMV4564 and JMV4674 analogues of JMV4463 in which statine moieties were substituted by γ-Leu or γ-Ala. The hydroxyl groups of the statine moieties are crucial for the CD inhibition so these compounds were supposed to be lesser inhibitors of the CD and non-toxic or less toxic *in vitro*.

-Compounds JMV4456 and 4457, analogues of JMV4463 that are devoid of the important for the internalization CPNP $(AMPA)_4$ moiety. These compounds were designed to be good inhibitors of the isolated CD but non-toxic *in vitro*.

Lastly, we synthesized a set of fluorescently labelled vectorized CD inhibitors to study their internalization potency (Table **III.5.1 E**). The fluorescein tag was connected to the N-terminus of the compounds via a β-Ala moiety so we can avoid side reactions as the one reported by Subra et al.[74]

All the bioconjugates that have been synthesized, their cytotoxicity and CD inhibiton results are reported in Table **III.5.1**.

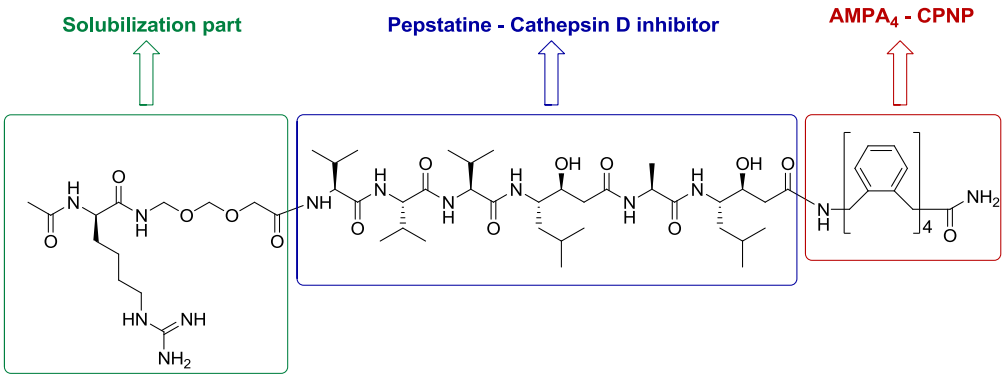

Figure III.5.1 *Compound JMV4463 – a bioconjugate composed of 3 distinctive parts. In red the CPNP $(AMPA)_4$ developed by our group, in blue the potent Cathepsin D inhibitor - pepstatine and in green a solubilizing moiety.*

Table III.5.1 *Summary of the Bioconjugates synthesized to study the vectorization of the pepstatine*

JMV Number	Compound	Cytotoxicity*	CD Inhibition**
A) First generation of vectorized pepstatine: Pepstatine-vector			
JMV2719	IsoVal-$(Val)_2$-Sta-Ala-Sta-$(AMPA)_4$-NH_2	Inconsistent results	Strong
JMV4216	IsoVal-$(Val)_2$-Sta-Ala-Sta-$(AMPA)_3$-NH_2	None	Strong
	IsoVal-$(Val)_2$-Sta-Ala-Sta-$(DBT)_4$-NH_2	None	Strong
	IsoVal-$(Val)_2$-Sta-Ala-Sta-$(Arg)_9$-NH_2	None	Strong
B) Second generation of vectorized pepstatine: Solubilizing moiety-Pepstatine-oligoAMPA			
JMV4461	Ac-D-Lys-O_2Oc-$(Val)_3$-Sta-Ala-Sta-$(AMPA)_4$-NH_2	High	Strong
JMV4462	Ac-D-Lys-O_2Oc-$(Val)_3$-Sta-Ala-Sta-$(AMPA)_5$-NH_2	High	Strong
JMV4463	Ac-D-Arg-O_2Oc-$(Val)_3$-Sta-Ala-Sta-$(AMPA)_4$-NH_2	High	Strong
JMV4464	Ac-D-Arg-O_2Oc-$(Val)_3$-Sta-Ala-Sta-$(AMPA)_5$-NH_2	High	Strong
JMV4622	H-D-Arg-$(Val)_3$-Sta-Ala-Sta-$(AMPA)_4$-NH_2	High	Strong
JMV4623	Ac-D-Arg-D-Arg-O_2Oc-$(Val)_3$-Sta-Ala-Sta-	Medium	Strong

	$(AMPA)_4$-NH_2		
JMV4624	Ac-O_2Oc-O_2Oc-$(Val)_3$-Sta-Ala-Sta-$(AMPA)_4$-NH_2	Medium	Strong
JMV4625	Ac-D-Asp-O_2Oc-$(Val)_3$-Sta-Ala-Sta-$(AMPA)_4$-NH_2	None	Strong
C) Second generation of vectorized pepstatine: Solubilizing moiety-Pepstatine-oligoDBT			
JMV4630	Ac-D-Arg-O_2Oc-$(Val)_3$-Sta-Ala-Sta-$(DBT)_4$-NH_2	None	Strong
D) Negative controls - compounds that are supposed to be less toxic or non-toxic *in vitro*			
JMV4215	IsoVal-$(Val)_2$-γ-Leu-Ala-γ-Leu-$(AMPA)_4$-NH_2	None	Medium
JMV4563	Ac-D-Lys-O_2Oc-$(Val)_3$-γ-Leu-Ala-γ-Leu-$(AMPA)_4$-NH_2	Medium	Medium
JMV4564	Ac-D-Arg-O_2Oc-$(Val)_3$-γ-Leu-Ala-γ-Leu-$(AMPA)_4$-NH_2	Medium	Medium
JMV4674	Ac-D-Arg-O_2Oc-$(Val)_3$-γ-Ala-Ala-γ-Ala-$(AMPA)_4$-NH_2	None	None
JMV4566	Ac-D-Lys-O_2Oc-$(Val)_3$-Sta-Ala-Sta-NH_2	None	Strong
JMV4567	Ac-D-Arg-O_2Oc-$(Val)_3$-Sta-Ala-Sta-NH_2	None	Strong
E) Fluorescently labelled compounds for internalization testes			
JMV4626	Fl-β-Ala-D-Arg-O_2Oc-$(Val)_3$-Sta-Ala-Sta-$(AMPA)_4$-NH_2	None	Strong
JMV4629	Fl-β-Ala-D-Arg-O_2Oc-$(Val)_3$-Sta-Ala-Sta-$(DBT)_4$-NH_2	None	Strong
JMV4631	Fl-β-Ala-D-Arg-O_2Oc-$(Val)_3$-Sta-Ala-Sta-NH_2	None	Strong
JMV4632	Fl-β-Ala-D-Arg-O_2Oc-$(Val)_3$-Sta-Ala-Sta-$(AMPA)_5$-NH_2	None	Strong
JMV4659	Fl-Ahx-D-Arg-O_2Oc-$(Val)_3$-Sta-Ala-Sta-$(AMPA)_4$-NH_2	None	Strong

* Cytotoxicity is classified as: **High** – IC_{50} of the cell growth in the range of 10^{-6} M to 10^{-5} M, **Medium** IC_{50} of the cell growth in the range of 10^{-5} M to 5. 10^{-5} M, **None** IC_{50} of the cell growth higher than 5.10^{-5}

** CD inhibition is classified as: **Strong** - residual CD proteolytic activity between 0 and 20%, **Medium** residual CD proteolytic between 20 and 60%, **None** residual CD proteolytic activity between 60 and 100%,

III.5.2. Test for inhibition of the isolated CD enzyme

Our first task was to asses if the vectorized pepstatine analogues have kept their ability to inhibit CD. Figure **III.5.2-1** shows the remaining proteolytic activity of the CD after incubation with different inhibitors and negative controls calculated by the method described in section **I.3.2**. All the compounds that possess the typical pepstatine moiety (JMV4567, 4463, 4626 and 4630) have high inhibition activity. In fact they seem to inhibit CD with higher efficiency than the simple pepstatine. This should be attributed to their better solubility in water. Compound JMV4564 with

statine moieties substituted by γ-Leu showed an intermediate inhibition, while compound JMV4674 in which the statine moieties were substituted by γ-Ala exhibited practically no inhibition. These results should be explained by the fact that pepstatine is a transition-state inhibitor of the CD in which the hydroxyl function of the statine residues were expected to give a tight interaction with the enzyme.

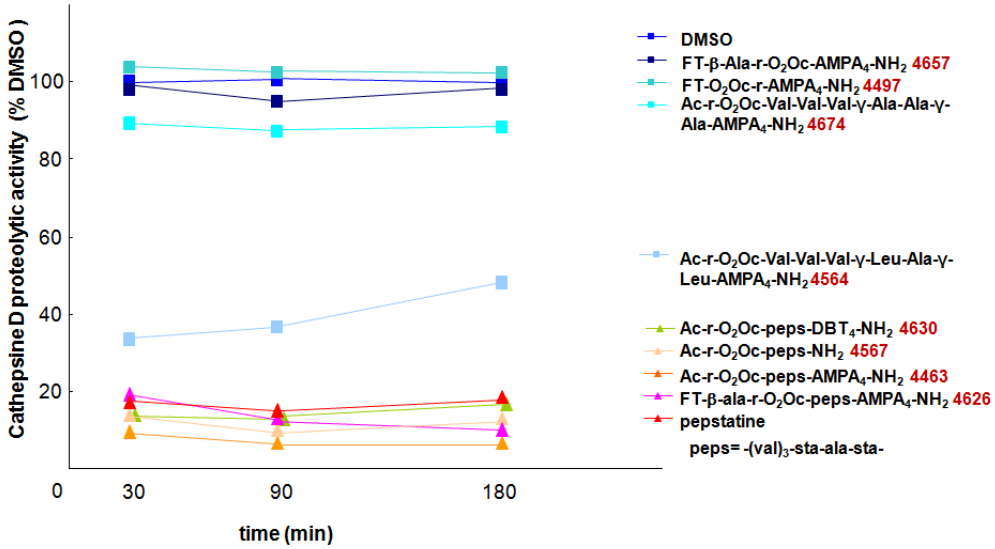

Figure III.5.2-1 *Remaining proteolytic activity of CD incubated with different inhibitors and negative controls at 10^{-5} M. As control we used 1 % DMSO solution in H_2O.*

These two compounds are very important negative controls because they are supposed to show reduced toxicity compared to JMV4463 during the *in vitro* experiments. Compounds JMV4497 and JMV4657 devoid of a pepstatine moiety, also tested as negative controls, did not show any inhibition of the CD activity. Proteolytic activity of the CD after incubation at 10 µM with the second generation of vectorized pepstatine derivatives (Table **III.5.1-1 B**) is reported in Figure **III.5.2-2**. The solubilizing moieties attached to the N-terminus of JMV2719 to produce the second generation of inhibitors did not affect the CD inhibition.

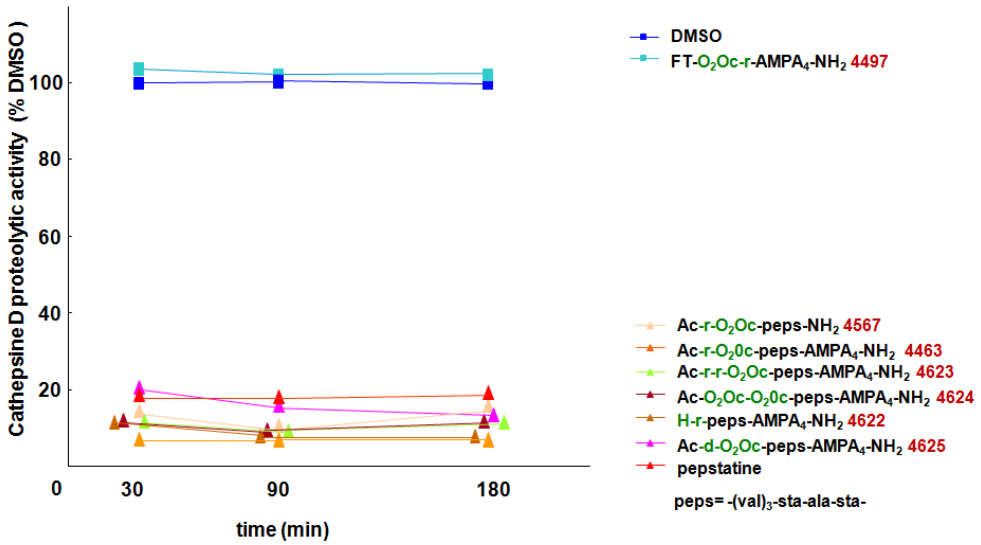

*Figure **III.5.2-2** Remaining proteolytic activity of the CD after incubation with the second generation of vectorized pepstatine derivatives at 10^{-5} M (table **III.5.1-1 B**). The solubilizing moieties attached to the N-terminus did not diminish the CD inhibition by the pepstatine moiety. As control we used 1 % DMSO solution in H_2O.*

These data showed that neither attachment of an oligo-AMPA or oligo-DBT as CPNP at the C-terminus of pepstatine nor the introduction of hydrophilic moieties or fluorescent dyes at the N-terminus diminish its ability to inhibit CD. However, any modifications of the pepstatine gave inhibitors with lower efficiency. The ability of all the tested compounds to inhibit CD is summarized in Table **III.5.1**.

III.5.3. *In vitro* tests for cytotoxicity

As mentioned in **III.5.1** our first positive results for cytotoxicity *in vitro* were obtained with compound JMV2719 but probably due to its poor solubility these results were inconsistent. To confront this problem we synthesized a series of compounds derivatized with solubilizing moieties on their N-terminus. JMV4622-4625, JMV4463 and pepstatine were incubated with MDA-MB-231 cells at 10 µM. The negative control was 1% solution of DMSO. Cell growth was measured after five days of incubation (Figure **III.5.3-1**). Pepstatine alone, as expected exhibited no cytotoxicity, probably due to its inability to cross the cellular membrane. Compounds 4463 and 4622 exhibeted remarkable toxicity completely inhibiting the cell growth after five days. The similarity of the toxicities of compounds 4463 and 4622 showed that the polyethylene glycol linker is not crucial for the activity. Compounds 4624 and especially 4625 were less toxic probably due to their lower solubility in aqueous media. Compound 4623 with two D-Arg residues showed an intermediate toxicity. It is possible that too many charged residues hamper the internalization of this compound.

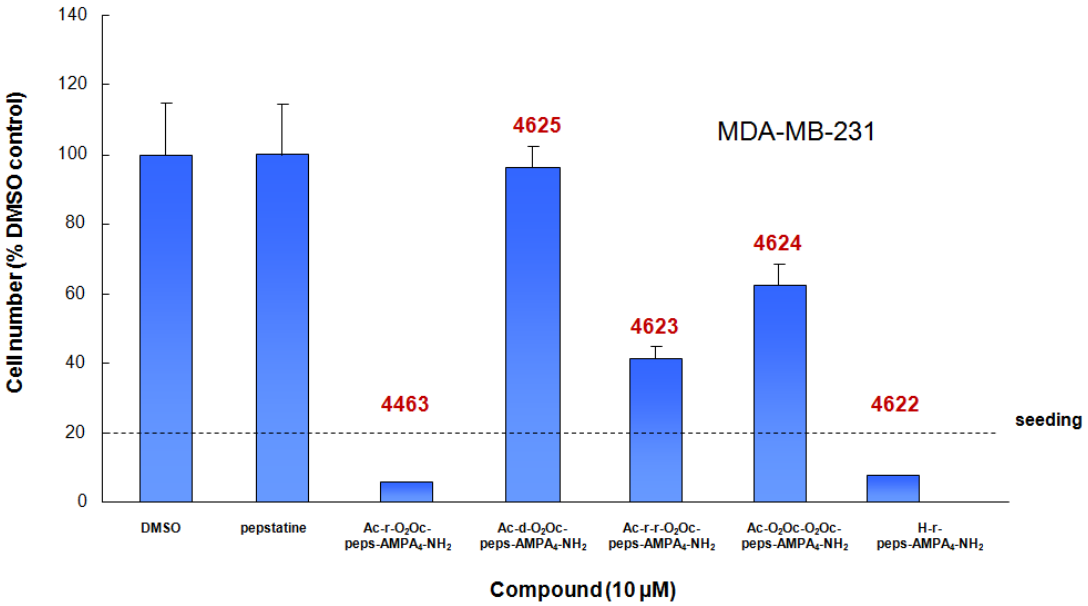

Figure III.5.3-1 *Cytotoxicity of the second generation of vectorized pepstatine inhibitors. Growth of MDA-MB-231 cells was measured after five day of incubation at 10 µM concentration. As control we used 1% DMSO solution in H_2O.*

Next we studied the importance of the charged amino acid in the solubilizing moiety and the length of the AMPA oligomer. Different cell lines were incubated with compounds JMV4461, JMV4462, JMV4463 and JMV4464 at 10µM. The cell growth was calculated after 5 days and compared to the cell growth after incubation with pepstatine (Figure **III.5.3-2**). The compounds were especially toxic to the two breast cancer cell lines (MDA-MB-231 and MCF7) but showed high cytotoxicity to all the cell

cultures. The HCT116 cell line seems to be less sensitive to these compounds. Altogether there was no significant difference between the toxicity of the tested compounds. This fact indicates that the nature of the charged group in the solubilizing moiety (amino or guanidino) does not influence the activity of the compounds.

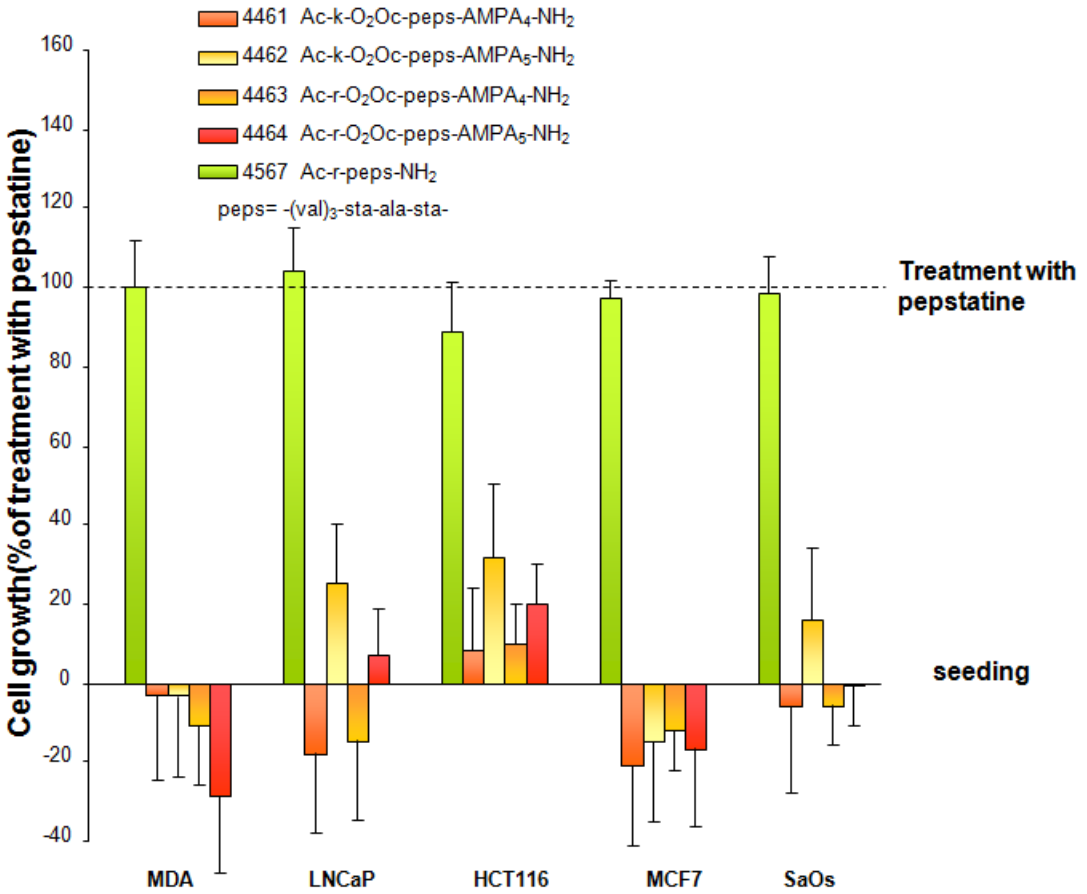

Figure III.5.3-2 *Cytotoxicity of pepstatine moiety connected to different CPNP and solubilizing moieties. Growth of different cell lines was measured after five days of incubation at 10 μM. As control we used 10 μM concentration of pepstatine.*

Next we incubated MDA-MB-231 cells with different concentrations of compounds JMV4462-4665, JMV4463 and pepstatine in order to calculate their IC_{50} after five days of incubation (Figure **III.5.3-3**). Oligomers JMV4463 and 4622 were the most efficient compounds with an IC_{50} equal to 2 and 3.10^{-6} M respectively. We chose JMV4463 as a leading compound for its high cytotoxicity and good solubility in water. Cytoxicity of this compound was further evaluated on prostate cancer cells, colon cancer cells, osteosarcome and two types of breast cancer cells and compared to compounds JMV4564, JMV4463, JMV4567 and pepstatine (Figure **III.5.3-4**).

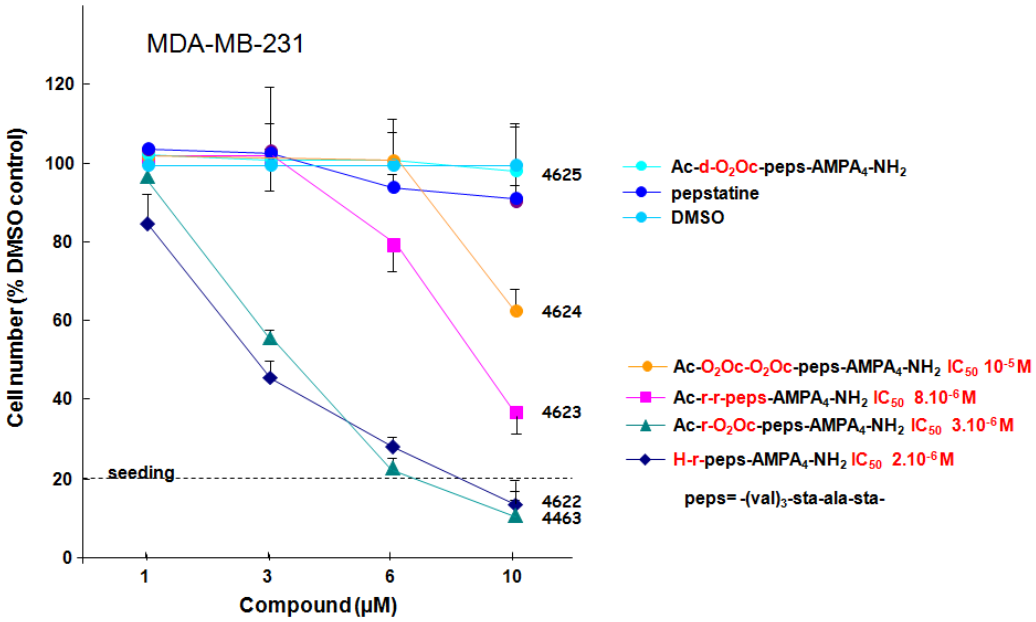

Figure III.5.3-3 *IC_{50} values of vectorized pepstatine inhibitors and negative controls on MDB-MB-232 cells growth after five days. As control we used 1 % DMSO solution in H_2O.*

As we expected pepstatine showed no cytotoxicity for all cell lines. JMV4463 was highly toxic for all cell lines. The HCT116 cells seemed more resistant to this compound compared to the others. Compound JMV4567 carrying water-solubilizing moiety 'Ac-O_2Oc-r-' but free of CPNP was non toxic for all the cell cultures. This result showed that the solubilizing moiety is not enough for the toxicity of the bioconjugates. Compound JMV4564 is a weaker inhibitor of the CD compared to the JMV4463 because of the substitution of its two statine moieties by γ-Leu. This compound showed reduced cytotoxicity compared to JMV4463 which is in accordance with its lower CD inhibition activity.

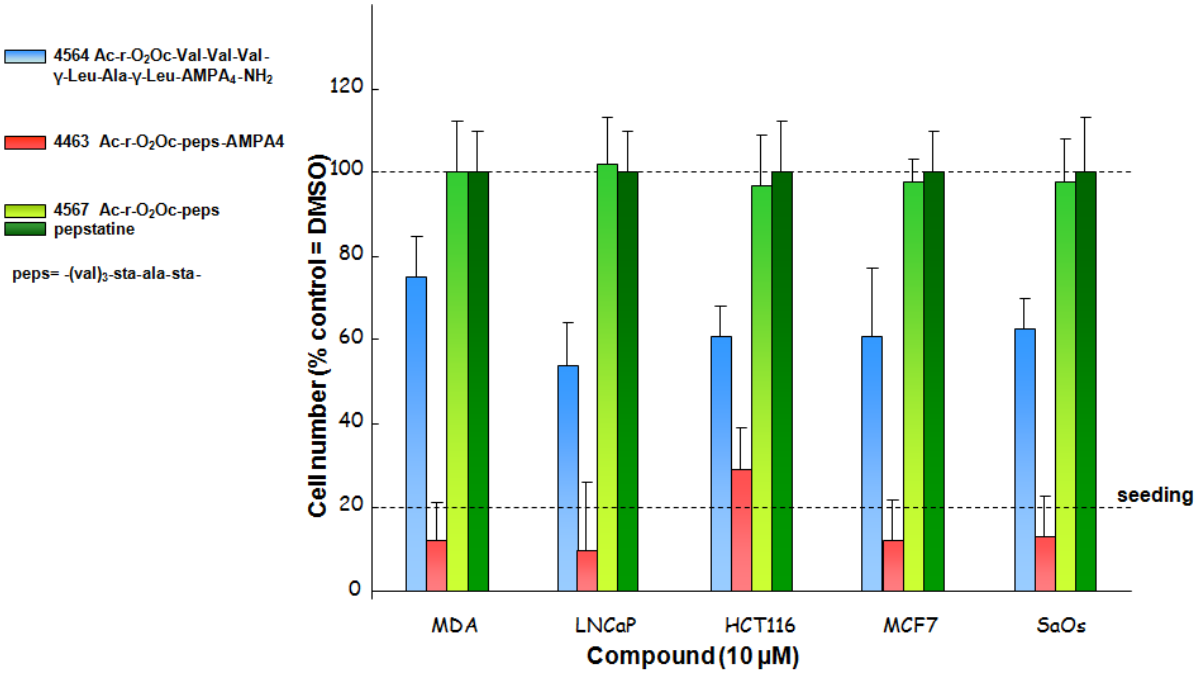

Figure III.5.3-4 *Cytotoxicity of JMV4463, 4564, 4567 and pepstatine to different cell lines incubated at 10 µM for 5 days. As control we used 1 % DMSO solution in H_2O.*

We also incubated MDA-MB-231 cancer cells for five days at different concentration of JMV4463, JMV4567, JMV4463, JMV4674 and Pepstatine in order to determine their IC_{50} values (Figure **III.5.3-5**)

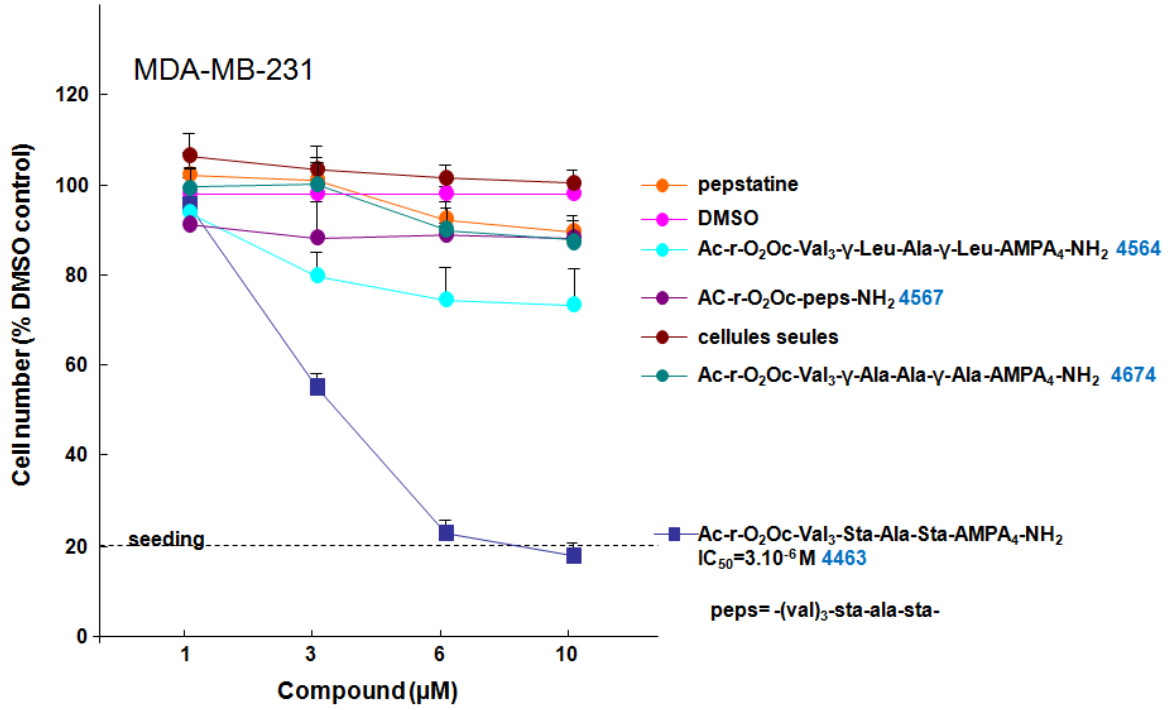

Figure III.5.3-5 *IC_{50} values of JMV4463 and negative controls on MDB-MB-232 cells growth after five days. As control we used 1 % DMSO solution in H_2O.*

The only compound that showed considerably toxicity was JMV4463. The weaker CD inhibitors JMV4674 and 4564 showed very limited inhibition of the cell growth. Compound 4567 devoid of AMPA oligomer and wild-type pepstatine were also non-toxic. This study shows the importance of the pepstatine and the CPNP – $(AMPA)_4$ moieties for the toxicity. There is a good correlation between the ability of the compounds to inhibit CD and their cytotoxicity. Compounds devoid of CPNP are non-toxic that should be ascribed to lack of penetration and thus their inability to reach the endosomes and the lysosomes.

Next a kinetic study of the JMV4463 cytotoxicity was performed. MDA-MB-231 cells were incubated with 10 µM of JMV4463 or different negative controls (Figure **III.5.3-6**). The cell growth was controlled after 2 hours, 9 hours and 5 days. After two hours treatment JMV4463 already showed considerable inhibition of the cell growth compared to the control (1% DMSO) while the other compounds showed no toxicity with the exception of JMV4564 that showed weak inhibition of the cell growth. After 9 hours of incubation the cells treated with JMV4463 were less than the seeding and about 20% of the control while the cell growth after incubation with the control compounds was only slightly inhibited. After five days of incubation with JMV4463 the number of cells in the essay was about half of the seeding number and about 15% of the control. From the negative controls only the pepstatine showed noticeable toxicity - cell growth about 80% of the control after 5 days. Altogether these results show the ability of JMV4463 to inhibit completely cell growth for less than 10 hours and to keep it lower than the seeding after 5 days.

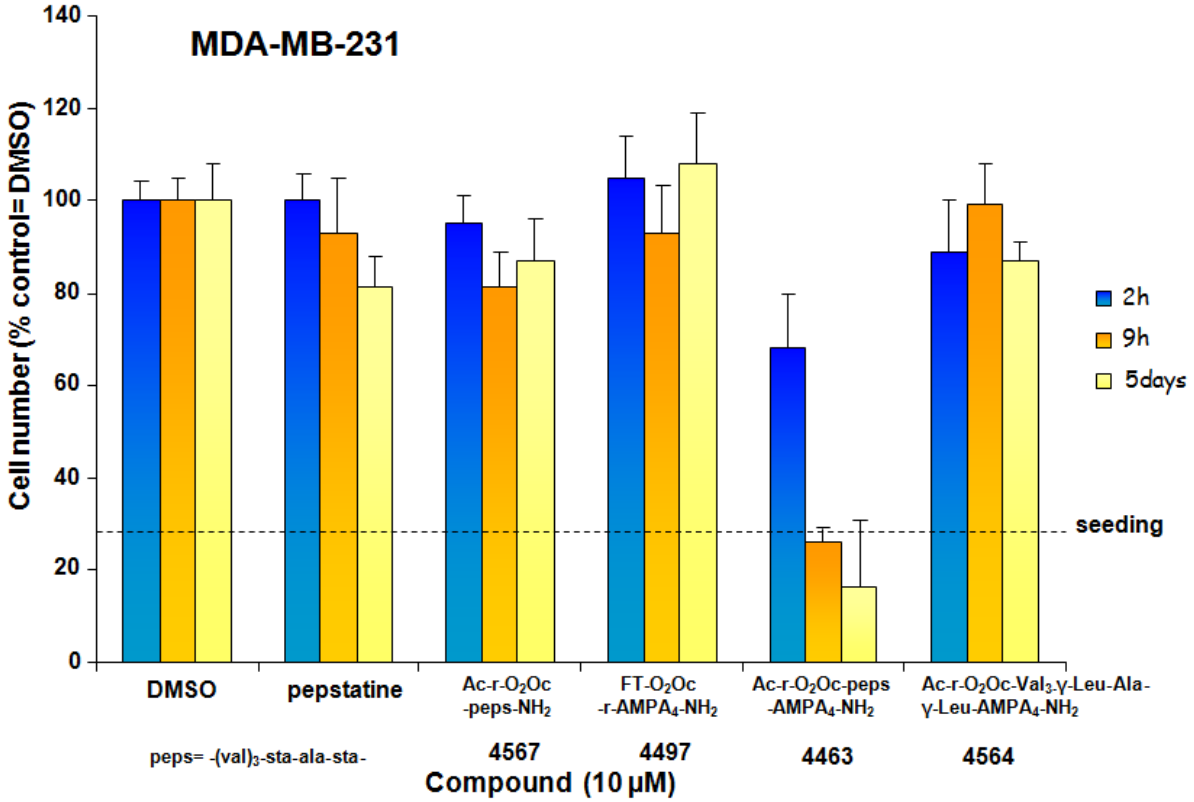

Figure III.5.3-6 *Kinetic study of the JMV4463 toxicity compared to different negative controls. MDA-MB-231 cells were incubated with 10 µM concentration. As control we used 1 % DMSO solution in H_2O.*

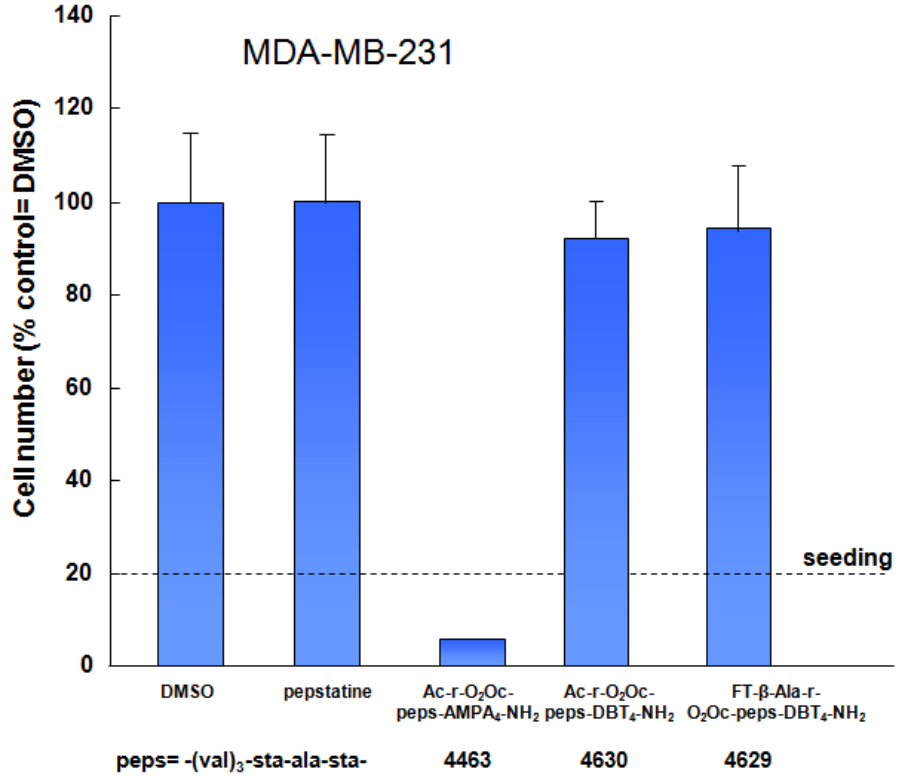

Figure III.5.3-7 *Cytotoxicity of compound JMV4630 compared to compound JMV4463. MDA-MB-231 cells were incubated at 10 µM concentration for five days. The control is 1% DMSO solution in H_2O.*

Encouraged by our results with compound JMV4463 we synthesized and tested for cytotoxicity the compound JMV4630 in which the $(AMPA)_4$ moiety was substituted by $(DBT)_4$. To our surprise even though this compound was able to inhibit the isolated CD (Figure **III.5.2-1**) it was non toxic *in vitro* after five days of incubation at 10^{-5} M (Figure **III.5.3-7**). A possible explanation is that this compound is not internalized in the same way as the JMV4463. We performed a series of internalization test that will be discussed in the next chapter.

III.5.4. Internalization essays of fluorescently labelled CD inhibitors

Confocal laser scanning microscopy (CLSM) (see section **I.2.3**) analyses were also performed on living cells (MDA-MB-231) to assess the internalization and intracellular distribution of the fluorescently labelled vectorized CD inhibitors. Cells were incubated with a membrane marker (lipid raft labelling). To gain more insight into the internalization, co-staining was performed with other fluorescent markers for subcellular components such as the nucleus and the lysosomes. These experiments were associated with a kinetic study of the bioconjugates internalization. First studied compound was JMV4626 which is the fluorescently labelled analogue of the toxic JMV4463. Co-staining with a membrane marker (lipid-raft labelling) indicated that this compound was not held in the lipid membrane after three hours and was internalized into the cell (Figure **III.5.4-1 A**). It was mainly localized in vesicular like compartments probably the endosomes or the lysosome. At the 16^{th} hour the compound was co-localized with the lysosome marker (Figure **III.5.4-1 B**). We performed a similar experiment with compound JMV4631 that was devoid of an oligoAMPA CPNP moiety. This compound was not internalized at all after 16 hours (Figure **III.5.4-2**). This fact proves the importance of the AMPA tetramer for the internalization of the pepstatine moiety. The extracellular localization of the FITC-conjugated compound (JMV4631) could explain the nontoxicity of its acetylated analogue (JMV4567)

Next we performed tests with compound JMV4629 (FITC-β-Ala-r-O_2Oc-peps-DBT_4-NH_2). The compound was not co-stained with the membrane marker at 3 or 24 hours and was very well internalized in the cell in vesicular compartments. At the 16^{th} hour the compound was co-localized with the lysosome marker.

The results of the CLSM with compounds JMV4629 and JMV4626 suggested the ability of the CPNP $(DBT)_4$ and $(AMPA)_4$ to deliver biologically relevant cargos (pepstatine) inside the cells. In the same time the pepstatine vectorized by these two classes of CPNP showed different biological activities. High toxicity was observed when vectorized by $(AMPA)_4$ and no toxicity at all when vectorized by $(DBT)_4$. The possible reasons for these differences will be discussed in the next chapter

III.5.5 Discussion

We have tested a series of pepstatine analogues linked to a CPP or CPNP at their C-terminus for their ability to inhibit the Cathepsin D and for their cytotoxicity *in vitro*. We obtained very encouraging results with compounds composed of pepstatine moiety linked to an AMPA tetramer at their C-terminus and cationic solubilizing moiety at their N-terminus. Our lead compound JMV4463 was able to inhibit the isolated CD and its fluorescent analogue 4626 was able to penetrate into MDA-MB-

231 cells. Analogues of this compound with modified pepstatine moiety were worst inhibitors of the CD and showed less or no toxicity. Compound JMV4622 devoid of polyethylene glycol linker showed similar cytotoxicity thus probably this linker is not crucial for the activity. Also compounds with different charged aminoacid (D-Lys instead of D-Arg) showed similar activity while compound with D-Asp instead of D-Arg showed no toxicity.

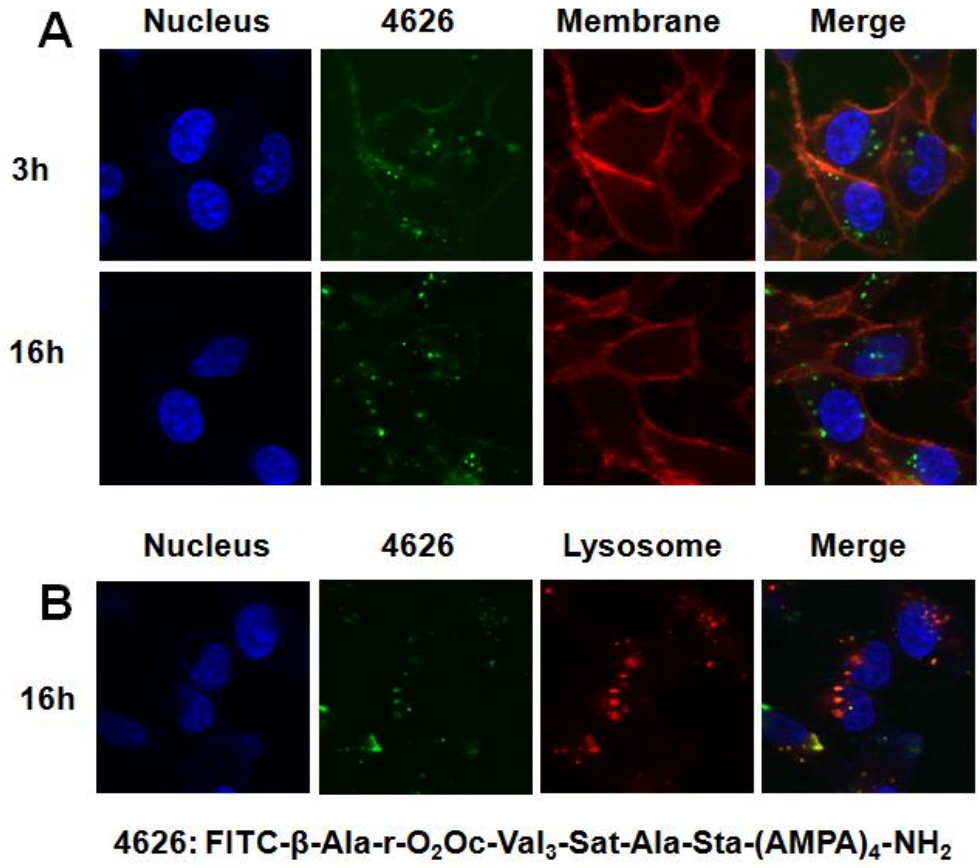

Figure III.5.4-1 *Confocal microscopy images of living MDA-MB-231 breast cancer cells incubated with compound JMV4626. Images are representative of at least 3 independent experiments.* ***A)*** *Distribution of JMV4626 after 3 and 16 hours of incubation at 37°C. Cells were incubated at 10^{-5} M* ***B)*** *Co-localization of JMV4626 with the lysosome marker at 16 h at 37°C.*

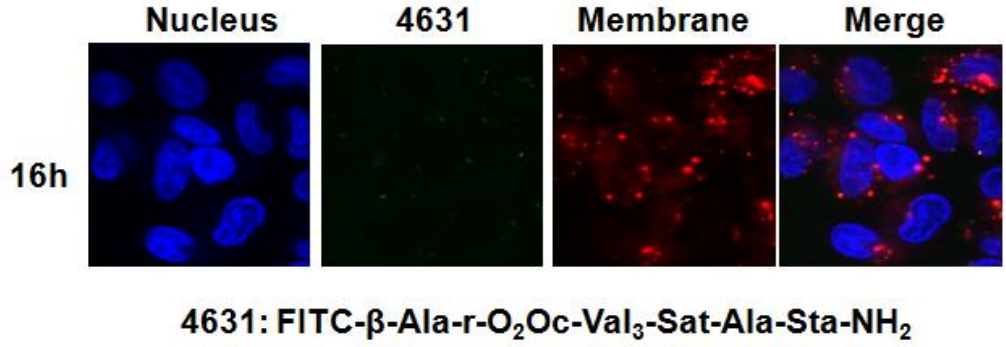

Figure III.5.4-2 *Confocal microscopy images of living MDA-MB-231 breast cancer cells incubated with compound JMV4631. Images are representative of at least 3 independent experiments and represent the distribution of JMV4631 after 16 hours of incubation at 10^{-5} M.*

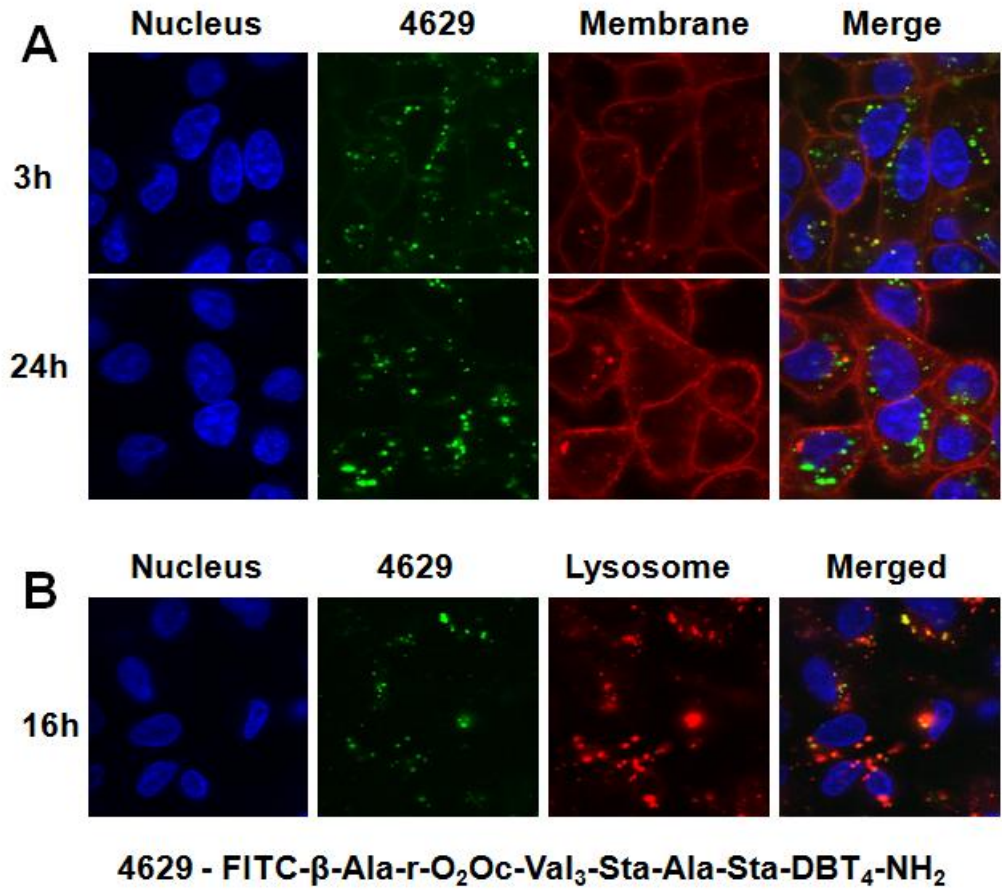

Figure III.5.4-3 *Confocal microscopy images of living MDA-MB-231 breast cancer cells incubated with compound JMV4629. Images are representative of at least 3 independent experiments.* ***A)*** *Distribution of JMV4629 after 3 and 24 hours of incubation at 37°C. Cells were incubated at* 10^{-5} *M* ***B)*** *Co-localization of JMV4629 with the lysosome marker after 16 h at 37°C.*

Probably a charged lysine or arginine residue is important mostly for the solubility of the compounds in aqueous media. Similar studies were performed with the DBT analogue of JMV4463 – JMV4630. JMV4630 is a potent inhibitor of the CD and its fluorescently labelled analogue was well internalized into the cells but it did not exhibit any cytotoxicity *in vitro*. One of the possible explanations is that JMV4463 toxicity is not related with CD inhibition but another yet unknown target. Another explanation is that compound JMV4630 is internalized in a different way so it is unable to interact with the CD. It is very important to understand the exact mechanism of action of JMV4463 so we could design even more powerful compounds. If this compound is truly toxic via its interaction with CD we could perform very important studies on the CD implication in cancer growth and development. The good results with JMV4463 encouraged us to perform tests *in vivo*. Tests for anti-cancer activity on mice are currently under way.

IV. CONCLUSION AND PERSPECTIVES

IV.1 Structural studies of DBT and AMPA oligomers

The protons of oligomers Ac-$(DBT)_n$-NH_2 n=[1-6] were assigned using a combination of 2D NOESY, 2D ROESY, 2D COSY and 2D TOCSY experiments. Numerous NOE interactions were detected in the Ac-$(DBT)_6$-NH_2 molecule by 2D NOESY experiments. The volumes of these interactions were integrated and converted to distance restrictions. The immediate perspective for this project is to use these distance restrictions for the determination of the DBT hexamer structure in solution by molecular modelization studies. Unfortunately for the time being the crystallization essays have not produced crystals suitable for X-Ray studies. Powder diffraction experiments are currently performed with compounds: -(Lys-$DBT)_3$-, -$(DBT)_3$- and Ac-$(DBT)_6$-NH_2.

If the structure of the DBT oligomers is determined we could use this moiety as a building block for biomimetics with correctly positioned crucial functions on a target-by-target basis. Such compounds could be used to disturb specific protein-protein interactions. Determination of the secondary structure of the DBT oligomers could give us also some indications for the internalization mechanism of these biomimetics.

IV.2 DBT and AMPA oligomers as cell penetrating non-peptides

DBT and AMPA tetramers have been described as a new class of cell penetrating non-peptides. These short oligomers share a lot of features – their small size, hydrophobic non-cationic nature and high intracellular uptake. Both compounds $(DBT)_4$ and $(AMPA)_4$ possess four aromatic unites that are probably an important feature for their internalization. Also both compounds are delivered to the lysosome via endocytosis. These CPNP could be used to deliver drugs for the treatment of cancer, lysosomal storage disease and Alzheimer's disease.

For the time being we have shown the ability of these compounds to deliver fluorescent dies and small peptides like the pepstatine inside the cell. Another interesting perspective is to synthesize bioconjugates between these CPNPs and drugs for the treatment of Alzheimer's disease as one of the enzyme implicated in the production of the amyloid peptide is mainly localized in the endosomes and the lysosomes.

Another important task is to better understand the internalization mechanism of these new CPNP so we could synthesize compounds with even higher intracellular uptake and well defined intracellular localization.

IV.3 A straightforward approach for cellular-uptake quantification of CPPs and CPNPs

We have described a straightforward and efficient method for the quantification of cell-penetrating compounds internalization. The originality of the methodology relies first on the use of the combination of HCCA as a UV-light-absorbing tag and the neutral HCCE matrix, which enabled the very sensitive detection of the compounds of interest by mass spectrometry even in complex biological medium. We have used this methodology to straightforward evaluate the intracellular concentration of two well known CPP – $(Arg)_8$, penetratine and our CPNP $(DBT)_4$.

One of the perspectives ahead us is to straightforward evaluate the intracellular concentration of our CPNP $(AMPA)_4$. Another direction for research is to design a new tag composed of HCCA connected to a specific peptide sequence that could be cleaved only inside the cell. The HCCA moiety will be connected to CPP or CPNP via this cleavable linker. Thus we could make a difference between the internalized CPP/CPNP and the CPP/CPNP that is attached to the membrane

IV.4 Vectorization of pepstatine

We have designed a vectorized inhibitor of the Cathepsin D enzyme (compound JMV4463) by the conjugation of the pepstatine moiety to $(AMPA)_4$ and a solubilizing moiety. This compound was still able to inhibit the isolated Cathepsin D and showed considerable toxicity *in vitro.*

An important quantity of JMV4463 has been synthesized and we are currently performing *in-vivo* test for anti-cancer activity on mice. JMV4463 is a potential anti-breast cancer drug. Very important for this project is to prove that our compound is toxic because of its interaction with CD and not some other target inside the cell. If this compound is truly toxic via its interaction with CD we could perform very important studies *in vitro* and in *vivo* on the CD implication on cancer growth and development

V. MATERIALS AND METHODS

V.1 Materials

All amino acid derivatives were purchased from Iris Biotech. The other chemicals were purchased from: commercial suppliers, Iris Biotech, Senn Chemicals, Merck, Carlo Erba, Fluka, Riedel-de Haën, Sigma Aldrich, Acros Organics, FluoroChem and VWR Prolabo. The 2-chlorotrityl chloride resin (100-200 Mesh, 1.55 mmol/g Cl/g resin) was purchased from Iris Biotech, stored at 4°C and dried under vacuum at least 24 hours before use. Fmoc Rink amide polystyrene resin (100-200 mesh, 0.46 mmol/g) was purchased from SENN chemicals, Gentilly, France. Fluorescein isothiocyanate (FITC) was purchased from Sigma-Aldrich, Lyon, France. The Solvents used for HPLC and LC/MS were of HPLC grade. All final compounds were purified by reversed-phase HPLC and the purity assessed by analytical reversed-phase HPLC was found superior to **98 %.**

V.2 Characterization of the compounds

Analysis of the compounds. HPLC: The samples were prepared in acetonitrile/water (50/50 v/v) mixture, containing 0.1% TFA. Samples that were not soluble in this mixture were prepared in DMSO. The HPLC system consisted of a Beckman 32 Karat System. All the analyses were carried out using a RP C18 VWR chromolith column, 50 mm x 3.9 mm. A flow rate of 5 mL/min and a gradient of (0–100)% B over 3 min were used. Eluent A: water/0.1% TFA; eluent B: acetonitrile/0.1% TFA. The detection was performed both at 214 nm and 254 nm.

LC/MS Analysis. Samples were prepared in acetonitrile/water (50/50 v/v) mixture, containing 0.1% TFA. The samples that were not soluble in this mixture were prepared in DMSO. The LC/MS system consisted of a Waters Alliance 2690 HPLC, coupled to a Waters-Micromass ZQ spectrometer (electrospray ionization mode, ESI+). All the analyses were carried out using a RP C18 monolithic Onyx Phenomenex 25 x 4.6 mm column. A flow rate of 3 mL/min and a gradient of (0–3 100)% B over 3 min were used. Eluent A: water/0.1% formic acid; eluent B: acetonitrile/0.1% formic acid. Positive ion electrospray mass spectra were acquired at a solvent flow rate of 100–500 µL/min. Nitrogen was used for both the nebulizing and drying gas. The data were obtained in a scan mode in 0.1s intervals; 10 scans were summed up to get the final spectrum.

The yield and the purity after HPLC purification, HPLC retention time, calculated monoisotopic mass and detected mass of the compounds reported in the manuscript are presented in table **V.4**

V.3 Liquid phase synthesis

Synthesis of Fmoc-DBT-OH

Section **III.1**

Synthesis of Boc-D-Cys-OH

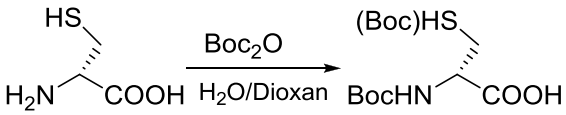

Compound	Mw (g.mol^{-1})	Equivalent	Mmol	Mass/volume
H-D-Cys-OH.HCl	159	1	125,786	20,00gr
Boc_2O*	218	1.5	188,679	41,14ml
Triethylamine(TEA)**	101	2	251,572	34,90ml

*- d_{Boc2O}=1,01
**- d_{TEA} =0.728

H-D-Cys-OH.HCl (20,000 gr, 125,786 mmol) was dissolved in mixture of 150ml of H_2O and 150 ml dioxan in a flask. The TEA (34,90ml, 251,572 mmol) was added and the reaction mixture was cooled down to 0°C with an ice bath. Boc_2O (41,14ml, 188,679 mmol) was dissolved in 50ml of dioxan and then was added dropwise. The reaction mixture was stirred at room temperature for four hours. Then 200 ml of the reaction mixture were evaporated under reduced pressure. The remaining solution was acidified to pH 3 by 1M solution of $KHSO_4$ and the aqueous phase was extracted three times with ethyl acetate. The organic phases were collected, washed with brine and dried over $MgSO_4$. Then the ethyl acetate was removed under reduced pressure to obtain 33,105 gr of Boc-D-Cys-OH as transparent oil. The weight of the obtained product was more than the calculated theoretical yield because of the presence of Boc-Cys(Boc)-OH.

Characterization:

HPLC: Rt = 1,10 mn ; MS (ESI): m/z 222 [$(M+H)^+$] ; $C_8H_{15}O_4NS$.

Synthesis (S)-2-(tert-butoxycarbonylamino)-3-(2-nitrophenylthio)propanoic acid (A)

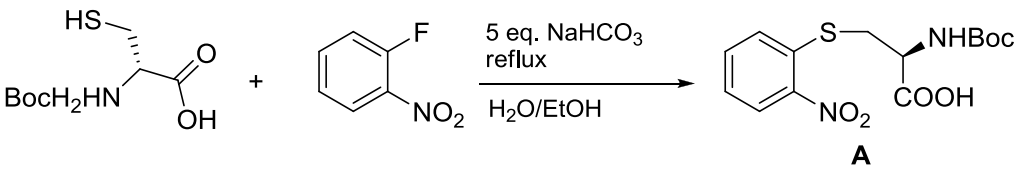

A

Compound	Mw (g.mol^{-1})	Equivalent	Mmol	Mass
Boc-D-Cys-OH*	221	1	125,79	33,11gr*
$NaHCO_3$	84	3	377,39	31,67gr
2-fluoronitrobenzen**	140	1	125,79	12,58ml

*Mixture of Boc-D-Cys-OH and Boc-D-Cys(Boc)-OH
** $d_{2\text{-fluoronitrobenzen}}$ =1.4

2-fluoronitrobenzen (12,58 ml, 125,79 mmol), Boc-D-Cys-OH (33,11 gr, 125,79 mmol) and $NaHCO_3$ (31,67 gr, 377,37mmol) were dissolved in a mixture of 300 ml H_2O and 300 ml EtOH . The reaction mixture was refluxed for 12 hours. Then we evaporated 400ml of the solvent and the resulting reaction mixture was washed 2 times by EtOEt in separatory funnel. The aqueous phase was acidified to pH 3 by 1M solution of $KHSO_4$ and extracted three times with ethyl acetate. The organic phases were collected, washed with brine and dried over $MgSO_4$. The ethyl acetate was removed under reduced pressure to obtain 44,11 gr of (**A**) as an yellow oil.

Expected mass of (A) =43.20 gr
Obtained mass=44,11 gr (residual solvent or salts)

Yield for the first two reaction – quantitative of chromatography pure product

Characterization:

HPLC: Rt = 1,56 mn ; MS(ESI): m/z 343.0 [$(M+H)^+$], 685.5 [$(2M+H)^+$] ; $[\alpha]_D^{20}$ = -75 (c 1.0, CH_3OH).
RMN ^{1}H ($CDCl_3$): conformer I (37%): 1.42 (s, 9H, (CH_3)$_3$C), 3.30 (m(br), 1H, S-*H*CH), 3.62 (m(br), 1H, S-*H*CH), 4.57 (m(br), 1H, NH-C*H*-CO), 7.05 (br, 1H, N*H*), 7.34 (d, J = 8.0 Hz, 1H, Ar-*H*), 7.60 (s, 1H, Ar-*H*), 8.21 (d, J = 8.0 Hz, 1H, Ar-*H*). conformer II (63%): 1.46 (s, 9H, (CH_3)$_3$C), 3.42 (m(br), 1H, S-*H*CH), 3.62 (m(br), 1H, S-*H*CH), 4.69 (m(br), 1H, NH-C*H*-CO), 5.46 (d, J = 6.5 Hz, 1H, N*H*), 7.32 (d, J = 8.0 Hz, 1H, Ar-*H*), 7.60 (s, 1H, Ar-*H*), 8.17 (d, J = 8.0 Hz, 1H, Ar-*H*).
RMN ^{13}C ($CDCl_3$): conformer I : 28.50 ((CH_3)$_3$*C*), 36.25 (S-*C*H_2), 53.51 (N-*C*H-CO), 81.16 ((CH_3)$_3$*C*), 125.74 (Ar-*C*H), 126.63 (Ar-*C*H), 127.44 (Ar-*C*H), 134.08 (Ar-*C*H), 136.41 (Ar-*C*), 147.12 (Ar-*C*), 157.10 (N-*C*O-O), 174.09 (*C*OOH), conformer II : 28.67 ((CH_3)$_3$*C*), 35.28 (S-*C*H_2), 52.85 (N-*C*H-CO), 81.34 ((CH_3)$_3$*C*), 125.93 (Ar-*C*H), 126.44 (Ar-*C*H), 128.15 (Ar-*C*H), 134.08 (Ar-*C*H), 135.73 (Ar-*C*), 147.50 (Ar-*C*), 155.84 (N-*C*O-O), 174.54 (*C*OOH).

Synthesis (S)-3-(2-aminophenylthio)-2-(tert-butoxycarbonylamino)propanoic acid (B)

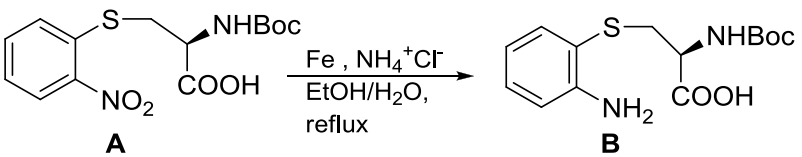

A **B**

Compound	Mw (g.mol^{-1})	Equivalent	Mmol	Mass
(A)		1	125,786	44,11 gr
Fe (Powder)		1 mass eq.		44,11gr
$NH_4^+Cl^-$		0,1 mass eq.		4,411gr

44,11 gr (125,79 mmol) of (**A**) were dissolved in a mixture of 300 ml of EtOH and 150 ml of H_2O in a flask and then the Fe powder (44,11 gr) and ammonium chloride (4,41 gr) were added. The reaction mixture was refluxed on stirring by mechanical agitation for 4 hours. Then the solution was filtered through celite, the celite was washed two times with boiling EtOH and the organic phases were collected. We evaporated 400 ml of the reaction mixture and added around 150 ml of H_2O to it. The aqueous phase was extracted 5 times with ethyl acetate. The collected organic phases were washed with brine, dried over $MgSO_4$, and the ethyl acetate was removed under reduced pressure to obtain 33,12 of (**B**) as a brown powder.

Expected weight 39,25 gr
Obtained weight 33,12 gr

Yield=84.34% of chromatographically pure

Characterization:

HPLC: Rt = 1,3 mn ; MS (ESI): m/z 312.9 [$(M+H)^+$], 621.3 [$(2M+H)^+$] ; $[\alpha]_D^{20}$ = +43 (c 1.0, CH_3OH) ; $C_{14}H_{20}O_4N_2S$.
RMN ^1H ($CDCl_3$): 1.26 (s, 9H, $(CH_3)_3C$), 3.06 (m(br), 1H, S-*H*CH), 3.14 (m(br), 1H, S-*H*CH), 4.28 (m(br), 1H, NH-C*H*-CO), 5.46 (br, 2H, NH_2), 5.79 (br, 1H, N*H*), 6.60 (t, $J_1 = J_2$ = 7.4 Hz, 1H, Ar-*H*), 6.66 (d, J = 7.4 Hz, 1H, Ar-*H*), 7.01 (t, $J_1 = J_2$ = 7.4 Hz, 1H, Ar-*H*), 7.31 (d, J = 7.4 Hz, 1H, Ar-*H*).
RMN ^{13}C ($CDCl_3$): 28.70 ($(CH_3)_3C$), 38.28 (S-CH_2), 55.18 (N-*C*H-CO), 80.46 ($(CH_3)_3C$), 116.57 (Ar-*C*H), 118.65 (Ar-*C*), 120.13 (Ar-*C*H), 130.50 (Ar-*C*H), 136.89 (Ar-*C*H), 147.86 (Ar-*C*), 156.12 (N-*C*O-O), 176.55 (*C*OOH).

Synthesis of (S)-tert-butyl 4-oxo-2,3,4,5-tetrahydrobenzo[b][1,4]thiazepin-3-ylcarbamate (C)

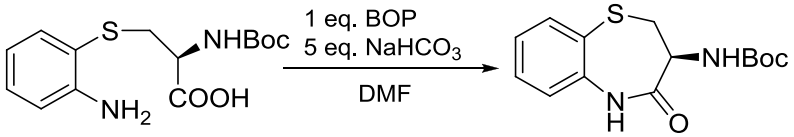

B **C** Yield=77%

Compound	Mw (g.mol^{-1})	Equivalent	Mmol	Mass
(B)	312	1	106.10	33,10gr
BOP	442	1	106.10	46.90gr
$NaHCO_3$	121.7	5	530,50	64,56gr

33,10 gr (106,10 mmol) of (**B**) were dissolved in 600ml of DMF and then the $NaHCO_3$ (64,56 gr, 530,50 mmol) and the BOP (46,56 gr, 106,10 mmol) were added. The reaction mixture was stirred for 24 hours at room temperature. After that the DMF

was evaporated under reduced pressure and the obtained oil was dissolved in ethyl acetate. The organic phase was subsequently washed 3 times by saturated solution of $NaHCO_3$ and brine and dried over $MgSO_4$. The ethyl acetate was removed under reduced pressure to obtain the crude (**C**) as a brown powder that was further purified by flash chromatography (AcOEt/Hex : 5/5) to obtain 18.31gr of white powder.

Expected weight=31,19gr
Obtained weight=18.31gr

Yield=58,70% of chromatography pure product

Characterization:

HPLC: Rt= 1,5 mn ; MS(ESI): m/z 295.0 $[(M+H)^+]$, 611.1 $[(2M+Na)^+]$; $[\alpha]_D^{20}$ = +274 (c 1.0, CH_3OH).
RMN ^1H ($CDCl_3$): 1.33 (s, 9H, $(CH_3)_3C$), 2.28 (t, $J_1 = J_2$ = 11.4 Hz, 1H, S-HCH), 3.75 (dd, J = 6.6 Hz et 11.4 Hz, 1H, S-HCH), 4.41 (m, 1H, NH-CH-CO), 5.61 (d, J = 7.8 Hz, 1H, NHBoc), 7.06 (d, J = 6.8 Hz, 1H, Ar-H), 7.10 (t, $J_1 = J_2$ = 6.8 Hz, 1H, Ar-H), 7.28 (t, $J_1 = J_2$ = 6.8 Hz, 1H, Ar-H), 7.53 (d, J = 6.8 Hz, 1H, Ar-H), 8.45 (s, 1H, NH).
RMN ^{13}C ($CDCl_3$): 28.71 ($(CH_3)_3C$), 39.66 (S-CH_2), 50.80 (N-CH-CO), 80.60 ($(CH_3)_3C$), 124.17 (Ar-CH), 127.14 (Ar-C), 127.65 (Ar-CH), 130.49 (Ar-CH), 135.79 (Ar-CH), 140.44 (Ar-C), 155.02 (N-CO-O), 172.88 (CONH).

Synthesis of (S)-tert-butyl 2-(3-(tert-butoxycarbonylamino)-4-oxo-3,4-dihydrobenzo[b][1,4]thiazepin-5(2H)-yl)acetate (D)

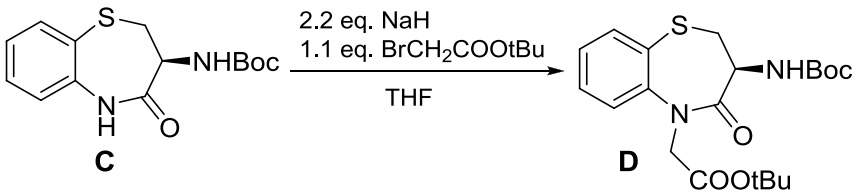

Yield 100%

Compound	**Mw** (g.mol^{-1})	Equivalent	Mmol	Mass
(C)	294	1	62.28	18.31gr
NaH	24	2	124,56	2,99gr
$BrCH_2COOtBu$*	195	1,1	68.51	10.11ml

***d**$_{BrCH2COOtBu=}$1.321

18,31 gr (62,28 Mmol) of (**C**) were dissolved in 150 ml of anhydrous THF in a flask under inert argon and after cooling to 0°C with ice bath, NaH (2,99 gr) was added slowly for about 20 minutes. When the release of H_2 was over a solution of $BrCH_2COOtBu$ (10,11 ml) in 40ml of anhydrous THF was added drop wise. The flask was closed under inert argon and the reaction mixture was stirred for 4 hours. After the completion of the reaction (HPLC controlled) 1M solution $KHSO_4$ was added drop wise to neutralize the residual NaH. After that 150 ml of 1M solution of $KHSO_4$ were added and the obtain mixture was extracted three times with ethyl acetate. The organic phases were collected, washed with brine and dried over $MgSO_4$. The ethyl

acetate was removed under reduced pressure to obtain 25.71gr of (**D**) as transparent oil.

Expected weight=25.55gr
Obtained weight=25.71gr

Yield = quantitaitve of chromatography pure product

Characterization:

HPLC: Rt = 1,97 mn ; MS(ESI): m/z 409.0 $[(M+H)^+]$; $C_{20}H_{28}O_5N_2S$

Synthesis of (S)-2-(3-amino-4-oxo-3,4-dihydrobenzo[b][1,4]thiazepin-5(2H)-yl)acetic acid (E)

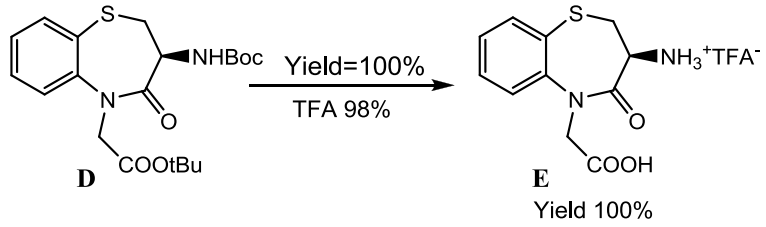

25.71gr (68,75 mmol) of (**D**) were dissolved in 150ml of 98% solution of TFA and the reaction mixture was stirred for 4 hours. The TFA was evaporated under reduced pressure. Five co-evaporations with 150 ml of EtOEt each were performed to take away the residual non-evaporated TFA. Then (**E**) was precipitated in EtOEt, filtered, washed many times with EtOEt and dried under reduced pressure to obtain 23.10 gr.

Expected weight=22.88gr
Obtained weight=23.10gr

Yield = quantitative of chromatography pure product

Characterization:

HPLC: Rt=0,87 mn ; MS(ESI): m/z 253.0 $[(M+H)^+]$

Synthesis of (3-S)[amino]-5-(carboxylmethyl)-2,3-dihydro-1,5-benzothiazepin-4(5H)-one Fmoc-DBT-OH (F)

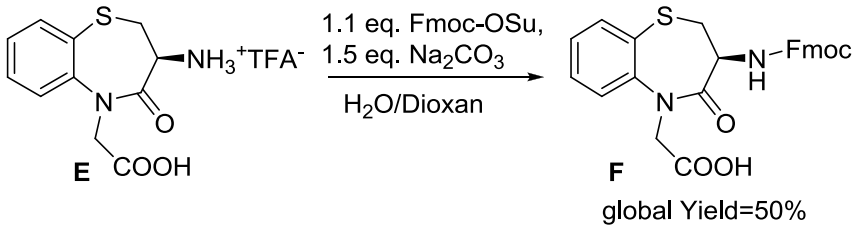

Compound	Mw (g.mol^{-1})	Eq	Mmol	Mass
FmocOSu	366	1.1	68.75	25,16 gr
(E)	336	1	62.5	22.88 gr
Na_2CO_3	106	1.5	93,75	9.94 gr

(**E**) (25,16 gr, 62,75 mmol) and Na_2CO_3 (9,94 gr, 93,75 mmol) were dissolved in a mixture of 300 ml H_2O and 300 ml dioxan. The reaction mixture was cooled down to 0°C and FmocOSu (25,16 gr, 68,75 mmol) was added drop wise dissolved in 100ml of dioxan. The reaction mixture was stirred for 12 hours at room temperature. After the completion of the reaction (controlled by HPLC) 400 ml of the solvent were evaporated. The aqueous phase was washed 2 times with EtOEt, acidified to pH 3 by $KHSO_4$ and extracted 3 times with ethyl acetate. The organic phases were collected, washed with brine and dried over $MgSO_4$. The ethyl acetate was removed under reduced pressure to obtain 29,10 gr of Fmoc-DBT-OH as white powder.

Expected weight=29,75
Obtained weight=29,10

Yield = 97,81% of chromatography pure product

Characterization:

HPLC: Rt = 1,88 mn ; MS(ESI): m/z 474.9 [$(M+H)^+$] ; $C_{26}H_{22}O_5N_2S$.
RMN ^1H ($CDCl_3$): 2.90 (t, $J_1 = J_2 = 11.1$ Hz, 1H, S-*H*CH), 3.45 (dd, J = 6.8 Hz et 11.1 Hz, 1H, S-*H*CH), 3.80 (t, $J_1 = J_2 = 7.6$ Hz, 1H, CO-O-CH_2-C*H*), 4.15 (d, J = 7.6 Hz, 2H, CO-O-CH_2-CH), 4.30 (d, J = 17.6 Hz, 1H, N-*H*CH), 4.50 (m, 1H, NH-C*H*-CO), 4.90 (d, J = 17.6 Hz, 1H, N-*H*CH), 5.85 (d, J = 7.8 Hz, 1H, N*H*Fmoc), 7.25 (d, J = 7.6 Hz, 2H, Ar-*H*), 7.35 (d, J = 7.6 Hz, 2H, Ar-*H*), 7.40 (d, J = 7.6 Hz, 2H, Ar-*H*), 7.45 (d, J = 7.6 Hz, 1H, Ar-*H*), 7.55 (m, 2H, Ar-*H*), 7.65 (d, J = 7.6 Hz, 1H, Ar-*H*), 7.75 (d, J = 7.6 Hz, 2H, Ar-*H*), 8.90 (br, 1H, CO_2H).

Synthesis of 2-aminomethyl-phenyl-acetic acid (Fmoc-AMPA-OH)

Section **III.1**

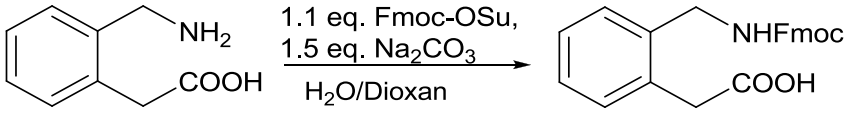

Compound	Mw (g.mol^{-1})	Eq	mmol	Mass
FmocOSu	337	1,1	27,30	9.20 gr
AMPA	201.65	1	24.80	5 gr
Na_2CO_3	106	1.5	37.20	3.94 gr

AMPA (5 gr, 24,80 mmol) was dissolved with Na_2CO_3 (3,94 gr, 37,20) in a mixture of 200 ml H_2O and 200 ml dioxan. The solution was cooled down to 0°C and FmocOSu (9,20 gr, 27,30 mmol) was added drop wise dissolved in 100ml of dioxan. The reaction mixture was stirred for 12 hours at room temperature. After the completion of the reaction (controlled by HPLC) about 300ml of the solvent were evaporated. The

aqueous phase was washed 2 times with EtOEt, acidified to pH 3 with $KHSO_4$ and extracted 3 times with ethyl acetate. The organic phases were collected, washed with brine and dried over $MgSO_4$. The ethyl acetate was removed under reduced pressure to obtain 8.81 gr of Fmoc-AMPA-OH as white powder.

Expected weight=9.60
Obtained weight=8.81

Yield = 91,77 % of chromatography pure product

Characterization:

HPLC: Rt = 1,70 mn ; MS(ESI): m/z 388 $[(M+H)^+]$; $C_8H_{15}O_4NS$.

V.4 SPPS

Anchoring on Rink amide-PS resin

Sections: **III.2.1, III.3.1.1, III.3.1.2, III.5.1**

Fmoc-Rink amide resin was conditioned for 30 minutes in DCM and submitted to the standard deportation cycle, using two times DMF/pip 80/20 v/v solution for 30 minutes. After washing steps, the first constrained dipeptide mimetic (Fmoc-LBT-OH/Fmoc-DBT-OH or Fmoc-AMPA-OH) motif or Fmoc protected amino acid was loaded onto the resin through a standard coupling cycle, using HBTU (3 eq.) as a coupling agent and DIEA (3 eq.) as a base.

Anchoring on 2-chlorotrityl chloride PS resin

Sections: **III.2.1**

The anchoring was carried out manually in a plastic syringe equipped with frit. 2 grams of 2-chlorotrityl chloride PS resin with theoretical charge of 1.55 mmol/gr (about 3,10 mMol) was conditioned for 30 minutes with anhydrous DCM. After that the resin was incubated with 3,67gr (7,75 mmol) of Fmoc-DBT-OH dissolved in 15ml of anhydrous DMF and 2,66ml (7,75 mmol) of DIEA and stirred mechanically overnight. By UV titration after the deprotection of the Fmoc group we determined a charge of 0.77 mmol/gr on the resin after the anchoring of the first DBT moiety.

Coupling steps

Sections: **III.2.1, III.3.1.1, III.3.1.2, III.5.1**

The Coupling reaction was carried out manually in plastic syringes equipped with frits. HBTU (3 eq) as a coupling agent, DIEA (3 eq) as a base and Fmoc protected moieties (D/L natural aminoacids, D/L BT, AMPA, Ahx, O_2Oc or β-Ala) or isovaleric acid (3eq according to resin loading) were solubilized in DMF and added to the resin. The reaction was stirred for 3 hours at room temperature. The reaction was monitored by the standard TNBS test.[76]

Deprotection step

Sections: **III.2.1, III.3.1.1, III.3.1.2, III.5.1**

Fmoc deprotection was carried out using DMF/piperidine 80/20 v/v solution two times for 30 minutes. Only in the case of deprotection of an AMPA moiety was used DMF/Piperidine/DBU 46/2/2 v/v/v solution two times for 45 minutes. This treatment allowed us to avoid incomplete deprotections that were observed with the standard DMF/Piperidine solution.

Washing steps

Sections: **III.2.1, III.3.1.1, III.3.1.2, III.5.1**

Washing steps were performed after each coupling and deprotection steps: one time methanol, one time DCM, 3 times DMF and 3 times DCM.

FITC coupling

Sections: **III.3.1.1, III.3.1.2, III.5.1**

FITC reaction was carried out manually in plastic syringes equipped with frits. 1.5 eq. of FITC and 3 eq. of DIEA (according to resin loading) were solubilized in DMF and added to the resin. The reaction was stirred for 2 hours at room temperature.

Acetylation

Acetylation was carried manually in plastic syringes equipped with frits using DCM/Ac_2O solution 2 times for 15 minutes.

Cleavage of Rink amide PS resin

Oligomers were cleaved from resin for 4 hours by 99% trifluoroacetic acid. After removal of the resin by filtration, the resin was washed multiple times with DCM. The DCM and trifluoroacetic acid filtrates were concentrated under reduced pressure. Compounds were precipitated by addition of diethyl ether and filtrated. They were dissolved in acetonitrile/water 50/50 solution containing 0.1% TFA and freeze dried.

Cleavage of 2-chlorotrityl chloride PS resin

Sections: **III.2.1**

In the case of DBT homo-oligomers the peptides were cleaved from the resin in the same reaction conditions as for the RA PS resin.

$(DBT\text{-}Lys)_n$ hetero-oligomers were cleaved from the resin for 3 hours by TFE/DCM 3/7 v/v solution. After removal of the resin by filtration, the resin was washed multiple times with DCM. The DCM and DCM/TFE filtrates were concentrated under reduced pressure. The products were precipitated by addition of diethyl ether and filtrated.

They were dissolved in acetonitrile/water 50/50 solution containing 0.1% TFA and freeze dried.

Microwave assisted solid phase peptide synthesis

Section: **III.4.1**

Residue coupling conditions: Fmoc-amino acids or Fmoc-DBT-OH (0.5 mmol, 0.2 M) in 2.5 mL of DMF were used for the stepwise synthesis following the solid phase peptide synthesis procedure, using a solution of HBTU in DMF (0.5 mmol, 0.5 M, 1 mL), and a solution of DIEA in DMF (1 mmol, 2M, 0.5 mL) under N_2 for 5 min at 23W and 70°C. These conditions were also used to couple Boc-HCCA and Boc HCCA(D) on the amino function of Ahx residue.

Fmoc deprotection: removal of the Fmoc protecting group was carried out using 20% piperidine in DMF (7 mL) at 40W for 30s at 75°C and then 20% piperidine in DMF (7 mL) at 35W for 3 min at 70°C. These conditions were also used to remove the Fmoc protecting group from Fmoc-Rink amide polystyrene resin (100-200 mesh, 0.46 mmol/g).

Cleavage and deprotection of amino-acid side chains: After performing all the coupling/deprotection cycles, the peptidyl or DBT-containing resin was cleaved with a TFA/TIS/H_2O 95/2.5/2.5 v/v/v) solution, for 120 minutes at room temperature, under gentle stirring. Resin was filtered, washed with cleavage solution and the filtrate was concentrated in vacuum. The residue was washed with diethyl ether and then dried at room temperature.

Purification of the compounds

All the compounds were purified by preparative HPLC (Waters 4000 apparatus) carried out on a C18 reversed-phase column (C18 Deltapak column, 100 mm x 40 mm, 15µm, 100Å) at a flow rate of 50 mL/min of a mixture of H_2O + 0.1% TFA and CH_3CN + 0.1% TFA in gradient mode with UV detection at 214 nm or 254 nm.

The yield and the purity after HPLC purification, HPLC retention time, calculated monoisotopic mass and detected mass of the compounds are reported in table **V.4**

Table V.4 *List of the synthesized compounds. Between brackets and in bold in the Mass spectrometry section are reported the expected masses of the compounds*

Compound	**Sequence**	**MS: Ion detected (expected mass)**	**Rt (min)**	**Yield**
Section **III.2.1.1**				
JMV4279	Ac-DBT-NH_2	$[M+H]^+$- 293.1(**293.07**)	1.15	60%
JMV4280	Ac-$(DBT)_2$-NH_2	$[M+H]^+$- 528.2 (**527.1**)	1.22	50%
JMV4281	Ac-$(DBT)_3$-NH_2	$[M+H]^+$- 762.2(**761.15**)	1.35	45%
JMV4169	Ac-$(DBT)_4$-NH_2	$[M+H]^+$-996.2 , $[M+2H]^{2+}$-498,6 (**995,2**)	1.51	35%
JMV4170	Ac-$(DBT)_5$-NH_2	$[M+H]^+$-1230.2 , $[M+2H]^{2+}$-615.6 (**1229.2**)	1.61	25%
JMV4172	Ac-$(DBT)_6$-NH_2	$[M+H]^+$-1464.4 ,	1.73	15%

		$[M+2H]^{2+}$-732.6 (**1463.3**)		
JMV4282	Ac-$(DBT)_7$-NH_2	$[M+2H]^{2+}$- 849.9 (**1697.3**)	1.88	13%
JMV4283	Ac-$(DBT)_8$-NH_2	$[M+2H]^{2+}$- 966.7(**1931.4**)	1.91	11%
JMV4286	Ac-DBT-LBT-DBT-LBT-NH_2	$[M+H]^{+}$-996.2 , $[M+2H]^{2+}$-498,6 (**995,2**)	1.41	34%
JMV4176	Ac-$(AMPA)_4$-NH_2	$[M+H]^{+}$-648.4, $[M+2H]^{2+}$-324.8, $[M+Na]^{+}$-670.3 (**647.4**)	1.30	52%
JMV4288	Ac-$(AMPA)_5$-NH_2	$[M+2H]^{2+}$-398.2 (**794.35**)	1.90	25%
JMV4086	Z(Br)-$(DBT)_5$-NH_2	$[M+H]^{+}$-1400,1 , $[M+2H]^{2+}$-700,7(**1399,2**)	1.98	20%
JMV4087	Z(Br)-$(DBT)_6$-NH_2	$[M+2H]^{2+}$-817,6 (**1633.2**)	2.04	15%
Section **III.2.1.2**				
JMV4675	-DBT-DBT-DBT-	$[M+H]^{+}$-703,2 (**702.12**)	1.62	17%
JMV4284	-DBT-DBT-DBT-DBT-	$[M+H]^{+}$- 937.1 (**936.16**)	1.78	23%
JMV4678	-(Lys-DBT-Lys-DBT-Lys-DBT)-	$[M+H]^{+}$- 1087.5; $[M+2H]^{2+}$-544.3 (**1086.4**)	0.87	27%
JMV4679	-(Lys-DBT-Lys-DBT-Lys-DBT-Lys-DBT)-	$[M+2H]^{2+}$- 725.4 $[M+3H]^{3+}$-483.9 (**1448.5**)	0.91	25%
Section **III.3.1.1**				
JMV2949	Fl-$(DBT)_2$-NH_2	$[M+H]^{+}$ - 875.00 (**874.1**)	1.70	35%
JMV2968	Fl-$(DBT)_3$-NH_2	$[M+H]^{+}$-1109.1 (**1108.2**)	1.87	30%
JMV3229	Fl-$(DBT)_4$-NH_2	$[M+H]^{+}$-1343.1 $[M+2H]^{2+}$-672.1 (**1342.2**)	1.80	24%
JMV4228	Fl-$(LBT)_4$-NH_2	$[M+H]^{+}$-1343.2, $[M+2H]^{2+}$-672.3 (**1342.2**)	1.80	25%
JMV4287	Fl-$(DBT\text{-}LBT)_2$-NH_2	$[M+H]^{+}$-1343.2$[M+2H]^{2+}$-672.2 (**1342.2**)	1.69	25%
JMV4236	Fl-$(AMPA)_3$-NH_2	$[M+H]^{+}$-848.24 , $[M+2H]^{2+}$-424.9 (**847.24**)	1.54	46%
JMV4237	Fl-$(AMPA)_4$-NH_2	$[M+H]^{+}$- 995.3, $[M+2H]^{2+}$-498.2 (**994.31**)	1.63	26%
JMV4497	Fl-O_2Oc-r-$(AMPA)_4$-NH_2	$[M+H]^{+}$-1296.5, $[M+2H]^{2+}$-649.0, $[M+3H]^{3+}$-433.0 (**1295.5**)	1.34	25%
Section **III.3.1.2**				
JMV4568	Fl-Ahx-$(DBT)_3$-Ahx-$(Arg)_9$-NH_2	$[M+4H]^{4+}$-686.2, $[M+5H]^{5+}$-549.1, $[M+6H]^{6+}$-457.8, $[M+7H]^{7+}$-392.7 (**2739.2**)	1.00	22%
JMV4569	Fl-Ahx-$(DBT)_4$-Ahx-$(Arg)_9$-NH_2	$[M+4H]^{4+}$-744.66, $[M+5H]^{5+}$-595.86, $[M+6H]^{6+}$-496.92 (**2973.2**)	1.09	20%
-	Fl-Ahx-$(Arg)_8$-NH_2	$[M+4H]^{4+}$-443, $[M+5H]^{5+}$-354.6 (**1767.9**)	**-**	30%
JMV3888	Fl-Ahx-$(Arg)_9$-NH_2	$[M+4H]^{4+}$-482, $[M+5H]^{5+}$-385,8 (**1924**)	**-**	25%

Section **III.4.1**				
JMV4239	HCCA-Ahx-$(DBT)_4$-NH_2	$[M+H]^+$-1238.3, $[M+2H]^{2+}$-619.65 (**1237.3**)	1.57	40%
JMV4240	HCCA(D_4)-Ahx-$(DBT)_4$-NH_2	$[M+H]^+$-1242.3, $[M+2H]^{2+}$-621.6 (**1241.3**)	1.57	41%
JMV4285	Ac-Ahx-$(DBT)_4$-NH_2	$[M+H]^+$-1109.3, $[M+2H]^{2+}$-555.15 (**1108.3**)	1.53	45%
Section **III.5.1**				
JMV2719	IsoVal-Val_2-Sta-Ala-Sta-$(AMPA)_4$-NH_2	$[M+H]^+$- 1273.6, $[M+2H]^{2+}$-637.3 (**1272.7**)	1.67	15%
JMV4215	IsoVal-$(Val)_2$-γLeu-Ala-γLeu-$(AMPA)_4$-NH_2	$[M+2H]^{2+}$-621.4, (**1240.8**)	1.78	10%
JMV4216	IsoVal-$(Val)_2$-Sta-Ala-Sta-$(AMPA)_3$-NH_2	$[M+H]^+$- 1126.7 $[M+2H]^{2+}$-563,8 (**1125.6**)	1.54	20%
JMV2729	IsoVal-Val_2-Sta-Ala-Sta-$(DBT)_4$-NH_2	$[M+H]^+$- 1621.5 $[M+2H]^{2+}$-811,25 (**1620.6**)	1.60	15%
JMV4461	Ac-D-Lys-O_2Oc-$(Val)_3$-Sta-Ala-Sta-$(AMPA)_4$-NH_2	$[M+2H]^{2+}$-802.5, $[M+3H]^{3+}$-535.6 (**1602.9**)	1.35	35%
JMV4462	Ac-D-Lys-O_2Oc-$(Val)_3$-Sta-Ala-Sta-$(AMPA)_5$-NH_2	$[M+2H]^{2+}$- 876.1, $[M+3H]^{3+}$-584.4 (**1749.9**)	1.41	25%
JMV4463	Ac-D-Arg-O_2Oc-$(Val)_3$-Sta-Ala-Sta-$(AMPA)_4$-NH_2	$[M+2H]^{2+}$- 816.4 $[M+3H]^{3+}$-544.6 (**1630.9**)	1.37	30%
JMV4464	Ac-D-Arg-O_2Oc-$(Val)_3$-Sta-Ala-Sta-$(AMPA)_5$-NH_2	$[M+2H]^{2+}$- 890.1, $[M+3H]^{3+}$-593.8 (**1877.9**)	1.42	23%
JMV4563	Ac-D-Lys-O_2Oc-$(Val)_3$-γLeu-Ala-γLeu-$(AMPA)_4$-NH_2	$[M+H]^{2+}$- 786.6, $[M+3H]^{3+}$-524.4 (**1571**)	1.41	25%
JMV4564	Ac-D-Arg-O_2Oc-$(Val)_3$-γLeu-Ala-γLeu-$(AMPA)_4$-NH_2	$[M+H]^{2+}$- 800.6, $[M+3H]^{3+}$-534.1 (**1599**)	1.41	26%
JMV4566	Ac-D-Lys-O_2Oc-$(Val)_3$-Sta-Ala-Sta-NH_2	$[M+H]^+$-1015.7, $[M+2H]^{2+}$-508.4 (**1014,6**)	1.07	30%
JMV4567	Ac-D-Arg-O_2Oc-$(Val)_3$-Sta-Ala-Sta-NH_2	$[M+H]^+$-1043.7, $[M+2H]^{2+}$-522.3 (**1042,6**)	1.04	18%
JMV4625	Ac-D-Asp-O_2Oc-$(Val)_3$-Sta-Ala-Sta-$(AMPA)_4$-NH_2	$[M+2H]^{2+}$- 795.8, $[M+3H]^{3+}$-531.4 (**1589,8**)	1.46	25%
JMV4626	Fl-betaAla-r-O_2Oc-$(Val)_3$-Sta-Ala-Sta-$(AMPA)_4$-NH_2	$[M+2H]^{2+}$- 1025.5, $[M+3H]^{3+}$-648.1 (**2048,9**)	1.46	26%
JMV4629	Fl-betaAla-r-O_2Oc-$(Val)_3$-Sta-Ala-Sta-$(DBT)_4$-NH_2	$[M+2H]^{2+}$- 1199,4, $[M+3H]^{3+}$-800 (**2396,8**)	1.55	28%
JMV4630	Ac-r-O_2Oc-$(Val)_3$-Sta-Ala-Sta-$(DBT)_4$-NH_2	$[M+2H]^{2+}$- 990,4, $[M+3H]^{3+}$-660,6 (**1978,8**)	1.48	25%
JMV4631	Fl-betaAla-r-O_2Oc-$(Val)_3$-Sta-Ala-Sta-NH_2	$[M+2H]^{2+}$- 731,3 (**1460,7**)	1.35	30%
JMV4659	Fl-Ahx-r-O_2Oc-$(Val)_3$-Sta-Ala-Sta-$(AMPA)_4$-NH_2	$[M+2H]^{2+}$- 1046.5, $[M+3H]^{3+}$-698.2 (**2091**)	1.46	22%
JMV4674	Ac-D-Arg-O_2Oc-$(Val)_3$-γ-Ala-Ala-γ-Ala-$(AMPA)_4$-NH_2	$[M+2H]^{2+}$- 758,4 (**1514,7**)	1.62	20%

V.5 Biological experiments

Cell Preparation and Treatment with Fluorescently Labelled Oligomers

Sections: **III.3.2.1, III.3.2.4. III.3.3 III.3.4, III.5.4**

We used 1 mM stock solutions of compounds dissolved in DMSO that were further diluted with serum-free medium to obtain a final concentration of 10^{-5} M. All compounds were protected from light during the experiments, and their fluorescence values were regularly verified. Human breast cancer MDA-MB-231 cells were maintained in monolayer cultures in Dulbecco's modified Eagle's medium (DMEM) supplemented with 10% fetal bovine serum (FBS) and 50 µg/mL gentamycin at 37 °C in 5% CO_2. One day prior to the experiment, cells were harvested using trypsin in phosphate-buffered saline (PBS), centrifuged, and resuspended with culture medium. The suspension containing 106 cells/mL was transferred into plastic 24-well plates (Becton Dickinson, Le Pont De Claix, France) (200 µL/well) and incubated overnight until they reached >90% confluency. On the day of the experiment, the culture medium was removed, and the cells were washed once with phenol red-free DMEM. Then, 200 µL of DMEM containing 10^{-5} M of compounds was dispersed on cells. Experiments were carried out in triplicate for each compound. To determine the amount of compounds assimilated by cells, including membrane-bound fractions, cells were washed twice with PBS. To determine the amount of internalized compounds, cells were washed with PBS and then treated for 5 min with 30 µL of a solution containing 0.5 mg/mL trypsin. After trypsinization, cells were resuspended in phenol red-free DMEM and centrifuged for 5 min at 800g. Adherent cells or cell pellets were lysed in 200 µL of cell culture lysis reagent (Promega, Charbonnie`res, France). After 30 min of incubation at room temperature, 200 µL of distilled water was added before analysis on a Gemini XS spectrofluorimeter (Molecular Devices, CA, USA), with the excitation wavelength adjusted to 485 nm and emission measured at 530 nm. All fluorescence values were normalized according to the fluorescence intensity of each compound at 10^{-5} M in lysis buffer in the presence of 2 $\times 10^5$ cells.

Kinetics of Internalization

Sections: **III.3.2.1**

One day before the experiment, $2x10^6$ MDA-MB-231 cells were seeded on plastic 24-well plates. The cells were then washed with DMEM and incubated for increasing times from 1 to 24 h with 10^{-5} M oligomer at 37°C. At the indicated time, cells were treated by trypsin and intracellular fluorescence measured as described above.

Visualization of Fluorescent Oligomers by CLSM

Sections: **III.3.2.2, III.3.3, III.3.4, III.3.4.1, III.5.4.2**

The day prior to the experiment, MDA-MB-231(MCF7 in section **III.3.3**) cells were seeded onto bottom glass dishes (World Precision Instrument, Stevenage, UK) at a density of 106 cells per square centimeter. On the day of the experiment, cells were washed once and incubated in 1 mL red-free medium containing fluorescent labelled

compounds at a concentration of 10^{-5} M for 3, 16, and 24 h. Thirty minutes before the end of incubation, cells were loaded with Hoechst 33342 (Invitrogen, Cergy Pontoise, France) for nuclear staining at a final concentration of 5 *μ*g/mL. For membrane labeling, a Vybrant lipid-raft labeling kit (Invitrogen) was used as described by the manufacturer. For endosome labeling, 20 min before the end of the experiment, 35 mg/mL of transferrin (Invitrogen) was added to the culture medium. For lysosome labeling, 3 h before the end of the experiment, 50 nM of lysotracker red DND-99 (Invitrogen) was added to phenol red-free DMEM. Before visualization, cells were washed gently with phenol redfree DMEM. Cells were then scanned with a LSM 5 LIVE confocal laser scanning mi croscope (Carl Zeiss, Le Pecq, France), with a slice depth (Z stack) of 0.67 *μ*m.

MTT viability assay

Section: **III.3.2.3, III.5.3**

Cellular toxicity of the fluorescent agents was examined using the 3-(4,5-dimethylthiazol-2-yl)-2,5-diphenyltetrazolium bromide (MTT) cell viability assay. Briefly, 5000 cells were seeded in 96-well plates. Two concentrations (10^{-5} and 10^{-6} M) of compounds were tested for 5 days. Following this incubation, the cells were incubated for 4 h with 0.5 mg/mL of MTT in media. After 4 h, the MTT/media solution was removed, and the precipitated crystals were dissolved in ethanol/DMSO (1/1). The solution absorbance was read at 540 nm. We confirmed this assay to be linear and to give comparable results as total DNA quantification by diaminobenzoic acid assay.[77]

Cell Preparation and Treatment with HCCA Labelled Oligomers

Section **III.4.1**

Cell penetration experiments

Stock solutions of cell penetrating compounds were prepared in DMSO at 1mM and then diluted with serum-free medium to obtain a final concentration of 10 µM. Human breast cancer MDA-MB-231 cells were cultured at 37°C in Dulbecco's modified eagle's medium (DMEM) supplemented with 10% foetal bovine serum (FBS) and 50 µg/mL gentamycin. In each 24-well (Becton Dickinson, France), 2.105 cells were incubated overnight prior to the experiment. For the experiments, cells were washed with phenol red-free DMEM, and then incubated for 3 h with the cell penetrating compound solution (200µL, 10 µM, in phenol red-free DMEM). Cells were then washed 2 times with 1mL of PBS.

Cell treatment for determination of cellular and membrane-bounded compounds

Cells were lysed with 400 µL of a lysis buffer containing 10 mM Tris and 1 mM EDTA. This mixture was incubated for 20 min at room temperature in lysis buffer, and lysates were then sonicated for 5 min. Classical buffer containing Triton was not used to avoid the PEG-like envelope of cations observed below 1200 Da during MALDI-TOF MS analysis.

Cell treatment for determination of internalised compounds

After washing, cells were treated for 5 min with 30 µL of 0.5 mg/mL trypsin. After trypsinization, cells were resuspended in phenol-red free medium and centrifuged for 5 min at 10,000 g. Cell pellets obtained were then incubated for 20 min with lysis buffer prior to a sonication for 5 min. In order to quantify more precisely the intracellular compounds, some samples obtained after trypsinization were centrifuged for 15 min at 15,000 g. This centrifugation step can eliminate all membrane fragments that could have been left after sonication and therefore all compounds sticked to the membranes.

Inhibition of the Cathepsin D

Section **III.5**

Cell Line, Culture and Products

MDA-MB-231, MCF7, LNCaP, SaOS2 and HCT116 were cultured in DMEM containing 10% foetal bovine serum (FBS) (Fisher Scientific, France), 100 U. ml^{-1} penicillin and 100 µg.ml^{-1} streptomycin at 37°C. Pepstatine was from Sigma Aldrich Chimie (France).

Stock solutions of compound were dissolved at 1 mM in DMSO. For experiment, compounds were further diluted with serum-free medium to obtain a final concentration of 10^{-5} M.

Enzyme kinetic essay

Section: **III.5.2**

Kinetic parameters were determined using the internally quenched fluorescent synthetic peptide substrate EDANS–C(O)–CH_2–CH_2–C(O)–Arg-pro-Ile-Phe-Phe-Arg-leu-Gln–DABCYL)–OH with a cleavage site of Phe-Phe, previously described by Baechle and collaborators.[73] The assays were carried out using a Gemini XS spectrofluorimeter (Molecular Devices, CA, USA). The excitation and emission wavelengths were respectively 335 nm and 538 nm with a cut off at 495 nm. The reaction was carried out at 37°C in a solution of 100 mM sodium acetate, 200 mM sodium chloride supplemented with 125 µL of NIH3T3 conditioned medium at pH 3.5. The observed fluorescence correspond to synthetic substrate hydrolysis by active cathepsin D. The fluorescence units were converted to percent of cathepsin D activity as a function of total enzyme in vehicle (DMSO).

Cell outgrowth assay

Section: **III.5.3**

Outgrowth assays were performed as described previously.[77] Briefly, 5,000 subconfluent cells were seeded in 96-well plates. The day after seeding, cells were treated with the indicated concentration of compounds in Dulbecco's modified Eagle's medium (DMEM) supplemented with 10% fetal bovine serum (FBS). 4 days after treatment, cells were quantified using a 3-(4,5-dimethylthiazol-2-yl)-2,5-diphenyltetrazolium (MTT) assay (200 µg/mL MTT for 4 h).

Western blot analysis

Protein extracts were resolved on SDS-PAGE gel and transfered to PVDF-membrane, which was probed with antibodies against cyclin E (1:500; sc-247, Santa Cruz Biotechnology), PCNA (1:500; sc-56, Santa Cruz Biotechnology), cdk-2 (1:500; sc-163, Santa Cruz Biotechnology), GAPDH (1:500; ab8245, abcam) and Bcl-2 (1:500; sc-492, Santa Cruz Biotechnology). The membrane was subsequently probed with a horseradish peroxidase-conjugated secondary antibody and developed with ECL PLUS (Amersham).

V.6 MALDI TOF experiments

MALDI-TOF mass spectrometry analysis.

Section **III.4.1**

The mass spectra were acquired with a Bruker Ultraflex Daltonics instrument (Bruker Daltonics, Wissembourg, France). A pulsed Nd:YAG laser at a wavelength of 355 nm was operated at a frequency of 100 Hz. External calibration was performed with commercial peptide mixture (Calibration peptide standard 2, Bruker Daltonics, Wissembourg, France). Data were acquired with the Flex Control software under the following MS conditions. The source was operated in the positive mode with an acceleration voltage of 25.0 kV and a delayed extraction time of 140 ns was applied. The reflectron mode was used for the peptides (voltages of 26.3 kV and 13.9 kV). Mass spectra were acquired from 200 laser shots, the laser fluence being adjusted for each studied sample (Laser Fluence 1). Ions were detected over a mass range from m/z 500 to 3000, the matrix ions being deflected up to m/z 500 to avoid detector saturation.

The [D_4]HCCA-tagged CPP solubilized in a mixture of acetonitrile/water/trifluoroacetic acid (50:50:0.1 v/v/v; 5 mL) at different concentrations was added to the cell sample (5 mL). After mixing and centrifugation, the mixture was analyzed by MALDI-TOF MS. To improve the signal resolution when the concentration of the internalized compound was very low, the mixture was concentrated by lyophilization and dissolved in acetonitrile/water/trifluoroacetic acid (50:50:0.1 v/v/v). Each sample was analyzed with both the HCCA and the HCCE matrix twice.When the HCCA matrix was used, 0.5 mL of the sample was mixed on the MALDI probe with 0.5 mL of the matrix solution (half-saturated in acetonitrile/water/trifluoroacetic acid 50:50:0.1 v/v/v). When the HCCE matrix was used, 0.5 mL of the HCCE matrix (saturated in acetone) was deposited and dried on the MALDI probe, and then the peptide solution (0.5 mL) was deposited. The isotopic group of peaks of each cell-penetrating compound was integrated with the FlexAnalysis software (version 2.2, Bruker Daltonics). The SNAP algorithm was used to determine the area of each isotopic pattern of light and heavy molecules by calculating their isotopic distribution.

V.7 NMR expreriments and structural studies

The NMR samples of Ac-$(DBT)_n$-NH_2 n=[1-8] were prepared by dissolving the oligomers in d_6-DMSO or $CDCl_3$ (500 µL) at a concentration of 0.5 mM.
NMR experiments were carried out on a Varian Inova 600 MHz spectrometer, equipped with a cryogenic probe optimized for ^1H detection. For the one-dimensional (1D) ^1H spectra, 64 scans were acquired with a spectral width of 6714.8 Hz, relaxation delay 1.5 s, 16384 data points for acquisition and 32768 for transformation. The 1D spectra in d_6-DMSO and $CDCl_3$ were recorded at temperature of 298 K. The two-dimensional (2D) [^1H,^1H] spectra: double quantum filtered correlated spectroscopy (DQF-COSY)[78], total correlation spectroscopy (TOCSY)[79], nuclear Overhauser effect spectroscopy (NOESY)[80], rotating-frame Overhauser effect spectroscopy (ROESY)[81], were acquired using the time-proportional phase-incrementation (TPPI) method to obtain complex data points in the t_1 dimension. Typically, 32 or 64 scans per t_1 increment were collected with a spectral width of 6714.8 Hz along both f_1 and f_2, 2048x256 data points in t_2 and t_1 respectively and recycle delay 1.5 s. Only in the case of ROESY the delay was 2s. Water suppression in d_6-DMSO was achieved by means of Double Pulsed Field Gradient Spin Echo (DPFGSE) sequence[82]. The TOCSY experiment was recorded using a DIPSI-2 mixing scheme of 70 ms with 7.7 KHz spin-lock field strength. The NOESY spectra were carried out at 298 K with a mixing time in the range of 150 - 400 ms. The mixing time of the ROESY experiment was in the range of 200 – 350 ms. The data were typically apodized with a square cosine window function and zero filled to a matrix of size 4096x1024 prior to Fourier transformation and baseline correction. Chemical shifts were referenced to internal residual signal of the DMSO. All NMR data were processed with Varian VNMRJ 1.1.D software and analyzed using Monoscope and NEASY[83], tools of CARA (http://www.nmr.ch)[84].

Experimental distance restraints for structure calculation of Ac-$(DBT)_6$-NH_2 were derived from the cross-peak volumes in the NOESY spectrum recorded in d_6-DMSO with a mixing time of 250 ms. NOESY cross-peaks were manually integrated using the NEASY software and converted to a target distance constraints according to an inverse sixth power peak volume-to-distance relationship:

$$Distance = \sqrt[6]{\frac{Const}{Volume\ (NOE)}}$$

As a reference to calculate the ‘Const’ we used the NOE volume of the interaction between HA DBT:B1 and HB2 DBT:B1. The distance between these two atoms was estimated at 2.86 Å by the crystallographic data obtained for the DBT monomer.[2]

The upper limits of the distances were caclulated as target distance plus 15%.

V.7.1 Proton chemical shifts of compounds Ac-$(DBT)_n$-NH_2

Chemical shits (in ppm) of Ac-DBT-NH_2 protons in DMSO at 25ºC

First residue (DBT:B1)									
HA	**HB3**	**HB2**	**HD2**	**HD3**	**HE1**	**HZ1**	**HZ2**	**HE2**	**H**
4,491	3,005	3,506	4,658	3,961	7,531	7,585	7,349	7,697	8,446

Chemical Shits (in ppm) of Ac-$(DBT)_2$-NH_2 protons in DMSO at 25ºC

First residue (DBT:B1)									
HA	**HB2**	**HB3**	**HD2**	**HD3**	**HE1**	**HZ1**	**HZ2**	**HE2**	**H**
4,467	3,481	2,977	4,735	4,060	7,455	7,538	7,335	7,673	8,407
Second residue (DBT:B2)									
4,571	3,533	3,016	4,636	4,048	7,580	7,58	7,373	7,708	8,534

Chemical Shits (in ppm) of Ac-$(DBT)_3$-NH_2 protons in DMSO at 25ºC

First residue (DBT:B1)									
HA	**HB2**	**HB3**	**HD2**	**HD3**	**HE1**	**HZ1**	**HZ2**	**HE2**	**H**
4,453	3,476	2,960	4,737	4,013	7,438	7,519	7,327	7,665	8,385
Second residue (DBT:B2)									
4,522	3,515	3,007	4,737	4,117	7,471	7,539	7,343	7,682	8,553
Third residue (DBT:B3)									
4,572	3,525	3,007	4,651	4,048	7,587	7,587	7,378	7,709	8,594

Chemical Shits (in ppm) of Ac-$(DBT)_4$-NH_2 protons in DMSO at 25ºC

First residue (DBT:B1)									
HA	**HB2**	**HB3**	**HD2**	**HD3**	**HE1**	**HZ1**	**HZ2**	**HE2**	**H**
4,486	3,512	2,996	4,775	4,049	7,430	7,509	7,319	7,663	8,356
Second residue (DBT:B2)									
4,505	3,513	2,976	4,744	4,075	7,459	7,523	7,335	7,674	8,545
Third residue (DBT:B3)									
4,526	3,527	3,010	4,757	4,104	7,482	7,535	7,351	7,687	8,617
Fourth residue (DBT:B4)									
4,586	3,527	3,010	4,654	4,052	7,586	7,586	7,372	7,711	8,617

Chemical Shits (in ppm) of Ac-$(DBT)_6$-NH_2 protons in DMSO at **25ºC**

First residue (DBT:B1)									
HA	**HB2**	**HB3**	**HD2**	**HD3**	**HE1**	**HZ1**	**HZ2**	**HE2**	**H**
4,449	3,471	2,956	4,738	4,009	7,426	7,506	7,304	7,660	8,355
Second residue (DBT:B2)									
4,498	3,513	2,986	4,744	4,071	7,450	7,501	7,320	7,669	8,524
Third residue (DBT:B3)									
4,506	3,514	2,986	4,761	4,068	7,467	7,508	7,333	7,675	8,583
Fourth residue (DBT:B4)									
4,523	3,518	2,991	4,768	4,069	7,469	7,519	7,344	7,680	8,622
Fifth residue (DBT:B5)									
4,536	3,520	2,999	4,764	4,108	7,482	7,523	7,354	7,690	8,640
Sixth residue (DBT:B6)									
4,592	3,523	3,004	4,663	4,054	7,591	7,595	7,372	7,708	8,626

V.7.2 Distance restrictions measured for compound Ac-$(DBT)_6$-NH_2 from 2D NOESY experiment performed at 25℃ in d_6-DMSO

*Table **V.7.2** includes NOE interactions detected in the Ac-$(DBT)_6$-NH_2 molecule, the measured volumes of these interactions and the calculated target distances and upper limits (Target distance plus 15%)*

H1	H2	Volume	Target distance	Uper limit (+15%)	Lower limit (-15%)
HD3 DBT:B1	HB3 DBT:B2	146400	4,9	5,7	4,2
H DBT:B6	HE1 DBT:B5	311000	4,4	5,0	3,7
H DBT:B4	HE1 DBT:B3	497500	4,0	4,6	3,4
H DBT:B5	HE1 DBT:B4	482200	4,0	4,7	3,4
H DBT:B3	HE1 DBT:B2	373300	4,2	4,9	3,6
H DBT:B2	HE1 DBT:B1	225800	4,6	5,3	3,9
HE2 DBT:B1	HB2 DBT:B1	174300	4,8	5,5	4,1
HE2 DBT:B1	HA DBT:B1	102300	5,2	6,0	4,5
HE2 DBT:B1	HB3 DBT:B1	91520	5,3	6,1	4,5
HE2 DBT:B4	HA DBT:B4	173600	4,8	5,5	4,1
HE2 DBT:B4	HB3 DBT:B4	218300	4,6	5,3	3,9
HE2 DBT:B4	HB2 DBT:B4	377000	4,2	4,8	3,6
HA DBT:B4	HB3 DBT:B4	3000000	3,0	3,4	2,5
HA DBT:B4	HB2 DBT:B4	5000000	2,7	3,1	2,3
HE1 DBT:B6	HD2 DBT:B6	1852000	3,2	3,7	2,7
HE1 DBT:B6	HD3 DBT:B6	1743000	3,3	3,8	2,8
HE1 DBT:B6	HA DBT:B6	125500	5,1	5,8	4,3
HD3 DBT:B3	HB2 DBT:B4	200000	4,7	5,4	4,0
HE1 DBT:B2	HB3 DBT:B3	230600	4,6	5,3	3,9

HE1 DBT:B2	HB2 DBT:B3	217200	4,6	5,3	3,9
HE1 DBT:B2	HD2 DBT:B2	3254000	2,9	3,4	2,5
HE1 DBT:B2	HA DBT:B2	467800	4,1	4,7	3,5
HE1 DBT:B2	HD3 DBT:B2	3070000	3,0	3,4	2,5
HZ1 DBT:B3	HD3 DBT:B3	380000	4,2	4,8	3,6
H DBT:B3	HB3 DBT:B3	2869000	3,0	3,5	2,6
H DBT:B3	HD2 DBT:B2	4125000	2,8	3,3	2,4
H DBT:B3	HA DBT:B6	121400	5,1	5,9	4,3
H DBT:B3	HB2 DBT:B3	1739000	3,3	3,8	2,8
H DBT:B3	HD3 DBT:B2	3432000	2,9	3,4	2,5
H DBT:B3	HA DBT:B3	1085000	3,5	4,1	3,0
HZ1 DBT:B1	HA DBT:B1	76440	5,5	6,3	4,7
HD2 DBT:B6	HB3 DBT:B6	143900	4,9	5,7	4,2
HE2 DBT:B2	HB3 DBT:B2	218300	4,6	5,3	3,9
HE2 DBT:B2	HB2 DBT:B2	377000	4,2	4,8	3,6
HE2 DBT:B2	HA DBT:B2	173600	4,8	5,5	4,1
HA DBT:B5	HB3 DBT:B5	3000000	3,0	3,4	2,5
HA DBT:B5	HB2 DBT:B5	5000000	2,7	3,1	2,3
HA DBT:B1	HB2 DBT:B1	3854000	2,9	3,3	2,4
HA DBT:B1	HB3 DBT:B1	2095000	3,2	3,6	2,7
HE2 DBT:B3	HB3 DBT:B3	218300	4,6	5,3	3,9
HE2 DBT:B3	HB2 DBT:B3	377000	4,2	4,8	3,6
HE2 DBT:B3	HA DBT:B3	173600	4,8	5,5	4,1
HE1 DBT:B4	HA DBT:B4	467800	4,1	4,7	3,5
HE1 DBT:B4	HB2 DBT:B5	300000	4,4	5,0	3,7
HE1 DBT:B4	HD3 DBT:B4	3070000	3,0	3,4	2,5
HE1 DBT:B4	HD2 DBT:B4	3254000	2,9	3,4	2,5
HE1 DBT:B3	HD3 DBT:B3	3070000	3,0	3,4	2,5
HE1 DBT:B3	HB2 DBT:B4	300000	4,4	5,0	3,7
HE1 DBT:B3	HD2 DBT:B3	3254000	2,9	3,4	2,5
HE1 DBT:B3	HA DBT:B3	467800	4,1	4,7	3,5
H DBT:B4	HA DBT:B4	1153000	3,5	4,0	3,0
H DBT:B4	HB3 DBT:B4	2902000	3,0	3,4	2,5
H DBT:B4	HD3 DBT:B3	3415000	2,9	3,4	2,5
H DBT:B4	HB2 DBT:B4	1545000	3,3	3,8	2,8
H DBT:B4	HD2 DBT:B3	3645000	2,9	3,3	2,5
HZ1 DBT:B6	HA DBT:B6	40230	6,1	7,0	5,2
HE2 DBT:B5	HA DBT:B5	173600	4,8	5,5	4,1
HE2 DBT:B5	HB3 DBT:B5	218300	4,6	5,3	3,9
HE2 DBT:B5	HB2 DBT:B5	377000	4,2	4,8	3,6
HZ1 DBT:B4	HD3 DBT:B4	380000	4,2	4,8	3,6
HA DBT:B6	HB3 DBT:B6	3243000	2,9	3,4	2,5
HA DBT:B6	HB2 DBT:B6	5216000	2,7	3,1	2,3
HA DBT:B2	HB3 DBT:B2	3000000	3,0	3,4	2,5
HA DBT:B2	HB2 DBT:B2	5000000	2,7	3,1	2,3
HZ1 DBT:B2	HD3 DBT:B2	380000	4,2	4,8	3,6

HD3 DBT:B4	HB3 DBT:B5	230000	4,6	5,3	3,9
HD3 DBT:B4	HB2 DBT:B5	200000	4,7	5,4	4,0
HD3 DBT:B2	HB3 DBT:B3	230000	4,6	5,3	3,9
HD3 DBT:B2	HB2 DBT:B3	200000	4,7	5,4	4,0
H DBT:B5	HA DBT:B5	1475000	3,4	3,9	2,9
H DBT:B5	HB3 DBT:B5	2902000	3,0	3,4	2,5
H DBT:B5	HD3 DBT:B4	3415000	2,9	3,4	2,5
H DBT:B5	HB2 DBT:B5	1545000	3,3	3,8	2,8
H DBT:B5	HD2 DBT:B4	3645000	2,9	3,3	2,5
H DBT:B1	HB2 DBT:B1	1104000	3,5	4,1	3,0
H DBT:B1	HA DBT:B1	845200	3,7	4,2	3,1
H DBT:B1	HB3 DBT:B1	2121000	3,2	3,6	2,7
HE2 DBT:B6	HB3 DBT:B6	110400	5,2	5,9	4,4
HE2 DBT:B6	HB2 DBT:B6	324600	4,3	5,0	3,7
HA DBT:B3	HB3 DBT:B3	3000000	3,0	3,4	2,5
HA DBT:B3	HB2 DBT:B3	5000000	2,7	3,1	2,3
HE1 DBT:B1	HD2 DBT:B1	2349000	3,1	3,6	2,6
HE1 DBT:B1	HA DBT:B1	151300	4,9	5,6	4,2
HE1 DBT:B1	HD3 DBT:B1	2038000	3,2	3,7	2,7
HE1 DBT:B5	HD3 DBT:B5	2761000	3,0	3,5	2,6
HE1 DBT:B5	HA DBT:B5	467800	4,1	4,7	3,5
HE1 DBT:B5	HD2 DBT:B5	3254000	2,9	3,4	2,5
H DBT:B6	HD3 DBT:B5	3415000	2,9	3,4	2,5
H DBT:B6	HD2 DBT:B5	3645000	2,9	3,3	2,5
H DBT:B6	HB3 DBT:B6	2902000	3,0	3,4	2,5
H DBT:B6	HA DBT:B6	987400	3,6	4,1	3,1
H DBT:B6	HB2 DBT:B6	1545000	3,3	3,8	2,8
H DBT:B2	HD2 DBT:B1	3597000	2,9	3,3	2,5
H DBT:B2	HB3 DBT:B2	2623000	3,0	3,5	2,6
H DBT:B2	HD3 DBT:B1	2884000	3,0	3,5	2,6
H DBT:B2	HB2 DBT:B2	1361000	3,4	3,9	2,9
HE1 DBT:B1	HA DBT:B2	87900	5,4	6,2	4,6
HE1 DBT:B1	HB3 DBT:B2	79020	5,5	6,3	4,6
HZ2 DBT:B2	HA DBT:B3	47510	6,0	6,8	5,1

ABBREVIATIONS

Ac_2O - Acetic anhydride
Ahx - Aminohexanoic acid
AMPA - 2-aminomethyl-phenyl-acetic acid
Bcl - B-cell lymphoma
BH3 - Bcl-2 homology domain 3
Boc_2O - Di-tert-butyl dicarbonate
BOP - Benzotriazole-1-yl-oxy-tris-(dimethylamino)-phosphonium hexafluorophosphate
CF - Carboxyfluorescein
CLSM - Confocal Laser Scanning Microscopy
COSY - Correlation Spectroscopy
DCM - Dichloromethane
d - density
DBT - (3S)-amino-5-(carboxylmethyl)-2,3-dihydro-1,5-benzothiazepin-4(5H)-one
DMF - Dimethylformamide
CD - Cathepsin D
CPNP - Cell Penetrating Non-peptide
CPP - Cell Penetrating Peptide
DABCYL - 4-(4-dimethylaminophenylazo) benzoic acid
DMSO - Dimethyl Sulfoxide
DIEA - N,N-Diisopropylethylamine
EDANS - 5-[(2-aminoethyl)amino]naphthalene-1-sulfonic acid
ESI - Electrospray Ionisation
FACS - Fluorescence-activated cell sorting
FITC - Fluorescein Isothiocyanate
Fmoc - 9-fluorenylmetoxycarbonyl
HBTU - O-Benzotriazole-N,N,N',N'-tetramethyl-uronium-hexafluoro-phosphate
HCCA - α-cyano-4-hydroxycinnamic acid
HCCE - cyano-4-hydroxycinnamic methyl ester
HDM2 – Human MDM2 (murine double minute)
HPLC - High-Performance Liquid Chromatography
LBT - (3 R)-amino-5-(carboxylmethyl)-2,3-dihydro-1,5-benzothiazepin-4(5H)-one one
NMR - Nuclear magnetic resonance
NOESY – Nuclear Overhauser effect spectroscopy
m – multiplet
MALDI-TOF - Matrix-assisted laser desorption/ionization Time
MS - Mass spectrometry
MT – Mixing time
MTT - 3-(4,5-Dimethylthiazol-2-yl)-2,5-diphenyltetrazolium bromide
p53 – Protein 53
pCD – Preprocathepsin D
O_2Oc - 8-amino-3,6-dioxaoctanoic acid
OSu - Succinimide
PMO - Phosphorodiamidate Morpholino Oligo
PNA - Peptide nucleic acid
PS – Polystyrene

RA – Rink Amide
RISC - RNA-Induced Silencing Complex
ROESY - Rotating frame Overhause Effect Spectroscopy
Rt - retention time
s – singlet
SiRNA – small interfering RNA
SPPS - standard solid phase peptide synthesis
tBu - *Tert*-Butyl
TEA - Triethylamine
TFA - Trifluoroacetic acid
TFE - 2,2,2-Trifluoroethanol
TFEM - Total Fluorescence Emission Measurement
THF – Tetrahydrofuran
TIS - Tri-isopropyl-silane
TLC - Thin Layer Chromatography
UV – Ultra violet
Z(Br) - 2-bromobenzyloxycarbonyl

REFERENCES

1. Raynal, N.; Averlant-Petit, M.-C.; Bergé, G.; Didierjean, C.; Marraud, M.; Duru, C.; Martinez, J.; Amblard, M., Molecular modeling study for a novel structured oligomer subunit selection: the example of 2-aminomethyl-phenyl-acetic acid. *Tetrahedron Letters* **2007,** *48* (10), 1787-1790.
2. Amblard, M., Raynal, N., Averlant-Petit, M. C., Didierjean, C., Calmes, M., Fabre, O., Aubry, A., Marraud, M., and Martinez, J., Structural elucidation of the beta-turn inducing (S)-[3-amino-4-oxo-2,3-dihydro-5H-benzo[b][1,4]thiazepin-5-yl] acetic acid (DBT) motif. *Tetrahedron Lett.* **2005,** *46*, 3733–3735.
3. Trabulo, S.; Cardoso, A. L.; Mano, M.; de Lima, M. C. P., Cell-Penetrating Peptides—Mechanisms of Cellular Uptake and Generation of Delivery Systems. *Pharmaceuticals* **2010,** *3* (4), 961-993.
4. Goodman, C. M.; Choi, S.; Shandler, S.; DeGrado, W. F., Foldamers as versatile frameworks for the design and evolution of function. *Nat Chem Biol* **2007,** *3* (5), 252-62.
5. Sawant, R. T., V., Intracellular transduction using cell-penetrating peptides. *Mol Biosyst* **2010,** *6* (4), 628-40.
6. Futaki, S.; Suzuki, T.; Ohashi, W.; Yagami, T.; Tanaka, S.; Ueda, K.; Sugiura, Y., Arginine-rich peptides. An abundant source of membrane-permeable peptides having potential as carriers for intracellular protein delivery. *J Biol Chem* **2001,** *276* (8), 5836-40.
7. Rothbard, J. B.; Garlington, S.; Lin, Q.; Kirschberg, T.; Kreider, E.; McGrane, P. L.; Wender, P. A.; Khavari, P. A., Conjugation of arginine oligomers to cyclosporin A facilitates topical delivery and inhibition of inflammation. *Nat Med* **2000,** *6* (11), 1253-7.
8. Lubomir L. Vezenkov, M. M., Jean-Francois Hernandez, Marie-Christine Averlant-Petit, Olivier Fabre, Ettore Benedetti, Marcel Garcia, Jean Martinez and Muriel Amblard, Noncationic Dipeptide Mimic Oligomers As Cell Penetrating Nonpeptides(CPNP). *Bioconjugate Chem.* **2010,** *21* (10), 1850-1854.
9. Bareford, L. A., and Swaan P. W., Endocytic mechanisms for targeted drug delivery. *Adv. Drug Delivery Rev* **2007,** *59*, 748–758.
10. Burlina, F.; Sagan, S.; Bolbach, G.; Chassaing, G., Quantification of the cellular uptake of cell-penetrating peptides by MALDI-TOF mass spectrometry. *Angew Chem Int Ed Engl* **2005,** *44* (27), 4244-7.
11. David Paramelle, G. S., Lubomir L. Vezenkov, Marie Maynadier, Christophe Andre, Christine Enjalbal, Monique Calmes, Marcel Garcia, Jean Martinez, and Muriel Amblard., A Straightforward Approach for Cellular-Uptake Quantification. *Angew. Chem. Int. Ed.* **2010,** *49* (44), 8240-8243.
12. Petr Benes, V. V. a. M. F., Cathepsin D - Many Functions of one aspartic protease. *Crit Rev Oncol Hematol.* **2008,** *68* (1), 12-28.
13. Bautista, A. D.; Craig, C. J.; Harker, E. A.; Schepartz, A., Sophistication of foldamer form and function in vitro and in vivo. *Curr Opin Chem Biol* **2007,** *11* (6), 685-92.
14. Seebach, D.; Ciceri, P. E.; Overhand, M.; Jaun, B. R., D., Probing the helical secondary structure of short-chain β-peptides. *Helv. Chim. Acta* **1996,** (79), 2043–2066.
15. Appella, D. H.; Christianson, L. A.; Karle, I. L.; Powell, D. R.; Gellman, S. H., β-Peptide Foldamers: Robust Helix Formation in a New Family of β-Amino Acid Oligomers. *Journal of the American Chemical Society* **1996,** *118* (51), 13071-13072.
16. Gellman, S. H., Foldamers: A Manifesto. *Accounts of Chemical Research* **1998,** *31* (4), 173-180.
17. (a) Cheng, R. P.; Gellman, S. H.; DeGrado, W. F., beta-Peptides: from structure to function. *Chem Rev* **2001,** *101* (10), 3219-32; (b) Seebach, D.; Hook, D. F.; Glattli, A., Helices and other secondary structures of beta- and gamma-peptides. *Biopolymers* **2006,** *84* (1), 23-37.
18. Sharma, G. V.; Jayaprakash, P.; Narsimulu, K.; Ravi Sankar, A.; Ravinder Reddy, K.; Radha Krishna, P.; Kunwar, A. C., A left-handed 9-helix in gamma-peptides: synthesis and

conformational studies of oligomers with dipeptide repeats of C-linked carbo-gamma4-amino acids and gamma-aminobutyric acid. *Angew Chem Int Ed Engl* **2006,** *45* (18), 2944-7.
19. Arndt, H. D.; Ziemer, B.; Koert, U., Folding propensity of cyclohexylether-delta-peptides. *Org Lett* **2004,** *6* (19), 3269-72.
20. Horne, W. S.; Gellman, S. H., Foldamers with heterogeneous backbones. *Acc Chem Res* **2008,** *41* (10), 1399-408.
21. Fischer, L.; Guichard, G., Folding and self-assembly of aromatic and aliphatic urea oligomers: towards connecting structure and function. *Org Biomol Chem* **2010,** *8* (14), 3101-17.
22. Zega, A., Azapeptides as pharmacological agents. *Curr Med Chem* **2005,** *12* (5), 589-97.
23. Smith, A. B., 3rd; Knight, S. D.; Sprengeler, P. A.; Hirschmann, R., The design and synthesis of 2,5-linked pyrrolinones. A potential non-peptide peptidomimetic scaffold. *Bioorg Med Chem* **1996,** *4* (7), 1021-34.
24. Li, X.; Yang, D., Peptides of aminoxy acids as foldamers. *Chem Commun (Camb)* **2006,** (32), 3367-79.
25. (a) Lee, B. C.; Zuckermann, R. N.; Dill, K. A., Folding a nonbiological polymer into a compact multihelical structure. *J Am Chem Soc* **2005,** *127* (31), 10999-1009; (b) Baldauf, C.; Gunther, R.; Hofmann, H. J., Helices in peptoids of alpha- and beta-peptides. *Phys Biol* **2006,** *3* (1), S1-9.
26. (a) Huc, I., Aromatic Oligoamide Foldamers. *European Journal of Organic Chemistry* **2004,** *2004* (1), 17-29; (b) Li, Z. T.; Hou, J. L.; Li, C.; Yi, H. P., Shape-persistent aromatic amide oligomers: new tools for supramolecular chemistry. *Chem Asian J* **2006,** *1* (6), 766-78.
27. Gillies, E. R.; Dolain, C.; Leger, J. M.; Huc, I., Amphipathic helices from aromatic amino acid oligomers. *J Org Chem* **2006,** *71* (21), 7931-9.
28. Joachim Garric, J.-M. L. g., Axelle Grelard, Masakazu Ohkitac and Ivan Huc, Solid state and solution conformation of 2-pyridinecarboxylic acid hydrazides: a new structural motif for foldamers. *Tetrahedron Letters* **2003,** *44*, 1421–1424.
29. Yuan, L.; Zeng, H.; Yamato, K.; Sanford, A. R.; Feng, W.; Atreya, H. S.; Sukumaran, D. K.; Szyperski, T.; Gong, B., Helical aromatic oligoamides: reliable, readily predictable folding from the combination of rigidified structural motifs. *J Am Chem Soc* **2004,** *126* (50), 16528-37.
30. Yin, H.; Lee, G. I.; Park, H. S.; Payne, G. A.; Rodriguez, J. M.; Sebti, S. M.; Hamilton, A. D., Terphenyl-based helical mimetics that disrupt the p53/HDM2 interaction. *Angew Chem Int Ed Engl* **2005,** *44* (18), 2704-7.
31. Gesell, J.; Zasloff, M.; Opella, S. J., Two-dimensional 1H NMR experiments show that the 23-residue magainin antibiotic peptide is an alpha-helix in dodecylphosphocholine micelles, sodium dodecylsulfate micelles, and trifluoroethanol/water solution. *J Biomol NMR* **1997,** *9* (2), 127-35.
32. Dahui Liu, S. C., Bin Chen, Robert J. Doerksen, Dylan J. Clements, Jeffrey D. Winkler, Michael L. Klein, and William F. DeGrado, Nontoxic Membrane-Active Antimicrobial Arylamide Oligomers. *Angew. Chem. Int. Ed.* **2004,** *43*, 1158-1162.
33. Klaus Nusslein, L. A., Jason Rennie, Cullen Owens and Gregory N. Tew, Broad-spectrum antibacterial activity by a novel abiogenic peptide mimic. *Microbiology* **2006,** *152*, 1913–1918.
34. Ernst, J. T.; Becerril, J.; Park, H. S.; Yin, H.; Hamilton, A. D., Design and application of an alpha-helix-mimetic scaffold based on an oligoamide-foldamer strategy: antagonism of the Bak BH3/Bcl-xL complex. *Angew Chem Int Ed Engl* **2003,** *42* (5), 535-9.
35. Sadowsky, J. D.; Schmitt, M. A.; Lee, H. S.; Umezawa, N.; Wang, S.; Tomita, Y.; Gellman, S. H., Chimeric (alpha/beta + alpha)-peptide ligands for the BH3-recognition cleft of Bcl-XL: critical role of the molecular scaffold in protein surface recognition. *J Am Chem Soc* **2005,** *127* (34), 11966-8.
36. Horne, W. S.; Boersma, M. D.; Windsor, M. A.; Gellman, S. H., Sequence-based design of alpha/beta-peptide foldamers that mimic BH3 domains. *Angew Chem Int Ed Engl* **2008,** *47* (15), 2853-6.

37. Lee, E. F.; Sadowsky, J. D.; Smith, B. J.; Czabotar, P. E.; Peterson-Kaufman, K. J.; Colman, P. M.; Gellman, S. H.; Fairlie, W. D., High-resolution structural characterization of a helical alpha/beta-peptide foldamer bound to the anti-apoptotic protein Bcl-xL. *Angew Chem Int Ed Engl* **2009,** *48* (24), 4318-22.
38. Nakase, I.; Takeuchi, T.; Tanaka, G.; Futaki, S., Methodological and cellular aspects that govern the internalization mechanisms of arginine-rich cell-penetrating peptides. *Adv Drug Deliv Rev* **2008,** *60* (4-5), 598-607.
39. Melaine Delcroix, L. W. R., Cell-Penetrating Peptides for Antiviral Drug Development. *Pharmaceuticals* **2010,** *3* (3), 448-470.
40. Vives, E.; Brodin, P.; Lebleu, B., A truncated HIV-1 Tat protein basic domain rapidly translocates through the plasma membrane and accumulates in the cell nucleus. *J Biol Chem* **1997,** *272* (25), 16010-7.
41. Derossi, D.; Joliot, A. H.; Chassaing, G.; Prochiantz, A., The third helix of the Antennapedia homeodomain translocates through biological membranes. *J Biol Chem* **1994,** *269* (14), 10444-50.
42. Rothbard, J. B.; Jessop, T. C.; Lewis, R. S.; Murray, B. A.; Wender, P. A., Role of membrane potential and hydrogen bonding in the mechanism of translocation of guanidinium-rich peptides into cells. *J Am Chem Soc* **2004,** *126* (31), 9506-7.
43. Nakase, I.; Niwa, M.; Takeuchi, T.; Sonomura, K.; Kawabata, N.; Koike, Y.; Takehashi, M.; Tanaka, S.; Ueda, K.; Simpson, J. C.; Jones, A. T.; Sugiura, Y.; Futaki, S., Cellular uptake of arginine-rich peptides: roles for macropinocytosis and actin rearrangement. *Mol Ther* **2004,** *10* (6), 1011-22.
44. (a) Rousselle, C.; Clair, P.; Lefauconnier, J. M.; Kaczorek, M.; Scherrmann, J. M.; Temsamani, J., New advances in the transport of doxorubicin through the blood-brain barrier by a peptide vector-mediated strategy. *Mol Pharmacol* **2000,** *57* (4), 679-86; (b) Lindgren, M.; Rosenthal-Aizman, K.; Saar, K.; Eiriksdottir, E.; Jiang, Y.; Sassian, M.; Ostlund, P.; Hallbrink, M.; Langel, U., Overcoming methotrexate resistance in breast cancer tumour cells by the use of a new cell-penetrating peptide. *Biochem Pharmacol* **2006,** *71* (4), 416-25.
45. (a) Fawell, S.; Seery, J.; Daikh, Y.; Moore, C.; Chen, L. L.; Pepinsky, B.; Barsoum, J., Tat-mediated delivery of heterologous proteins into cells. *Proc Natl Acad Sci U S A* **1994,** *91* (2), 664-8; (b) El-Andaloussi, S.; Holm, T.; Langel, U., Cell-penetrating peptides: mechanisms and applications. *Curr Pharm Des* **2005,** *11* (28), 3597-611.
46. Jiang, T.; Olson, E. S.; Nguyen, Q. T.; Roy, M.; Jennings, P. A.; Tsien, R. Y., Tumor imaging by means of proteolytic activation of cell-penetrating peptides. *Proc Natl Acad Sci U S A* **2004,** *101* (51), 17867-72.
47. Won Jong Kim, L. V. C., Seongbong Jo, James W. Yockman, Ji Hoon Jeong,; Kim, Y.-H. K. a. S. W., Cholesteryl Oligoarginine Delivering Vascular Endothelial Growth Factor siRNA Effectively Inhibits Tumor Growth in Colon Adenocarcinoma. *MOLECULAR THERAPY* **2006,** *14*.
48. Morris, M. C.; Vidal, P.; Chaloin, L.; Heitz, F.; Divita, G., A new peptide vector for efficient delivery of oligonucleotides into mammalian cells. *Nucleic Acids Res* **1997,** *25* (14), 2730-6.
49. Hawiger, J., Cellular import of functional peptides to block intracellular signaling. *Curr Opin Immunol* **1997,** *9* (2), 189-94.
50. Crespo, L.; Sanclimens, G.; Montaner, B.; Perez-Tomas, R.; Royo, M.; Pons, M.; Albericio, F.; Giralt, E., Peptide dendrimers based on polyproline helices. *J Am Chem Soc* **2002,** *124* (30), 8876-83.
51. Watkins, C. L.; Brennan, P.; Fegan, C.; Takayama, K.; Nakase, I.; Futaki, S.; Jones, A. T., Cellular uptake, distribution and cytotoxicity of the hydrophobic cell penetrating peptide sequence PFVYLI linked to the proapoptotic domain peptide PAD. *Journal of Controlled Release* **2009,** *140* (3), 237-244.
52. Todd A. Aguilera, E. S. O., Margaret M. Timmers, Tao Jiangac; Tsien, a. R. Y., Systemic in vivo distribution of activatable cell penetrating peptides is superior to that of cell penetrating peptidesw. *Integr. Biol* **2009,** *1*.

53. Rueping, M.; Mahajan, Y.; Sauer, M.; Seebach, D., Cellular uptake studies with beta-peptides. *Chembiochem* **2002,** *3* (2-3), 257-9.
54. Wender, P. A.; Mitchell, D. J.; Pattabiraman, K.; Pelkey, E. T.; Steinman, L.; Rothbard, J. B., The design, synthesis, and evaluation of molecules that enable or enhance cellular uptake: peptoid molecular transporters. *Proc Natl Acad Sci U S A* **2000,** *97* (24), 13003-8.
55. Cooley, C. B.; Trantow, B. M.; Nederberg, F.; Kiesewetter, M. K.; Hedrick, J. L.; Waymouth, R. M.; Wender, P. A., Oligocarbonate molecular transporters: oligomerization-based syntheses and cell-penetrating studies. *J Am Chem Soc* **2009,** *131* (45), 16401-3.
56. (a) Fillon, Y. A.; Anderson, J. P.; Chmielewski, J., Cell penetrating agents based on a polyproline helix scaffold. *J Am Chem Soc* **2005,** *127* (33), 11798-803; (b) Geisler, I.; Chmielewski, J., Probing length effects and mechanism of cell penetrating agents mounted on a polyproline helix scaffold. *Bioorg Med Chem Lett* **2007,** *17* (10), 2765-8.
57. (a) Umezawa, N.; Gelman, M. A.; Haigis, M. C.; Raines, R. T.; Gellman, S. H., Translocation of a beta-peptide across cell membranes. *J Am Chem Soc* **2002,** *124* (3), 368-9; (b) Potocky, T. B.; Menon, A. K.; Gellman, S. H., Effects of conformational stability and geometry of guanidinium display on cell entry by beta-peptides. *J Am Chem Soc* **2005,** *127* (11), 3686-7.
58. Gillies, E. R.; Deiss, F.; Staedel, C.; Schmitter, J. M.; Huc, I., Development and biological assessment of fully water-soluble helical aromatic amide foldamers. *Angew Chem Int Ed Engl* **2007,** *46* (22), 4081-4.
59. Okuyama, M.; Laman, H.; Kingsbury, S. R.; Visintin, C.; Leo, E.; Eward, K. L.; Stoeber, K.; Boshoff, C.; Williams, G. H.; Selwood, D. L., Small-molecule mimics of an alpha-helix for efficient transport of proteins into cells. *Nat Methods* **2007,** *4* (2), 153-9.
60. Creaser, S. P.; Peterson, B. R., Sensitive and Rapid Analysis of Protein Palmitoylation with a Synthetic Cell-Permeable Mimic of Src Oncoproteins. *Journal of the American Chemical Society* **2002,** *124* (11), 2444-2445.
61. Rajendran, L.; Schneider, A.; Schlechtingen, G.; Weidlich, S.; Ries, J.; Braxmeier, T.; Schwille, P.; Schulz, J. B.; Schroeder, C.; Simons, M.; Jennings, G.; Knolker, H. J.; Simons, K., Efficient inhibition of the Alzheimer's disease beta-secretase by membrane targeting. *Science* **2008,** *320* (5875), 520-3.
62. J. P. Richard, K. M., E. Vives, C. Ramos, B. Verbeure, M. J. Gait, L. V. Chernomordik, B. Lebleu,, A REEVALUATION OF THE MECHANISME OF CELLULAR UTPAKE. *J. Biol. Chem.* **2003,** *278*, 585-590.
63. Omerod, M. G., Flow Cytometry - A practical approach. 3rd edition. *Oxford University press* **2000**.
64. Pawley, J., Handbook of Biological Confocal Microscopy (3rd ed.). *Berlin: Spinger* **2006**.
65. Kurreck, J., RNA Interference: From Basic Research to Therapeutic Applications. *Angew. Chem. Int. Ed.* **2009,** *48*, 1378 – 1398.
66. Ohri SS, V. A., Proctor M, Fusek M, Vetvicka V., Depletion of Procathepsin D Gene Expression by RNA Interference: A Potential Therapeutic Target for Breast Cancer. *Cancer Biol* **2007,** *6* (7), 1081-1087.
67. Vetvicka V, V. J., Fusek M., Anti-human procathepsin D activation peptide antibodies inhibit breast cancer development. *Breast Cancer Res Treat* **1999,** *57*, 261–269.
68. Marcel Garcia, N. P., Emmanuelle Liaudet, Valérie Laurent, Danielle Derocq, Jean-Paul Brouillet, Henri Rochefort, Biological and Clinical Significance of Cathepsin D in Breast Cancer Metastasis. *STEM CELLS* **1996,** *14*, 642-650.
69. Martin Fusek, V. V., DUAL ROLE OF CATHEPSIN D: LIGAND AND PROTEASE. *Biomed. Papers* **2005,** *149* (1), 43-50.
70. Abdel-Meguid SS., Inhibition of aspartyl proteinases. *Med. Res.Rev.* **1993,** *13*, 731–778.
71. Guy Berchem, M. G., Michel Gleizes, Jean-Paul Brouillet, FrancËoise Vignon, Marcel Garcia and Emmanuelle Liaudet-Coopman, Cathepsin-D affects multiple tumor progression steps in vivo: proliferation, angiogenesis and apoptosis. *Oncogene* **2002,** *21*, 5951 – 5955.

72. Sergei V. Gulinka, L. I. S., Pavel Majer, Jack Collins, Bradley P. Kene, Doald G. Johnson, John W. Erickson, Design of sensitive fluorogenic substrates for human cathepsin D. *FEBS J* **1997,** *413* (2).
73. D. Baechle, A. C., R. Fischer, J. Brandenburg, T. Burster, C. Driessen and H. Kalbacher, Biotinylated fluorescent peptide substrates for the sensitive and specific determination of cathepsin D activity. *J Pept Sci.* **2005,** *11* (3), 166–174.
74. Magali Jullian, A. H., Amelie Maurras, Karine Puget, Muriel Amblad, Jean Martinez, Gilles Subras, N-Terminus FITC labeling of peptides on solid support: the truth behind the spacer. *Tetrahedron Lett.* **2009,** *50*, 260-263.
75. David Lascoux, D. P., Gilles Subra, Michal Heymann, Christophe Geourjon, Jean Martinez, and Eric Forest, Discrimination and Selective Enhancement of Signals in the MALDI Mass Spectrum of a Protein by Combining a Matrix-Based Label for Lysine Residues with a Neutral Matrix. *Angew. Chem. Int. Ed.* **2007**, 5690 –5693.
76. Hancock, W. S., Battersby, J. E., and Harding, D. R. K., Use of Picric Acid as a Simple Monitoring Procedure for Automated Peptide-Synthesis. *Analytical Biochemistry* **1975,** *69*, 497-503.
77. Marie Maynadier, J.-M. R., Anne-Marie Cathiard, Nadine Platet, Delphine Gras, Michel Gleizes, M. Saeed Sheikh, Philippe Nirde, and Marcel Garcia, Unliganded estrogen receptor α inhibits breast cancer cell growth through interaction with a cyclin-dependent kinase inhibitor (p21WAF1). *Faseb J* **2008,** *22* (3), 671-681.
78. Rance M, Sørensen OW, Bodenhausen G, Wagner G, Ernst RR, Wüthrich K. Improved spectral resolution in cosy 1H NMR spectra of proteins via double quantum filtering. *Biochem. Biophys. Res. Commun*. 1983, **117**, 479-485.
79. Braunschweiler L, Ernst RR. Coherence transfer by isotropic mixing—application to proton correlation spectroscopy. *J. Magn. Reson.* **1983**, 53, 521–528.
80. Anil-Kumar, Ernst RR, Wüthrich K. A two-dimensional nuclear Overhauser enhancement (2D NOE) experiment for the elucidation of complete proton–proton cross-relaxation networks in biological macromolecules. *Biochem. Biophys. Res. Commun*. **1980**, 95, 1-6.
81. Griesinger C, Ernst RR. Frequency offset effects and their elimination in NMR rotating-frame cross-relaxation spectroscopy. *J. Magn. Res*. **1987**, 75, 261-271
82. Hwang TL, Shaka AJ. Water suppression that works: excitation sculpting using arbitrary wave-forms and pulsed-field gradients. *J. Magn. Reson. A* **1995**, 112, 275–279
83. Bartels C, Xia T, Billeter M, Wüthrich K. The program XEASY for computer-supported NMR spectral analysis of biological macromolecules. *J. Biomol. NMR* **1995**, 5, 1-10.
84. Keller R. The Computer Aided Resonance Assignment Tutorial. ISBN 3-85600-112-3, CANTINA Verlag, **2004**.

SCIENTIFIC PRODUCTION LIST

Publications and patents index

L. L. Vezenkov, M. Maynadier, J. F. Hernandez, M. Averlant-Petit, O. Fabre, E. Benedetti, M. Garcia, J. Martinez and M. Amblard, Noncationic Dipeptide Mimic Oligomers As Cell Penetrating Nonpeptides(CPNP). *Bioconjugate Chem.* ***2010,*** *21(10), 1850–1854*

D. Paramelle, G. Subra, **L. L. Vezenkov**, M. Maynadier, C. Andre, C. Enjalbal, M. Calmes, M. Garcia, J. Martinez, and M. Amblard., A Straightforward Approach for Cellular-Uptake Quantification. *Angew. Chem. Int. Ed.* ***2010,*** *49(44), 8240-8243*

M. Amblard, J. Martinez, **L. L. Vezenkov**, J. F. Hernandez, M. Garcia, M. Maynadier, Utilisation d'oligomères mimes contraints de dipeptides et tripeptides en tant qu'agents de vectorisation. *FR0955427* **2009**.

Communications index

Personal oral communications:

L. L. Vezenkov, M. Maynadier, J.F. Hernandez, E. Benedetti, M. Garcia, J. Martinez, M. Amblard, *Non-cationic dipeptide mimetic oligomers as cell penetrating non peptides (CPNP)*. 12th Naples Workshop on Bioactive Peptides: Naples, Italy, **04-07 Jun 2010**.

L. L. Vezenkov, M. Maynadier, J.F. Hernandez, M. Garcia, E. Benedetti, J. Martinez, M. Amblard, *Oligomères de mimes contraints de dipeptides comme vecteurs de pénétration cellulaire*. 19ème Journée Chimie Grand Sud-Ouest.: Toulouse-France, **13 Nov 2009**.

Personal poster communications:

L. L. Vezenkov, M. Maynadier, J. F. Hernandez, M. Averlant-Petit, O. Fabre, E. Benedetti, M. Garcia, J. Martinez, M. Amblard, *Oligomères de mimes contraints de dipeptides comme vecteurs de pénétration cellulaire*. . XVIIème Journée Jeunes Chercheurs Paris: Paris-France, **05 Feb 2010**.

G. Subra, D. Paramel., M. Maynadier, **L. L. Vezenkov**, C. André, C. Enjalbal, M. Calmès, M. Garcia, J. Martinez, M. Amblard, *Quantification of the Cellular uptake of Cell Penetrating compounds by MALDI-TOF MS using HCCA*. 12th Naples Workshop on Bioactive Peptides: Naples-Italy, **04-07 Jun 2010**.

L. L. Vezenkov, M. Maynadier, J. F. Hernandez, N. Floquet, M. Garcia, J. Martinez, M. Amblard, *Short artificial oligomers as non-charged transduction compounds.* PEPVEC 2009 : 3th Intracellular Delivery of Therapeutics Molecules: Montpellier-France, **31 Aug – 02 Sep 2009**. Participation with fellowship

L. L. Vezenkov, M. Maynadier, J. F. Hernandez, M. Garcia, J. Martinez, *Short artificial oligomers as non-charged transduction compounds.* Conseil Scientifique de l'Institut des Biomolécules Max Mousseron,: Montpllier, **26 Mar 2008**.

Poster and oral communications given by teammates:

L. L. Vezenkov, M. Maynadier, J.F. Hernandez, E. Benedetti, M. Garcia, G. Subra, J. Martinez, M. Amblard, *Short constrained dipeptide mimic oligomers as uncharged cell penetrating compounds*. 11th Chinese International Peptide Symposium: Lanzhou-China, **05.07-08.07 2010**.

D. Paramelle, M. Maynadier, **L. L. Vezenkov**, C. André, C. Enjalbal, M. Calmès, M. Garcia, J. Martinez, G. Subra, M. Amblard, *Quantification of the Cellular uptake of Cell Penetrating compounds by MALDI-TOF MS using HCCA/HCCE discrimination effect: application to a Cell penetrating non peptide (CPNP) oligomer.* 11th Chinese International Peptide Symposium: Lanzhou-China, **05-08 Jul 2010**

D. Paramelle, M. Maynadier, **L. L. Vezenkov**, C. André, C. Enjalbal, M. Calmès, M. Garcia, J. Martinez, G. Subra, M. Amblard, *Quantification of the cellular uptake of cell penetrating compounds by Maldi-Tof using HCCA/HCCE discrimination effect: application to a cell penetrating non peptide (CPNP) oligomer.* Probes for Peptides Science: **08 – 09 Apr 2010**

G. Subra, D. Paramel., M. Maynadier, J. F. Hernandez, M. Garcia, **L. L. Vezenkov**, J. Martinez, M. Amblard, *Cell Penetrating Non Peptides (CPNPS)*: *Short Artificial Oligomers As Non-charged Intracellular Transduction Compounds.* 8th Australian Peptide Conference: **11 – 16 Oct 2009**.

Experience abroad

As part of a joint program between Italy and France ("co-tutelle de thèse Italie-France"), this PhD work has been carried out at the "Dipartimento delle Scienze Biologiche", University "Federico II" of Napoli (Italy), where I spent half of my PhD working time (18 months), under the direction of Prof. Ettore BENEDETTI, and at the "Institut des Biomolécules Max Mousseron" IBMM UMR 5247 of Montpellier (France), where I spent the second half (18 months), under the direction of Prof. Jean MARTINEZ. My mobility between Italy and France was sponsorized by the "Università italofrancese" of Torino (Italy) through the "Bando VINCI 2008" and by the "MIUR" through the "Internazionalizzazione del Sistema Universitario 2004-2006 DM 5 agosto 2004 n°262 art. 26".